A Practical Manual on Groundwater Modelling

Water and Mineral Resources
Groundwater Modelling

Series Number CSC(93)WMR-16
Technical Paper 292

Practical Manual on Groundwater Modelling

by

Festus F Akindunni
Beak Consultants Limited
14 Abacus Road
Brampton, Ontario

and

E O Frind
Waterloo Centre for Groundwater Research
University of Waterloo
Waterloo, Ontario

February 1993

Commonwealth Science Council

Printed and published by
The Commonwealth Secretariat

May be purchased from
Commonwealth Secretariat Publications
Marlborough House
London SW1Y 5HX

ISBN 0 85092 393 X

TABLE OF CONTENTS

1. INTRODUCTION

This manual presents the basic theories of groundwater flow and contaminant transport as applied to the construction of numerical models. Chapter one discusses some of the practical questions that may be investigated with a numerical model, the capabilities and limitations of such models, a review of the different ways of approximating solutions to groundwater problems and the general procedure for constructing a model.

Important equations that govern groundwater flow and solute transport are reviewed in chapter two. Numerical modelling involves approximation of the equations especially to describe systems that have variable properties and irregular geometry. Analytical solutions are often not available for such systems. Numerical procedures used to describe groundwater problems create systems of equations that must be solved simultaneously. The equations must also be solved efficiently and fairly accurately. Some of the methods widely used to solve simultaneous equations are therefore discussed in chapter three.

Most groundwater models are based on either the finite difference or the finite element formulation. Basic principles of the two methods are discussed in chapters four and five respectively. Examples and case studies are provided for both methods in each chapter while details of the case studies are provided in appendices 1 to 3. Particle tracking methods are presented in chapter six as alternatives to finite difference and finite element methods for the simulation of contaminant transport.

A list of references is provided in chapter seven and a glossary of selected terms is given in chapter eight. Appendix 4 contains a list of some groundwater modelling codes which are based on the formulations presented in this manual.

1.1 Definition and Purpose of Modelling

Models (be they physical, analog or mathematical) are an attempt to represent reality. In groundwater studies, numerical models are often used as tools that help us understand the physical, chemical, and biochemical processes taking place in groundwater systems. They also help us understand the intricate interactions between these processes and provide the information we need in order to manage these processes beneficially, without harm to the environment. Numerical models are now used in virtually all areas of groundwater hydrology.

Groundwater models can be broadly grouped into two categories: water quantity (generally requiring flow models) and water quality (requiring transport models). In the water quantity category, models are used in aquifer management, well field design, recharge enhancement, determination of optimum yield, well interference studies, studies of groundwater-streamflow interactions, and similar problems. Models of this type have been well proven in many years of use.

In the groundwater quality category, numerical models are used to study the consequences of groundwater contamination, the means that are needed to prevent contamination, the design of remediation measures and to test effectiveness of alternative remediation schemes. Specifically, models can shed light on typical questions such as the following:

- what is the migration path of a contaminant in the groundwater?
- will the contaminant reach a specific location of interest, such as a water well?
- if migration to the location occurs, how long will it take?
- how important are attenuation mechanisms such as dilution, dispersion, and chemical or biochemical transformations?
- can the contaminant be removed by a specific remedial action?

- how effective are natural or artificial remediation processes in removing the contaminant?

Numerical models for basic transport processes such as advection-dispersion are also well proven. In more advanced areas (such as flow in variably saturated media, flow in fractured media and the transport of multiple chemically or biochemically interacting substances in a spatially discrete and dynamic framework) some models have been developed and intensive research is continuing.

1.2 Proper and Misuse of Models

Because models are representations of real-world systems, they are generally as good as our understanding of the systems being modelled.

Natural groundwater systems are often highly complex and a complete description of the physical characteristics is in most cases impossible. Instead, the physical properties of the system are generally described either in terms of averages or in the form of statistical distributions. Also, physical/chemical/biochemical processes can interact in complex ways and some of these interactions (i.e. reaction kinetics) are not yet fully understood.

In view of these complexities, the use of models in a purely predictive-deterministic mode is risky and generally justified only in simple situations. Groundwater models are properly used for purposes of, for example:

- obtaining insight into complex processes,
- assessing the relative importance of the various processes occurring in a given situation by means of sensitivity analyses,
- analyzing "worst-case", "special case" or "what if" situations,

- making probabilistic predictions.

Models also play a vital role in research into the behaviour of hazardous contaminants in the subsurface. For example, large-scale field experiments involving chlorinated hydrocarbons cannot be conducted in most industrialized countries because the discharge of these liquids into the environment is prohibited by law. Laboratory-validated numerical models provide a means to simulate such experiments without risk to the environment.

1.3 General Format for Model Construction

To construct a numerical model of a groundwater system, we first define, as closely as possible, the geological units and their hydrogeologic properties within the domain of interest. The domain should be selected such that conditions along its boundaries can be defined unambiguously.

If the model is designed for water quality studies, we then define processes that may play a role in the transport of contaminants. These processes will include, for example:

- groundwater flow,
- advective transport,
- dispersive/diffusive transport,
- chemical interactions,
- radioactive or biological decay,
- gravity forces,
- thermal processes,
- capillarity.

In most cases, only a limited number of these processes act at the same time. When the relevant processes are simple and act sequentially we speak of a linear system. For example,

advective-dispersive transport of a non-reacting dilute solute is a linear process. When the processes are coupled in complex relationships, or when the parameters controlling a process depend on the process itself, we speak of a nonlinear system. A nonlinear process occurs, for example, when the transport of a solute affects the flow system through the fluid density, or when an oxidation reaction depends on the amount of oxygen available while the oxygen available in turn depends on the amount consumed. Nonlinear systems are more difficult and costly to solve. While exact solutions are available for most linear problems, nonlinear problems are nearly always solved by means of numerical methods.

The processes taking place in a groundwater system are subject to physical laws such as:

- constitutive laws (Darcy's Law, Fick's Law),
- conservation laws for fluid mass, solute mass, thermal energy,
- force equilibrium laws.

These physical laws can be expressed mathematically in terms of governing equations which are usually partial differential equations. In cases of linear processes with simple geometry, these equations can generally be solved by analytical methods. In general cases involving nonlinear processes or complex geometry, the equations are solved numerically.

The mathematical description of the relevant physical laws, together with the description of the hydrogeology and the definition of the boundaries, constitute the *conceptual model* of the system. In order to solve the mathematical equations numerically, the system is *discretized* and the partial differential equations are approximated by algebraic equations at a finite number of points (*nodes*) in the domain. The *numerical solution* then solves the resulting sets of algebraic equations. Typically, several thousands of simultaneous equations are solved repeatedly in contaminant transport problems.

The entire solution process is formally expressed in a *computer code*. Although often the

computer code is seen as "the numerical model", the most important component is actually the conceptual model which has been selected to represent the real physical system and the processes taking place within this system. Thus great care must be taken in defining the conceptual model.

Model Verification, Validation and Calibration

Before the model can be applied to a real system, it must first be *verified* to ensure that the algebraic equations are solved correctly and that the code is error-free. This is generally done by comparison of model results with corresponding results produced by an analytical solution applied to a geometrically simple system subject to the same processes.

The model must also be *validated* (Tsang, 1991) to ensure that it actually represents the physical processes it is supposed to represent. This is done by comparing model results to field or laboratory observations. The comparison need not necessarily yield an exact agreement, but should provide proof that the physical/chemical/biochemical processes are validly and unambiguously represented in the model.

Disagreements between model results and field observation may be due to factors such as a lack of completeness in the data, measurement error, or less-than-perfect knowledge of the physical parameters. To obtain an improved match, the model can be *calibrated* by adjusting some of its parameters. However, only a small number of parameters can be adjusted in this way to preserve the *uniqueness* of the results. If different combinations of parameters values lead to the same result, the simulations will be non-unique.

Once the model is properly verified and validated, it can be applied to simulate the processes occurring in a real system, to perform sensitivity analysis, and to investigate "worst-case" situations. At this stage, the goal of the modeller should be to use the model to obtain the best possible insight into the system, and to use this insight in developing appropriate

strategies for achieving the overall objectives of the study.

1.4 Overview of Numerical Methods for Groundwater Models

The types of numerical methods that are most often used in groundwater modelling are *Finite Differences*, *Finite Elements*, and *Particle Tracking*. The first two of these approaches share the basic formulation of the solution as a boundary value problem. They originate from the two classical concepts of differentiation and integration in mathematics. The finite difference method has the advantage of being conceptually simple, while the finite element method is more flexible in representing domains with irregular geometry or anisotropic and heterogeneous media. In terms of accuracy, both methods are equivalent. Either of these two methods can be applied to the solution of flow and transport problems, and either allows the incorporation of chemical/biochemical interactions.

The user of numerical models should be aware of certain pitfalls which may affect the quality of the results obtained. One of these pitfalls is *numerical dispersion*, which may arise in the solution of the transport equation by either finite differences or finite elements. Techniques for its control have been developed and are easy to implement. Other pitfalls occur in the solution of nonlinear equations which describe flow in variably saturated porous media and transport with chemical or biochemical reactions.

The third of the commonly-used numerical methods, *Particle Tracking*, is applicable to the solution of transport problems only. This technique does not solve a boundary value problem, but instead considers the fate of contaminant particles as they migrate through the flow system. Particle tracking models are usually coupled with either finite difference or finite element models for determining the flow field. The main advantages of this technique are a simple and understandable concept, and a lack of susceptibility to numerical dispersion. A disadvantage is that chemical/biochemical interactions cannot be easily incorporated in a general way. The method is particularly useful for the simulation of hydraulic remediation

measures.

An excellent text on groundwater modelling at the introductory level is Kinzelbach (1986). Huyakorn and Pinder (1983) give an advanced treatment of numerical methods with a strong mathematical basis. Luckner and Schestakow (1986) present a comprehensive survey of all types of migration processes in groundwater, with some basic numerical methods. Other texts of valuable topics include Wang and Anderson (1982), Bear and Verruijt (1987); and Molson *et al.* (in preparation).

2. REVIEW OF GOVERNING EQUATIONS

The main equations that govern the physics of groundwater flow and contaminant transport are the Darcy equation, the groundwater flow equation, and the transport equation. These are supplemented by the appropriate relationships expressing chemical and biochemical transformations.

2.1 Darcy Equation

The Darcy equation relates the flow of water through a porous medium to the driving force, which is the hydraulic gradient. In general, natural groundwater systems are anisotropic (i.e. exhibiting preferred directions of flow) due to geologic factors such as the sedimentary structure of the medium, or fracturing. In the case of anisotropy due to the sedimentary structure, flow parallel to the layering is generally favoured over flow across the layering.

The general form of the Darcy equation for three dimensional (3D) anisotropic media is (Bear, 1979; Freeze and Cherry, 1979):

$$q_x = -K_{xx}\frac{\partial \phi}{\partial x} -K_{xy}\frac{\partial \phi}{\partial y} -K_{xz}\frac{\partial \phi}{\partial z}$$

$$q_y = -K_{yx}\frac{\partial \phi}{\partial x} -K_{yy}\frac{\partial \phi}{\partial y} -K_{yz}\frac{\partial \phi}{\partial z}$$

$$q_z = -K_{zx}\frac{\partial \phi}{\partial x} -K_{zy}\frac{\partial \phi}{\partial y} -K_{zz}\frac{\partial \phi}{\partial z}$$

or in short form

$$q_i = -K_{ij}\frac{\partial \phi}{\partial x_j}$$

where $x_i = (x,y,z)$ are the coordinates of a point, q_i is the specific discharge or Darcy flux (L/T) in the direction i in the medium, K_{ij} is the hydraulic conductivity tensor (L/T), $\phi = p/\rho g + Z$ is the hydraulic head (L), with p being the pressure, ρ the density, g the gravitational acceleration, and Z the elevation head. The term $\rho g \phi$ describes the potential energy of the water at point (x,y,z). The physical meaning of a typical term in K_{ij}, say K_{xy}, is literally "the ease at which water flows in the x-direction due to a driving force acting in the y-direction". The negative sign indicates that groundwater flows toward the direction of decreasing hydraulic gradient.

When the coordinate axes are aligned parallel and perpendicular to the direction of the stratification (the principal directions of flow), a driving force applied in one of the coordinate directions will produce flow only in that direction. The Darcy equation then simplifies to:

$$q_{x'} = -K_{x'x'}\frac{\partial \phi}{\partial x'}$$

$$q_{y'} = -K_{y'y'}\frac{\partial \phi}{\partial y'}$$

$$q_{z'} = -K_{z'z'}\frac{\partial \phi}{\partial z'}$$

where (x′,y′,z′) refers to the principal directions of the medium, and $K_{i'i'}$ refers to the principal components of the hydraulic conductivity tensor.

2.2 General Groundwater Flow Equation

The flow equation is based on the continuity of fluid mass in the porous medium. The general form for heterogeneous isotropic media, without sources or sinks, is (Bear, 1979):

$$\frac{\partial}{\partial x_i}\left(K_{ij}\frac{\partial \phi}{\partial x_j}\right) = S_s\frac{\partial \phi}{\partial t}$$

where t is time, and $S_s = \rho g(\alpha+\theta\beta)$ is the specific storage of the porous medium, with θ being the porosity, α the compressibility of the porous medium, and β the compressibility of the fluid.

The above equations are valid for one-, two- and three-dimensional systems. Although most natural aquifer systems are, strictly speaking, three dimensional, 3D models require large amounts of data and are therefore applied mainly in specialized situations, or for research purposes. In practical applications, two-dimensional (2D) forms are used wherever possible. Two types of 2D models, the areal model for confined or unconfined aquifers, and the cross-sectional model for flow systems with depth-dependent processes, are in common use. The governing equations for these two types of models are discussed below.

2.3 Confined/Unconfined Aquifer Equations

If flow in an aquifer is predominantly horizontal (Fig. 1), the general 3D equation can be integrated vertically over the aquifer thickness to obtain, in the case of a confined aquifer (Bear, 1979):

$$\frac{\partial}{\partial x}\left(T\frac{\partial \phi}{\partial x}\right) + \frac{\partial}{\partial y}\left(T\frac{\partial \phi}{\partial y}\right) - \frac{K'}{b'}(\phi - \phi') + Q = S\frac{\partial \phi}{\partial t}$$

where T = Kb is the aquifer transmissivity, with b = b(x,y) being the aquifer thickness, S = S_sb is the aquifer storativity, K′/b′(ϕ-ϕ′) represents the leakage flux from neighbouring aquifers, with K′ being the vertical conductivity of the aquitard, b′ being the aquitard thickness, and ϕ′ the hydraulic head in the neighbouring aquifer. The term Q represents the water injected or withdrawn at wells.

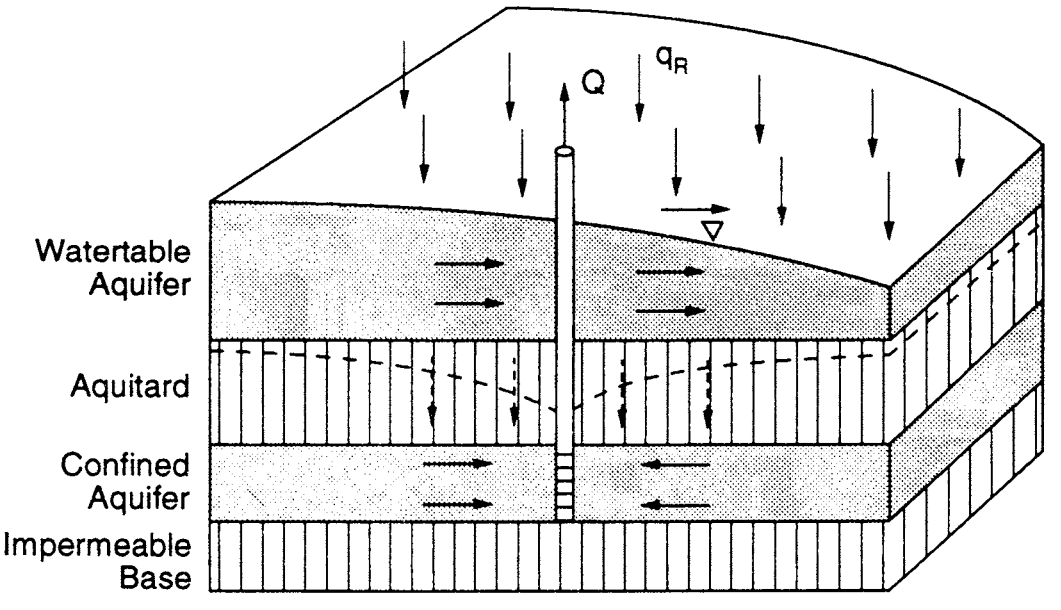

Figure 1: Confined/unconfined aquifer system

In the case of a watertable aquifer, the equation can be written as:

$$\frac{\partial}{\partial x}\left(Kb\frac{\partial h}{\partial x}\right) + \frac{\partial}{\partial y}\left(Kb\frac{\partial h}{\partial y}\right) + q_R + Q = S_y\frac{\partial h}{\partial t}$$

where h is the hydraulic head at the watertable, b=h(x,y)-B(x,y) is the saturated thickness, with B being the hydraulic head at the aquifer bottom, S_y is the specific yield, and q_R is the recharge at the watertable. The watertable aquifer equation is nonlinear since the effective transmissivity Kb depends on the unknown head h through the saturated thickness b.

The boundary around the periphery of the domain (Fig. 2) should follow some identifiable natural feature. One possible feature is an open body of water such as a stream which is in contact with the aquifer, providing a fixed head (*first-type* or *Dirichlet*) boundary condition of the form:

$$\phi = h_w$$

where h_w is the hydraulic head at the boundary. An impermeable barrier (or a hydrological divide) is also a suitable boundary which provides a zero flux (*second-type* or *Neumann*) boundary condition of the form:

$$q_n = 0$$

Other possible choices are a boundary where the flux is known, or a boundary following a streamline, giving again a zero-flux boundary condition.

The basic assumptions in areal aquifer models or multi-aquifer models are:

- flow in the aquifer is essentially horizontal,
- flow in the aquitards is essentially vertical,
- storage in the aquitards is negligible.

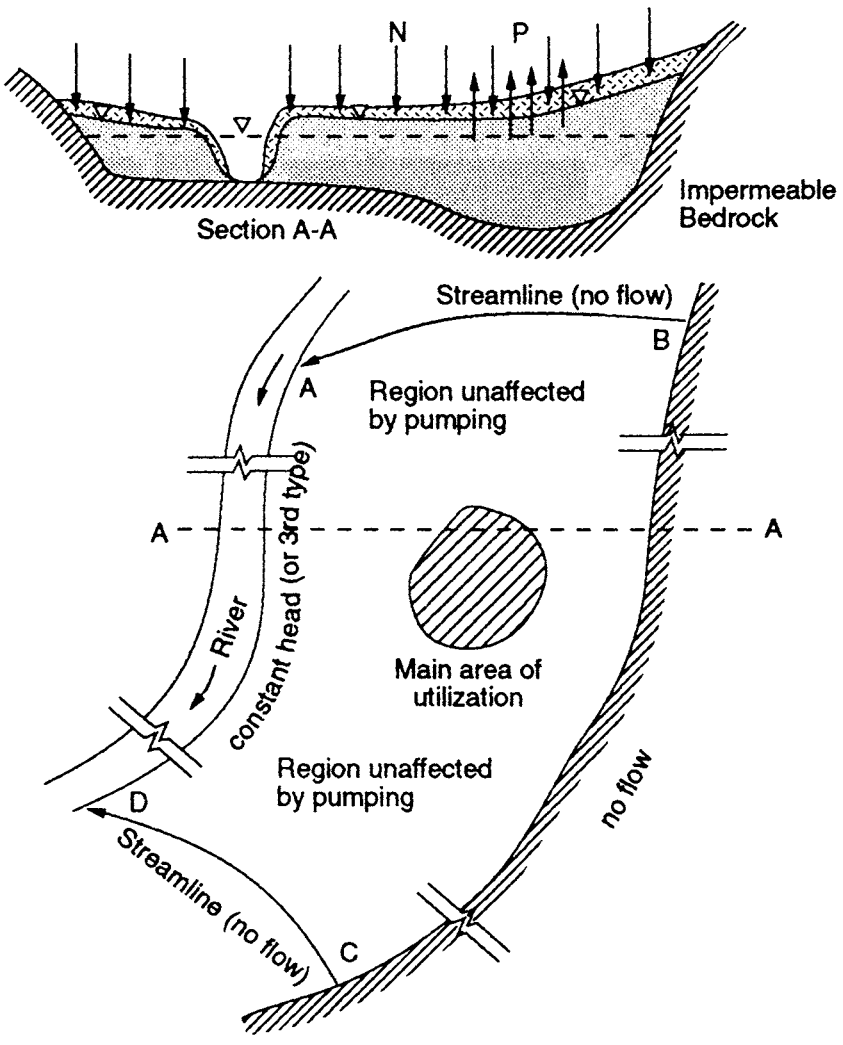

Figure 2: Boundary condition for areal flow model (modified from Bear, 1979)

These three assumptions form the basis for representing flow as 2D in the areal plane of the aquifer, and as one dimensional (1D) vertical in the aquitards with vertical flow being proportional to the head difference between the neighbouring aquifers. The validity of these assumptions must be considered when interpreting the results of 2D plan-view models. The first two assumptions are reasonable whenever the permeability contrast between the aquifers and aquitards is at least 2 orders of magnitude. The third assumption neglects the transient response in the aquitard which will normally occur when a head change is imposed in one of the aquifers. The time taken to equilibrate the system is given by (Frind, 1979):

$$t_e = \frac{S_s' \, (b')^2}{K'}$$

where S_s' is the aquitard specific storage. On the basis of this relationship, the third assumption above is reasonable if t_e is small in relation to the time period of interest.

2.4 Potential/Streamfunction Equations

Potential/streamfunction models applied in the cross-section are useful in situations where chemical or biochemical reactions play a role. Such reactions are often depth-dependent since the necessary reactants (e.g. oxygen, organic carbon, sulfides) occur at concentrations that vary with depth. Also, the reactions may be nonlinear due to the limited availability of the reactants. For these reasons, the individual transport processes cannot be averaged in the vertical over the aquifer thickness; instead, the vertical dimension must be represented explicitly in the model.

A contaminant entering the ground will first pass through the unsaturated soil zone and then enter the saturated groundwater zone. Although both of these zones can be modelled together

(Akindunni *et al.*, 1991; Akindunni and Gillham, 1992), the modelling scale is generally different. In order to stimulate unsaturated flow in a physically valid way, the soil moisture profiles must be adequately resolved in the model; this generally results in spatial discretizations of the order of centimeters. This means that, in order to keep the model manageable, its size will be restricted to a few meters (Akindunni, 1987).

In the saturated groundwater zone, on the other hand, the spatial scale of interest in contamination problems is often of the order of hundreds or thousands of meters, since both the source and the destination must be included in the model. The time scale may be of the order of several years. Therefore in problems where migration processes in the saturated zone are relevant, the unsaturated zone is often excluded. Although the flow direction in the saturated zone is predominantly horizontal, vertical velocity components are important because they can play a controlling role in chemical or biochemical reactions. We will focus here on saturated groundwater systems exclusively.

A cross-sectional flow and transport model can therefore be bounded at the top by the watertable. If the longer time scale is of interest, seasonal fluctuations are generally neglected and a long-term average flow system is assumed. The model domain can be visualized as a slice of unit thickness cut from the aquifer in the direction of groundwater flow (Fig. 3). The cut should follow the watertable gradient.

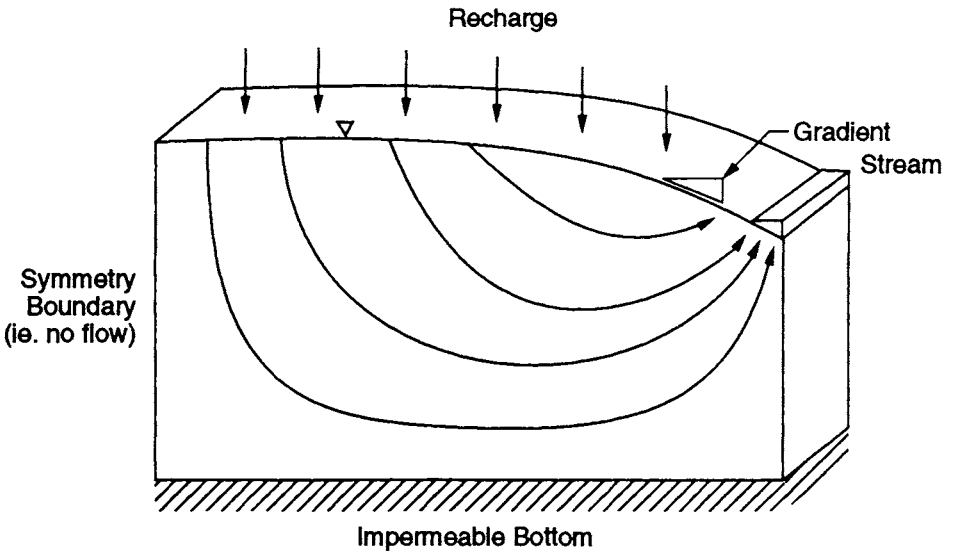

Figure 3: Typical cross-sectional flow diagram

A numerical problem can arise in cross-sectional transport modelling on account of the spatial scale. This arises because the length of the cross-sectional domain can be greater by several orders of magnitude than the width (i.e. the aquifer thickness), that is, the model domain can be very long and thin. The contrast between the horizontal and vertical scales can cause serious inaccuracies in the calculation of the groundwater velocities by means of Darcy's equation. This can in turn cause problems in the accurate definition of the flow paths that are needed in order to position the plume at the correct depth in the aquifer, and to facilitate the correct simulation of spatially dependent reactions.

This problem can be overcome by formulating the flow problem both in terms of the hydraulic potential ϕ and the streamfunction ψ. The steady-state form of the potential equation is used in this approach. The two governing equations are, in general form (Frind and Matanga,

1985):

$$\frac{\partial}{\partial x_i}\left(K_{ij}\frac{\partial \phi}{\partial x_j}\right) = 0$$

$$\frac{\partial}{\partial x_i}\left(\frac{1}{|K|}K_{ij}\frac{\partial \psi}{\partial x_j}\right) = 0$$

or, for the case where the coordinate axes coincide with the principal directions:

$$\frac{\partial}{\partial x}\left(K_{xx}\frac{\partial \phi}{\partial x}\right) + \frac{\partial}{\partial y}\left(K_{yy}\frac{\partial \phi}{\partial y}\right) = 0$$

$$\frac{\partial}{\partial x}\left(\frac{1}{K_{yy}}\frac{\partial \psi}{\partial X}\right) + \frac{\partial}{\partial y}\left(\frac{1}{K_{xx}}\frac{\partial \psi}{\partial y}\right) = 0$$

where the streamfunction ψ has dimensions of discharge (L^2/T). In the above two equations, the primes to designate principal directions have been omitted.

The Darcy equation is related to the streamfunction through the relationship:

$$\begin{Bmatrix} qx \\ qy \end{Bmatrix} = -\begin{bmatrix} K_{xx} & K_{xy} \\ K_{yx} & K_{yy} \end{bmatrix}\begin{Bmatrix} \frac{\partial \phi}{\partial x} \\ \frac{\partial \phi}{\partial y} \end{Bmatrix} = \begin{Bmatrix} \frac{\partial \psi}{\partial y} \\ \frac{\partial \psi}{\partial x} \end{Bmatrix}$$

In an isotropic medium, the potential contours ϕ and the streamfunction contours (the streamlines) ψ intersect at right angles.

A useful property of the streamfunction is that the discharge in a streamtube, ΔQ, equals the streamfunction increment $\Delta\psi$ (Fig. 4). The specific discharge (Darcy velocity) is therefore:

$$q = \frac{\Delta Q}{\Delta p} = \frac{\Delta \psi}{\Delta p}$$

which is the streamfunction increment divided by the streamtube width Δp. Therefore, the streamfunction allows the determination of groundwater velocities independent of the Darcy equation. For long thin systems, streamfunction-derived velocities are usually more accurate than potential-derived velocities (Frind *et al.*, 1985).

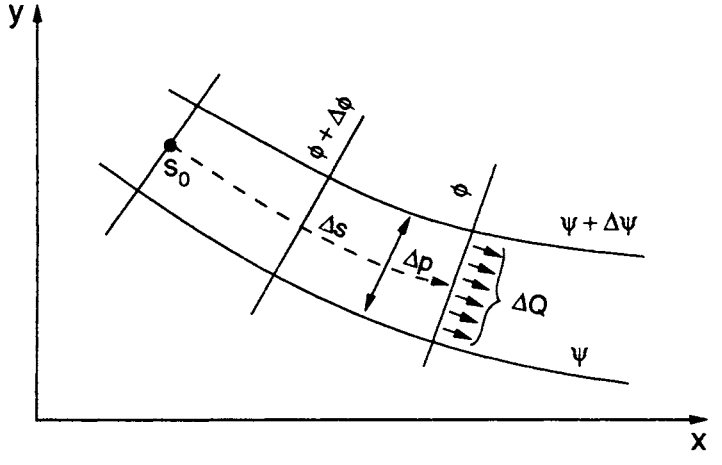

Figure 4: Streamtube in isotropic system

The streamfunction further relates the advective travel distance Δs to the travel time Δt through:

$$\Delta t = \frac{\theta}{\Delta \psi} \int_{s_o}^{s_o+\Delta s} \Delta p \; ds$$

which is simply the area of the streamtube between the points s_o and $s_o + \Delta s$, multiplied by a constant (see Fig. 4).

To solve the governing equations, boundary conditions with respect to both ϕ and ψ must be provided (Fig. 5). For the case where the location of the watertable is known, the watertable boundary condition for ϕ is:

$$\phi = h_w$$

where h_w is the watertable head. The boundary condition for ψ is expressed in terms of the component of the streamfunction gradient g_n^{ψ} in the direction normal to the boundary, which is (Frind and Matanga, 1985):

$$g_n^{\psi} = -\Delta h_w$$

Thus the normal component of the streamfunction gradient is equal to the negative rate of change of head along the watertable.

For the case where the recharge is defined at the watertable but the watertable location is unknown, the boundary condition for ψ is given in terms of the Darcy flux as:

$$q_n = q_w$$

where q_w is the specified recharge flux in the direction normal to the boundary. The boundary

condition for ψ is specified in terms of the streamfunction value along the watertable, which is obtained by summing the recharge entering the system along that boundary:

$$\psi = \psi_o = \int_b q_n \, db$$

where ψ_o is a reference value, and b designates the boundary.

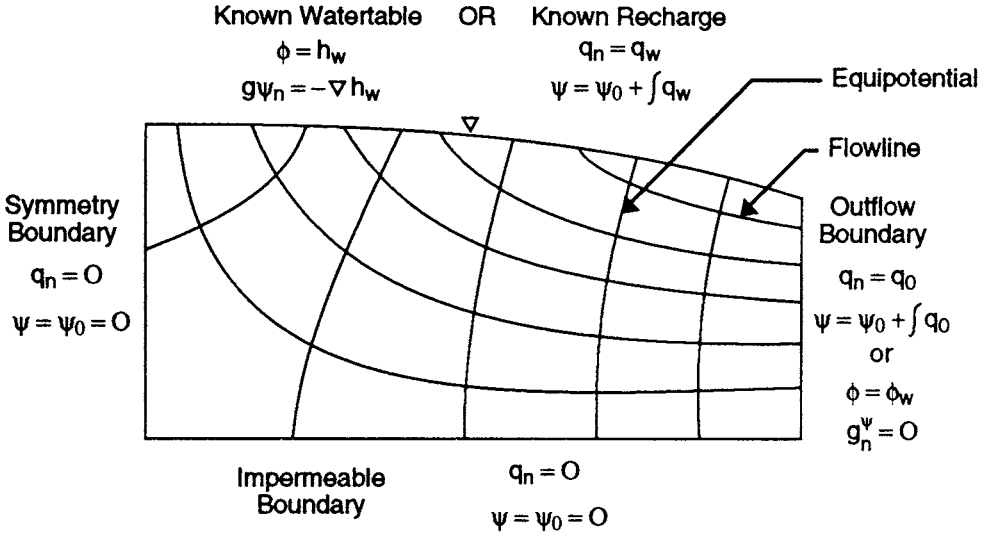

Figure 5: Boundary conditions for cross-sectional flow model

Along the bottom of the domain, we usually assume an impermeable boundary. The boundary conditions are:

$$q_n = 0$$

$$\psi = \psi_0 = 0$$

which expresses that the flux across an impermeable boundary is zero, and that the boundary is a streamline, the value of which is usually set to zero. Similar boundary conditions can be defined for the lateral boundaries.

Due to the basic assumption of flow in the plane of the cross-section, source/sink conditions such as pumping or injection wells are excluded, except when placed perpendicular to the plane of the section.

2.5 Transport Equation

The equation governing the advective-dispersive transport of a solute, subject to linear sorption and first-order decay, is (Bear, 1979; Luckner and Schestakow, 1986):

$$\frac{\partial}{\partial x_i}\left(D_{ij}\,\frac{\partial c}{\partial x_j}\right) - v_i\,\frac{\partial c}{\partial x_i} - R\lambda c = R\frac{\partial c}{\partial t}$$

where c is the concentration (usually expressed as relative with respect to the source concentration c_0, or c/c_0), D_{ij} is the dispersion tensor, $v_i = q_i/\theta$ is the average groundwater velocity, and $\lambda = \ln 2/t_{1/2}$ is the decay constant, with $t_{1/2}$ being the half-life. The retardation coefficient R is defined in standard form as (Freeze and Cherry, 1979):

$$R = 1 + \frac{\rho_b}{\theta}\,K_d$$

where ρ_b is the bulk density of the medium, and K_d is the linear distribution coefficient. The

governing equation is based on the assumption that both the adsorbed and the dissolved phases decay. Further assumptions are that the fluid is incompressible, that there are no internal sources or sinks, and that the medium does not deform.

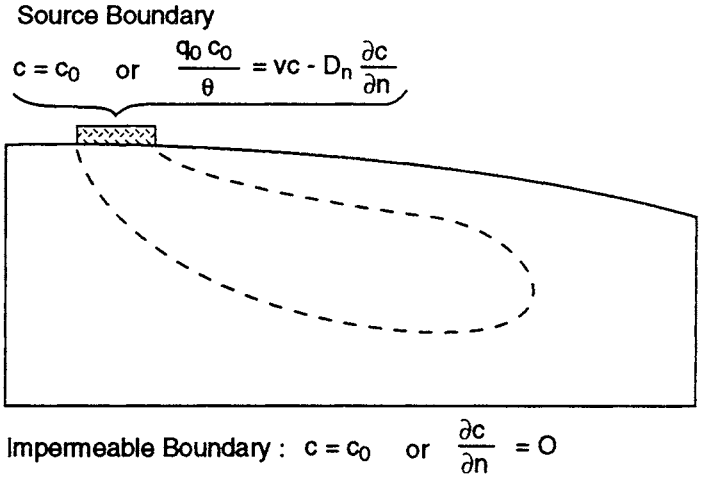

Figure 6: Boundary conditions for 2D cross-sectional transport model

The transport equation requires boundary conditions all around the domain (Fig. 6) for solution. One possible form of boundary condition is in the form of a specified concentration, which can be used in cases such as that of a waste lagoon in contact with the watertable. This gives the *first-type* or *Dirichlet* boundary condition. Alternatively, the boundary condition can be specified in the form of a known mass flux, which applies in cases such as a leaking landfill situated above the watertable where leachate is produced by rainwater percolating through the waste and the unsaturated zone to the watertable. This is known as a *third-type*

or *Cauchy* boundary condition, which takes the form:

$$\frac{q_0 c_0}{\theta} = vc - D_n \frac{\partial c}{\partial n}$$

where q_0 is the known boundary recharge, c_0 is the concentration of the solute carried by the recharge water, and D_n is the dispersion coefficient in the direction normal to the boundary.

At parts of the watertable outside of the source, the above boundary condition holds with c_0=0. The remaining boundaries of the model (2D or 3D) are usually selected such that the contaminant does not reach the boundary. A boundary condition of either c = 0 or $\partial c/\partial n = 0$ (*second type* or *Neumann* boundary condition) can then be used. When a contaminant plume reaches a boundary, the correct boundary condition is the free exit boundary (Frind, 1988), which is built into the numerical solution and does not require any specified boundary values.

2.6 The Classical Concept of Dispersion

The classical definition of the 3D dispersion tensor for a medium that is isotropic with respect to dispersion is (Bear, 1979):

$$D_{ij} = \alpha_T |v| \delta_{ij} + (\alpha_L - \alpha_T) \frac{v_i v_j}{|v|} + D^* \delta_{ij}$$

where α_L and α_T are the longitudinal and transverse dispersivities, respectively, $D^* = D_d \tau$ is the effective diffusion coefficient in the porous medium, with D_d being the molecular diffusion coefficient in solution and τ the tortuosity of the medium, and δ is the Kronecker delta. For 1D transport, this simplifies to:

$$D = \alpha_L v + D^*$$

In two dimensions, the components of the symmetrical dispersion tensor take on the form:

$$D_{xx} = \alpha_L \frac{v_x^2}{|v|} + \alpha_T \frac{v_y^2}{|v|} + D^*$$

$$D_{yy} = \alpha_T \frac{v_x^2}{|v|} + \alpha_L \frac{v_y^2}{|v|} + D^*$$

$$D_{xy} = (\alpha_L - \alpha_T) \frac{v_x v_y}{|v|}$$

In a coordinate system following the principal directions of the dispersion tensor, which are parallel and perpendicular to the flow lines, the above components become:

$$D_{xx} = \alpha_L v + D^*$$

$$D_{yy} = \alpha_T v + D^*$$

$$D_{xy} = D_{xz} = D_{yz} = 0$$

The above classical definition is based on the assumption that the medium is isotropic with respect to dispersion, which means that unique values of longitudinal and transverse dispersivity can be defined for a given medium. As a consequence of that assumption, a contaminant plume would always exhibit unique spreading characteristics in the longitudinal direction as well as in the traverse direction, regardless of the direction of flow in the aquifer. We will discuss this premise further in the next section.

Figure 7 shows a typical advective-dispersive plume in 2D, based on the above theory. An analytical solution developed by Cleary and Ungs (Wexler, 1989) was used to generate the plume. The analytical solution is valid for the case of a 2D semi-infinite medium, a

continuous symmetrical line source at the origin, and a first-type source boundary condition. The plume is shown both in the form of concentration contours (a), and in the form of the concentration profile at the centerline of the plume (b). The base case parameters are v=0.1m/day, α_L=1.0 m, α_T=0.1 m, R = 1.0, no decay.

In Figure 8, the parameters are varied one at a time, except for the velocity, and the resulting effect is compared with the base case. We see that increasing α_L (a) produces a typical stretching of the profile, while increasing α_T by the same proportion (b) gives a much different response due to the increased transverse spreading which depresses the profile. Doubling R reduces both the advective advance and the dispersion by one half. Introducing a decay term with $t_{1/2}$=1 year generates a profile that appears to be dominated by the exponential decay component.

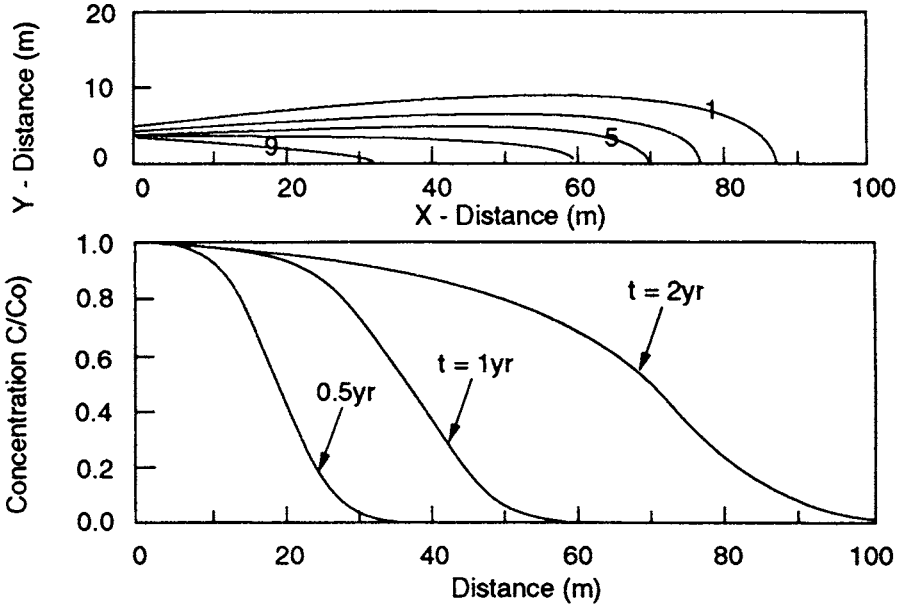

Figure 7: Advective-dispersive plume, contours and profiles

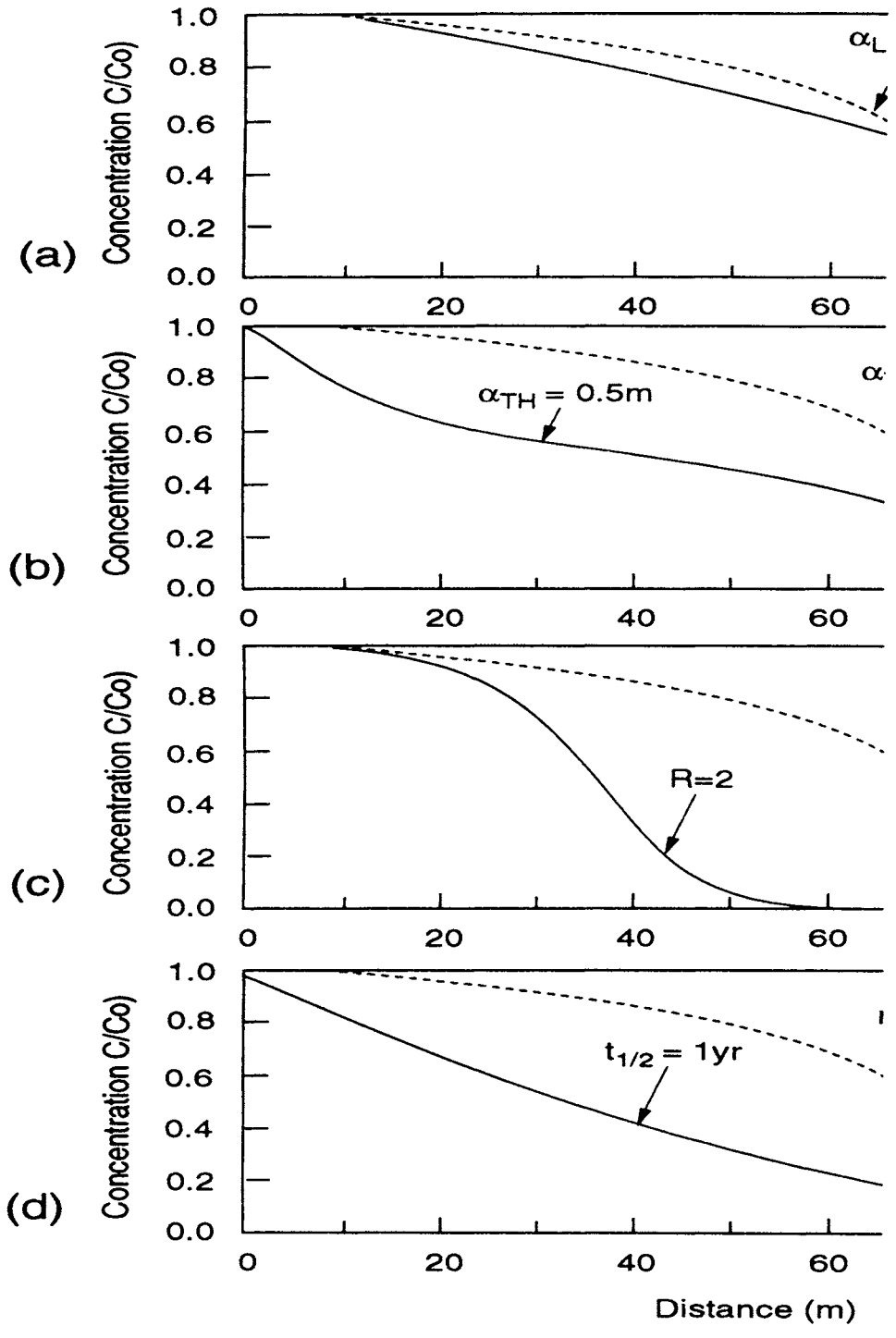

Figure 8: Advective-dispersive plume profiles at 2 years showing longitudinal, transverse dispersivity and retardation factor.

2.7 Scale-Dependent and Asymptotic Dispersion

The assumptions underlying the classical definition of dispersion are now known to be valid only at the microscale, i.e., the scale of the pores and grains in the medium. For natural heterogeneous media, it is known that transverse dispersion differs in the horizontal and vertical directions, and that the dispersivity itself may increase with scale. The scale dependence of dispersivity is a result of the heterogeneity of natural aquifer materials. As a contaminant enters the aquifer at the source, the initial dispersing mechanism is governed by the local pore-grain structure. As the contaminant migrates through the system, it progressively encounters more heterogeneities which cause the dispersing mechanism to increase. The dispersivity increases until a plateau value, the asymptotic dispersivity, is reached. Gelhar and Axness (1983) derived, on the basis of statistical analysis, expressions for the components of the asymptotic dispersivity tensor. They found that if flow is in a general direction (i.e., not parallel to the stratification), the dispersivity components are all controlled by the heterogeneity of the medium and will therefore all attain asymptotic values. For the special case where flow is parallel to the stratification, only the longitudinal dispersivity becomes asymptotic while the transverse dispersivities remain controlled by local processes.

Sudicky *et al.* (1983) showed by means of detailed field measurements that the transverse dispersivity in a natural aquifer differs in the horizontal and vertical directions. This can be explained by the differences in the sedimentary structure with respect to these directions. For the case of flow parallel to the stratification, the principal components of the asymptotic dispersion tensor can be represented as:

$$D_{xx} = (A_{11} + \alpha_L)v + D*$$

$$D_{yy} = \alpha_{TH}v + D*$$

$$D_{zz} = \alpha_{TV}v + D*$$

where α_L is the local longitudinal dispersivity, and α_{TH} and α_{TV} are the transverse horizontal and transverse vertical dispersivities, respectively. The asymptotic longitudinal dispersivity A_{11} is defined as (Gelhar and Axness, 1983):

$$A_{11} = \sigma_y^2 \frac{\lambda}{\gamma^2}$$

where σ_y^2 is the variance of the logarithm of the hydraulic conductivity, λ is the correlation length of the heterogeneities of the medium, and γ is a flow factor which was later found to be equal to 1.

Sudicky (1986) examined the spatial variability of hydraulic conductivity of a sandy aquifer in Ontario by means of highly detailed permeameter tests. He found the sand to consist of numerous thin and discontinuous lenses. He also found the hydraulic conductivity of the sand to vary over more than one order of magnitude. The resulting log conductivity variance was reported to be 0.38 and the correlation lengths of the lenses 2.8 m and 0.12 m in the horizontal and vertical directions, respectively. This study provided the first data suitable for the calculation of asymptotic dispersivities.

The asymptotic dispersivity relationships $A_{11}=\sigma_y^2\lambda$ was validated in 2D by Frind *et al.* (1987).

The physical basis of the asymptotic growth arises from the process of advective-diffusive exchange that takes place in a heterogeneous medium consisting of lenses having higher and lower values of hydraulic conductivity. In such a medium, a solute will advance advectively faster in a high-conductive zone and the resulting concentration gradient between high- and low-conductive zones will give rise to transverse diffusive transport. Mass is thus removed from the front of the plume and stored temporarily in the low-conductive layers. When the plume has passed the low-conductive zone, the concentration gradient reverses and the mass moves back into the high-conductive zone to be added to the tail end of the plume. In an aquifer containing many of these zones of differing conductivity, the aggregate of these mass exchanges, seen over the system as a whole, results in an apparent growth of the overall dispersivity. Eventually, the process stabilizes at the level of the asymptotic dispersivity. The study also confirmed that the transverse vertical dispersivity remains at its local value.

The dispersivity reaches its asymptotic value at a travel distance of about 40-50 correlation lengths from the source (Frind *et al.*, 1987). For pre-asymptotic conditions, unfortunately, rigorously valid scale-dependent dispersivity relationships that are easy to implement in numerical models have not yet been developed. Although the microscale approach is valid, its cost renders it impractical in normal situations. A dilemma therefore arises in the modelling of advective-dispersive transport in the pre-asymptotic range. One possible option may be to select an empirical dispersivity function that takes on a local value at the source and grows to the required asymptotic value. Fortunately, field problems may not be overly sensitive to the precise value of the dispersivity as long as it is in the correct range (Frind and Molson, 1989).

3. SOLUTION OF SIMULTANEOUS EQUATIONS

Numerical solutions of problems in groundwater studies create systems of simultaneous equations which could be very large. The number of unknown parameters in these equations are often between 100 and 1000, sometimes up to one million. The equations are also generally banded. Efficient techniques are required to solve these equations. The equations

are usually represented using matrix notations.

Consider the following set of linear equations:

$$\begin{aligned} 2x_1 - 5x_2 + x_3 &= 6 \\ -x_1 + 7x_2 - 2x_3 &= -2 \\ 4x_2 + 9x_3 &= 1 \end{aligned}$$

In matrix notation, this set of equations is written as:

$$\begin{bmatrix} 2 & -5 & 1 \\ -1 & 7 & -2 \\ 0 & 4 & 9 \end{bmatrix} \begin{Bmatrix} x_1 \\ x_2 \\ x_3 \end{Bmatrix} = \begin{Bmatrix} 6 \\ -2 \\ 1 \end{Bmatrix}$$

or in the general form:

$$\begin{bmatrix} a_{11} & a_{12} & \cdots & a_{1n} \\ a_{21} & a_{22} & \cdots & a_{2n} \\ a_{31} & a_{32} & \cdots & \\ a_{n1} & a_{n2} & \cdots & a_{nn} \end{bmatrix} \begin{Bmatrix} x_1 \\ x_2 \\ \cdot \\ \cdot \\ x_n \end{Bmatrix} = \begin{Bmatrix} b_1 \\ b_2 \\ \cdot \\ \cdot \\ b_n \end{Bmatrix}$$

The *coefficients* are contained in [A], the vector of *knowns* is {b} while {x} is the vector of *unknowns*. The matrix equation can be written in a more simplified notation as [A] {x} = {b}, where [A] may have *n* rows and *m* columns. When *n* is equal to *m*, the matrix is described as a SQUARE matrix. Other special forms of matrices include the following:

- SYMMETRIC MATRIX - The elements in the matrix are symmetric with respect to the diagonal, (i.e., $a_{ij} = a_{ji}$)

- SKEW SYMMETRIC MATRIX - A square matrix with a negative symmetrY with respect to the diagonal (i.e. $a_{ij} = a_{ji}$ for $i \neq j$)

- DIAGONAL MATRIX - A square matrix in which all elements are zero except at the diagonal (i.e., $a_{ij} = 0$ for $i \neq j$)

- IDENTITY (or UNIT) MATRIX - A diagonal matrix with diagonal elements equal to unity (i.e., $a_{ij} = 0$ for $i \neq j$; $a_{ij} = 1$ for i=j). It is denoted as [I].

- TRIANGULAR MATRIX - A square matrix with all - zero elements either above or below the diagonal elements.

- NULL MATRIX - A matrix in which all elements are zero (i.e., $a_{ij} = 0$).

3.1 Matrix Operations

3.1.1 Addition and Subtraction

Two matrices, [A] and [B] can be added (or subtracted) to obtain [C] only if their dimensions are the same. The procedure requires that corresponding elements of [A] and [B] are added (or subtracted) to obtain [C] such that $c_{ij} = a_{ij} \pm b_{ij}$ for all values of i and j.

3.1.2 Multiplication

A matrix [A] can be multiplied by [B] only if the column size of [A] is identical to the row size of [B]. The product formed, [C] = [A] [B] will have the column size of [A] and the row size of [B]. The elements in the product are obtained as:

$$c_{ij} = \sum_{k=1}^{m} a_{ik}\, b_{kj} \; (i=1, \ldots, n;\; j=1, \ldots, r)$$

Note that matrix multiplication is not commutative (i.e. [A] [B] ≠ [B] [A]). In many cases, [A] [B] may be defined while [B] [A] is undefined.

3.1.3 Transpose of a Matrix

The transpose of a matrix, denoted as $[A]^T$ can be obtained from [A] by interchanging the column and row elements such that:

$$a^T_{ij} = a_{ji}$$

The transpose of a product is obtained by:

$([A]\,[B])^T = [B]^T\,[A]^T$

3.2 Definitions

3.2.1 Determinant of a Matrix

The determinant of a matrix [A] (denoted as det A or $|A|$), and defined only for a square matrix) is obtained as:

$$|A| = \sum_{i=1}^{n} a_{ij} \cdot [cof(a_{ij})] = \sum_{j=1}^{n} a_{ij} \cdot [cof(a_{ij})]$$

where the cofactor (cof) is defined by:
and the minor is the determinant of the submatrix obtained by deleting the *i*th row and the *j*th

$$cof\ (a_{ij}) = (-1)^{i+j} \cdot [minor\ (a_{ij})]$$

column of the original matrix. Using the definition above, the determinant of a 2 x 2 matrix can be obtained as:

$$|A| = \begin{vmatrix} a_{11} & a_{12} \\ a_{21} & a_{22} \end{vmatrix} = a_{11}\ a_{22} - a_{21}\ a_{12}$$

Similarly, the determinant of a 3 x 3 matrix can be obtained as:

$$|A| = \begin{vmatrix} a_{11} & a_{12} & a_{13} \\ a_{21} & a_{22} & a_{23} \\ a_{31} & a_{32} & a_{33} \end{vmatrix} = a_{11}(+1) \begin{vmatrix} a_{22} & a_{23} \\ a_{32} & a_{33} \end{vmatrix} + a_{12}(-1) \begin{vmatrix} a_{21} & a_{23} \\ a_{31} & a_{33} \end{vmatrix} + a_{13}(+1) \begin{vmatrix} a_{21} & a_{22} \\ a_{31} & a_{32} \end{vmatrix}$$

3.2.2 Inverse of a Matrix

The inverse of a matrix (denoted as $[A]^{-1}$) is defined by:

$$[A]^{-1} = \frac{1}{|A|}\ adj\ [A] \qquad\qquad |A| \neq 0$$

where the adjoint (adj [A]) is obtained as:

$$\text{adj } [A] = [\text{cof } A]^T$$

For example,

$$adj \begin{bmatrix} a_{11} & a_{12} & a_{13} \\ a_{21} & a_{22} & a_{23} \\ a_{31} & a_{32} & a_{33} \end{bmatrix} = \begin{bmatrix} cofa_{11} & cof\ a_{21} & cof\ a_{31} \\ cof\ a_{12} & cof\ a_{22} & cof\ a_{32} \\ cof\ a_{13} & cof\ a_{23} & cof\ a_{33} \end{bmatrix}$$

The inverse satisfies the equalities:

$$[A]^{-1}[A] = [A][A]^{-1} = [I] \qquad \text{(Identity matrix)}$$

3.3 Matrix Solution by Inversion

Given a set of simultaneous equations:

$$[A]\{X\} = \{B\}$$

The vector of unknown parameters can be obtained by pre-multiplying each side of the matrix equation by the inverse of [A], thus:

$$[A]^{-1}[A]\{X\} = [A]^{-1}\{B\}$$

i.e. $[I]\{X\} = [A]^{-1}\{B\}$

or $\{X\} = [A]^{-1}\{B\}$

Exercise:

Solve by Inversion

$$\begin{bmatrix} 2 & 0 & 1 \\ 4 & 6 & -5 \\ 0 & 1 & 5 \end{bmatrix} \begin{Bmatrix} x \\ y \\ z \end{Bmatrix} = \begin{Bmatrix} 7 \\ 1 \\ 4 \end{Bmatrix}$$

3.4 Cramer's Rule

This is a convenient method for hand calculations of small (2x2 or 3x3) system of equations:

$$[A]\ \{ x \} = \{ B \}$$

The k^{th} term in the unknown vector {x} is:

$$x_k = \frac{\det A_k}{\det A} = \frac{| A_k |}{| A |} \qquad | A | \neq 0$$

$|A_k|$ is obtained by replacing the k^{th} column in |A| with the vector {B}:

$$| A_k | = \begin{vmatrix} a_{11} & a_{12} & a_{13} \cdots & a_{1,k-1} & b_1 & a_{1,k+1} & \cdots & a_{1n} \\ a_{21} & & & a_{2,k-1} & b_2 & a_{2,k+1} & \cdots & a_{2n} \\ | & & & & | & & & | \\ | & & & & | & & & | \\ a_{n1} & & & & b_n & & & a_{nn} \end{vmatrix}$$

The number of operations (multiplication and division) is On^4 (of the order of n^4) where n is the band width.

Exercise

Solve by Cramer's rule:

$$\begin{bmatrix} 2 & 1 & 2 \\ 3 & 1 & -1 \\ 1 & 4 & 1 \end{bmatrix} \begin{Bmatrix} x \\ y \\ z \end{Bmatrix} = \begin{Bmatrix} 10 \\ 2 \\ 12 \end{Bmatrix}$$

3.5 Gaussian Elimination

This is the most widely used method of solving simultaneous equations.

3.5.1 Elementary Row Operations

Consider the system:

$$\begin{matrix} 1) \\ 2) \\ 3) \\ 4) \end{matrix} \begin{bmatrix} a_{11} & a_{12} & a_{13} & a_{14} \\ a_{21} & a_{22} & a_{23} & a_{24} \\ a_{31} & a_{32} & a_{33} & a_{34} \\ a_{41} & a_{42} & a_{43} & a_{44} \end{bmatrix} \begin{Bmatrix} x_1 \\ x_2 \\ x_3 \\ x_4 \end{Bmatrix} = \begin{Bmatrix} b_1 \\ b_2 \\ b_3 \\ b_4 \end{Bmatrix}$$

From (2), subtract (1) x a_{21}/a_{11} to obtain (2′).

For example:

$$a_{21} - \frac{a_{21}}{a_{11}} a_{11} = 0$$

$$a_{22} - \frac{a_{21}}{a_{11}} a_{12} = a_{22}'$$

$$\vdots \qquad\qquad \vdots$$

$$b_2 - \frac{a_{21}}{a_{11}} b_1 = b_2'$$

In a similar manner, subtract (1) x a_{31}/a_{11} from (3) and (1) x a_{41}/a_{11} from (4).
(a_{11} is the pivot). This results in:

Next, subtract (2′) x a_{32}'/a_{22}' from (3′) and (2′) x a_{42}'/a_{22}' from (4′) to obtain:
Note that the new pivot is a_{22}'. Then subtract (3″) x a_{43}''/a_{33}'' from (4″) to obtain:

$$
\begin{matrix} 1\,) \\ 2')\\ 3')\\ 4') \end{matrix}
\begin{bmatrix} a_{11} & a_{12} & a_{13} & a_{14} \\ 0 & a_{22}' & a_{23}' & a_{24}' \\ 0 & a_{32}' & a_{33}' & a_{34}' \\ 0 & a_{42}' & a_{43}' & a_{44}' \end{bmatrix}
\begin{Bmatrix} x_1 \\ x_2 \\ x_3 \\ x_4 \end{Bmatrix}
\begin{Bmatrix} b_1 \\ b_2' \\ b_3' \\ b_4' \end{Bmatrix}
$$

$$
\begin{matrix} 1 \\ 2' \\ 3'' \\ 4'' \end{matrix}
\begin{bmatrix} a_{11} & a_{12} & a_{13} & a_{14} \\ 0 & a_{22'} & a_{23'} & a_{24'} \\ 0 & 0 & a_{33''} & a_{34''} \\ 0 & 0 & a_{43''} & a_{44''} \end{bmatrix}
\begin{Bmatrix} x_1 \\ x_2 \\ x_3 \\ x_4 \end{Bmatrix}
=
\begin{Bmatrix} b_1 \\ b_2' \\ b_3'' \\ b_4'' \end{Bmatrix}
$$

$$
\begin{bmatrix} a_{11} & a_{12} & a_{13} & a_{14} \\ 0 & a_{22}' & a_{23}' & a_{24}' \\ 0 & 0 & a_{33}'' & a_{34}'' \\ 0 & 0 & 0 & a_{44}''' \end{bmatrix}
\begin{Bmatrix} x_1 \\ x_2 \\ x_3 \\ x_4 \end{Bmatrix}
=
\begin{Bmatrix} b_1 \\ b_2' \\ b_3'' \\ b_4''' \end{Bmatrix}
$$

We can now solve for x, starting at the bottom, thus:

$$x_k = \frac{b_4'''}{a_{44}'''}$$

$$x_3 = \frac{1}{a_{33}''} (b_3'' - a_{34}'' x_4)$$

$$x_2 = \frac{1}{a_{22}'} (b_2' - a_{23}' x_3 - a_{24}' x_4)$$

$$x_1 = \frac{1}{a_{11}} (b_1 - a_{12} x_2 - a_{13} x_3 - a_{14} x_4)$$

3.5.2 Gauss-Jordan Elimination

The elimination is also done on the upper part of the matrix above the diagonal. Each row is divided by the appropriate pivot, resulting in:

$$\begin{bmatrix} 1 & & & 0 \\ & 1 & & \\ & & 1 & \\ 0 & & & 1 \end{bmatrix} \begin{Bmatrix} x_1 \\ x_2 \\ x_3 \\ x_4 \end{Bmatrix} = \begin{Bmatrix} b_1' \\ b_2'' \\ b_3''' \\ b_4'''' \end{Bmatrix}$$

The reader is referred to section 6.4 in Hornbeck (1975) for details. Because we always divide by the pivot, it is numerically important that the pivot is non-zero.

3.5.3 Matrix Inversion by Gauss-Jordan Elimination

For a square matrix [A], an inverse $[A]^{-1}$) is defined such that the product gives a unit matrix, thus:

$$[A]\ [A]^{-1} = [I]$$

i.e. [A] is transformed to [I]:

$$[A]\ [A^{-1}] = \begin{bmatrix} 1 & & & \\ & 1 & & \\ & & 1 & \\ & & & 1 \end{bmatrix}$$

The same transformation is performed on the right-hand side to obtain $[A]^{-1}$:

$$[I]\ [A]^{-1} = [A]^{-1}$$

3.5.4 Generalized Gauss Elimination Procedure (L - U Decomposition)

This procedure is useful in problems with repeated right-hand sides such as in time marching schemes or multiple loading conditions. Consider:

$$[A]\ \{ x \} = \{ B \}$$

If this corresponds to a real physical system ([A] is positive-definite), then [A] can be decomposed or factored into unique upper and lower triangular matrices:

$$[A] = [L]\ [U]$$

so:

$$[L]\ [U]\ \{ X \} = \{ B \}$$

let:

$$[U]\ \{ X \} = \{ Y \}$$

then:

$$[L]\ \{ Y \} = \{ B \}$$

Solve for y:

$$\begin{bmatrix} l_{11} & & 0 \\ l_{21} & l_{22} & \\ l_{31} & l_{32} & l_{33} \\ | & & \\ | & & \\ l_{n1} & & \end{bmatrix} \begin{Bmatrix} y_1 \\ y_2 \\ y_3 \\ | \\ | \\ y_n \end{Bmatrix} = \begin{Bmatrix} b_1 \\ b_2 \\ b_3 \\ | \\ | \\ b_n \end{Bmatrix}$$

$$y_1 = \frac{b_1}{l_{11}}$$

$$y_2 = \frac{b_2 - l_{21}\, y_1}{l_{22}}$$

etc.

Solve for x from:

$$[U] \{ x \} = \{ Y \}$$

$$\begin{bmatrix} u_{11} & u_{12} & & u_{1n} \\ & & & u_{2n} \\ & & & | \\ & & & | \\ 0 & & u_{n-1\,,\,n-1} & u_{n-1\,,\,n} \\ & & & u_{nn} \end{bmatrix} \begin{Bmatrix} x_1 \\ x_2 \\ | \\ | \\ x_{n-1} \\ x_n \end{Bmatrix} = \begin{Bmatrix} y_1 \\ y_2 \\ | \\ | \\ y_{n-1} \\ y_n \end{Bmatrix}$$

$$X_{n-1} = \frac{y_{n-1} - u_{n-1,n}\, x_n}{u_{n-1,n-1}}$$

The sequence of elementary row operations can be expressed as (for 4 x 4)

$$[L_3][L_2][L_1][A]\{ x \} = [L_3][L_2][L_1]\{ B \}$$

$$x_n = \frac{y_n}{u_{nn}}$$

where:

$$[L_1] = \begin{bmatrix} 1 & & & \\ \frac{a_{21}}{a_{11}} & 1 & & \\ \frac{-a_{31}}{a_{11}} & 0 & 1 & \\ \frac{-a_{41}}{a_{11}} & 0 & 0 & 1 \end{bmatrix}$$

let:

$$[L_3][L_2][L_1] = [L^*]$$

$$[L_2] = \begin{bmatrix} 1 & & & \\ 0 & 1 & & \\ 0 & \frac{-a_{32}'}{a_{22}'} & 1 & \\ 0 & \frac{a_{42}'}{a_{22}'} & 0 & 1 \end{bmatrix}$$

$$[L_3] = \begin{bmatrix} 1 & & & \\ 0 & | & & \\ 0 & 0 & | & \\ 0 & 0 & \frac{a_{43}''}{a_{33}''} & 1 \end{bmatrix}$$

then:

$$[L^*][A]\{ x \} = [L^*]\{ B \}$$

but the result of the elementary row operations is an upper triangular matrix. Since the decomposition must be unique, this means that:

$$[L^*][A] \equiv [U]$$

likewise:

$$[L^*]\{ B \} \equiv \{ Y \}$$

since:

$$[U]\{ x \} = \{ Y \}$$

Premultiply above equation by $[L^*]^{-1}$:

$$[L^*]^{-1}[L^*][A] = [L^*]^{-1}[U]$$

therefore:

$$[A] = [L^*]^{-1}[U]$$

$$= [L]\ [U]$$

$$[L^*]^{-1}[L^*]\{B\} = [L^*]^{-1}\ \{Y\}$$

$$\{\ B\ \} = [L]\ \{\ Y\ \}$$

Thus, after obtaining [L] and [U], the right hand side {B} can be handled independently. So:

$$[L] = [L^*]^{-1}$$

$$= ([L_3][L_2][L_1])^{-1}$$

$$= [L_1]^{-1}[L_2]^{-1}[L_3]^{-1}$$

$$= \left(\begin{bmatrix} 1 & & & \\ 0 & 1 & & \\ 0 & 0 & 1 & \\ 0 & 0 & \frac{a_{43}''}{a_{33}''} & 1 \end{bmatrix} \begin{bmatrix} 1 & & & \\ 0 & 1 & & \\ 0 & \frac{a_{32}'}{a_{22}'} & 1 & \\ 0 & \frac{-a_{42}'}{a_{22}'} & 0 & 1 \end{bmatrix} \begin{bmatrix} 1 & & & \\ \frac{a_{21}}{a_{11}} & 1 & & \\ \frac{a_{31}}{a_{11}} & 0 & 1 & \\ \frac{-a_{41}}{a_{11}} & 0 & 0 & 1 \end{bmatrix} \right)^{-1}$$

$$= \begin{bmatrix} 1 & & & \\ \frac{a_{21}}{a_{11}} & 1 & & \\ \frac{a_{31}}{a_{11}} & 0 & 1 & \\ \frac{a_{41}}{a_{11}} & 0 & 0 & 1 \end{bmatrix} \begin{bmatrix} 1 & & & \\ 0 & 1 & & \\ 0 & \frac{a_{32}'}{a_{22}'} & 1 & \\ 0 & \frac{a_{42}'}{a_{22}'} & 0 & 1 \end{bmatrix} \begin{bmatrix} 1 & & & \\ 0 & 1 & & \\ 0 & 0 & 1 & \\ 0 & 0 & \frac{a_{43}''}{a_{33}''} & 1 \end{bmatrix}$$

multiply out:

$$L = \begin{bmatrix} 1 & & & \\ \frac{a_{21}}{a_{11}} & 1 & & \\ \frac{a_{31}}{a_{11}} & \frac{a_{32}'}{a_{22}'} & 1 & \\ \frac{a_{41}}{a_{11}} & \frac{a_{42}'}{a_{22}'} & \frac{a_{43}''}{a_{33}''} & 1 \end{bmatrix}$$

[L] contains the pivots used in the elementary row operations to obtain [U].

The general procedure to solve [A] {x} = {B} is as follows:

1. Decompose [A] to obtain [L] and [U]

   - obtain [U] from elementary row operations
   - store pivot elements in [L]

2. Solve [L] {Y} = {B}

3. Solve [U] {x} = {y}

Repeat steps 2 and 3 only for repeated right-hand sides.

3.5.5 Ill-Conditioning

If *det* A is small in relation to the norm (magnitude) of the matrix, it may be ill-conditioned.

$$norm\ A = \sqrt{\sum_{i=1}^{n} \sum_{j=1}^{n} a_{ij}^2}$$

However, if the matrix represents a real, well-posed physical problem that is known to have a unique solution, ill-conditioning does not generally occur.

3.5.6 Row and Column Interchange

If a pivot is small, it may cause problems due to roundoff errors (note that a zero pivot will cause a solution failure). This can often be avoided by re-arranging rows or columns to place the largest element in the pivot position, thus:

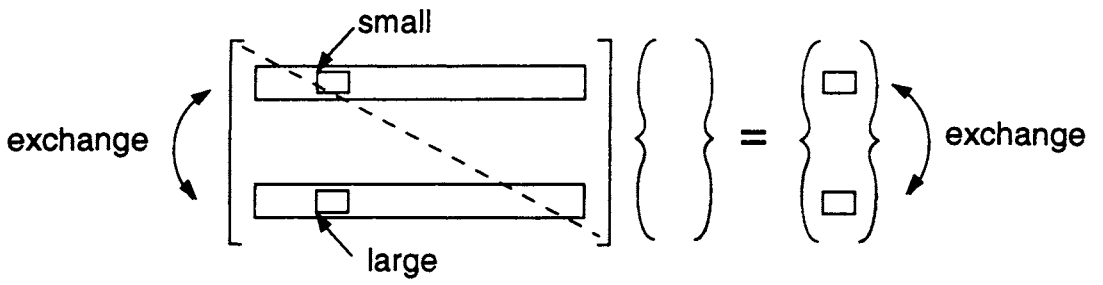

Row interchange

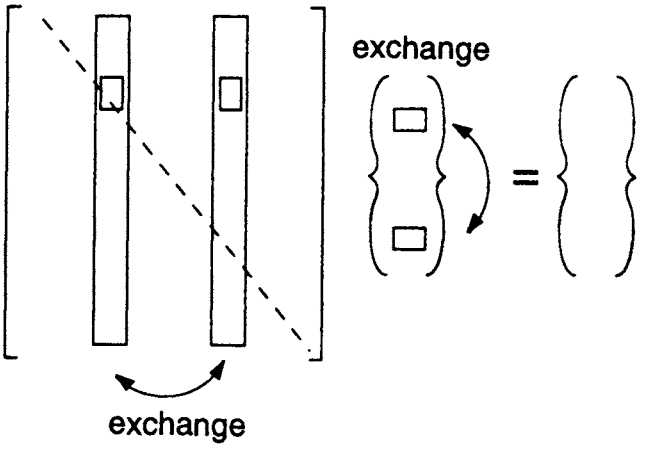

Column interchange

Note: Column interchanges must be kept track of in order to replace the unknowns to their

original positions after solving the equations.

3.5.7 Banded Matrices

Most physical problems lead to banded matrices.

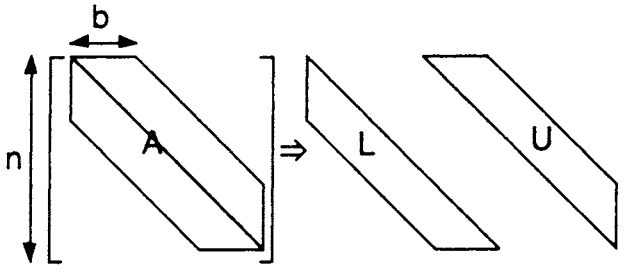

Banded matrices

Operations Count

To solve [A] {x} = [B] with A banded, requires the following number of operations (multiplication and division):

- about nb^2 operations are required to decompose, and
- 2nb operations are required to solve

To solve by inversion and back multiplication $\{x\} = [A]^{-1}\{B\}$ requires:

- inversion - about n^3 (Gauss-Jordan method)
- multiply - about n^3

Note that the advantage of the band is lost when solving by inversion.

3.6 Cholesky Method

This method is applicable to symmetric positive-definite matrices only. Being symmetric the lower and upper triangular matrices obtained after decomposition will be the transpose of each other.

$$[A] = [L]\,[U]$$

$$= [L]\,[L]^T = [U]^T[U]$$

$$\begin{bmatrix} u_{11} & & & & & \\ u_{12} & u_{22} & & & & \\ u_{13} & u_{23} & u_{33} & & & \\ | & & & | & & \\ | & & & & | & \\ u_{1n} & & & & & u_{nn} \end{bmatrix} \begin{bmatrix} u_{11} & u_{12} & u_{13} & & & u_{1n} \\ & u_{22} & u_{23} & & & \\ & & u_{33} & & & \\ & & & | & & \\ & & & & | & \\ & & & & & u_{nn} \end{bmatrix}$$

$$= \begin{bmatrix} a_{11} & a_{12} & a_{13} & - & - & a_{1n} \\ a_{21} & a_{22} & & & & \\ a_{31} & & & & & \\ | & & & & & \\ | & & & & & \\ a_{n1} & & & & & a_{nn} \end{bmatrix}$$

Multiply out:

Row 1:

$$u_{11}^2 = a_{11} \qquad \rightarrow u_{11} = \sqrt{a_{11}}$$

$$u_{11}\, u_{12} = a_{12} \qquad \rightarrow \qquad u_{12} = \frac{a_{12}}{u_{11}}$$

$$u_{11}\, u_{13} = a_{13} \qquad \rightarrow u_{13} = \frac{a_{13}}{u_{11}}$$

Row 2:

$$u_{12}^2 + u_{22}^2 = a_{22} \rightarrow \sqrt{a_{22} - u_{12}^2}$$

$$u_{12}u_{13} + u_{22}u_{23} = a_{23} \rightarrow u_{23} = \frac{a_{23} - u_{12}u_{13}}{u_{22}}$$

etc.

In general, the decomposition is:

$$u_{ii} = \sqrt{a_{ii} - \sum_{k=1}^{i-1} u_{ki}^2}$$

$$u_{ij} = \frac{a_{ij} - \sum_{k=1}^{i-1} u_{ki}u_{kj}}{u_{ii}}$$

This is done independently of the right-hand side. The solution is completed by forward and backward substitution.

Equation with multiple right-hand sides:

$$[A]\{x\}_l = \{B\}_l$$

Forward substitution:

$$\begin{bmatrix} u_{11} & & & \\ u_{12} & u_{22} & & 0 \\ u_{13} & u_{23} & u_{33} & \\ | & & & \\ | & & & \\ u_{1n} & - & - & u_{nn} \end{bmatrix} \begin{Bmatrix} y_1 \\ y_2 \\ | \\ | \\ y_n \end{Bmatrix}_l = \begin{Bmatrix} b_1 \\ b_2 \\ | \\ | \\ b_n \end{Bmatrix}_l$$

$$y_i = \frac{1}{u_{ii}} \left[b_i - \sum_{k=1}^{i-1} (u_{ki}\, y_k) \right]$$

Backward Substitution:

$$\begin{bmatrix} u_{11} & u_{12} & & & u_{1n} \\ & u_{22} & | & & \\ & & & | & \\ & & & | & \\ & & & | & \\ & & u_{n-1,n-1} & u_{n-1,n} & \\ & & & & u_{nn} \end{bmatrix} \begin{Bmatrix} x_1 \\ x_2 \\ | \\ | \\ x_n \end{Bmatrix}_l = \begin{Bmatrix} y_1 \\ y_2 \\ | \\ | \\ y_n \end{Bmatrix}_l$$

$$x_i = \frac{1}{u_{ii}} \left[y_i - \sum_{k=i-1}^{n} (u_{ik}\, x_k) \right]$$

3.7 Thomas Algorithm

This method is applicable to tridiagonal matrices.

$$A = \begin{bmatrix} d_1 & f_1 & & & \\ e_2 & d_2 & f_2 & & \\ & & & f_{n-1} & \\ & & & d_{n-1} & \\ & & e_n & d_n & \end{bmatrix}$$

It can be shown that if [A] is banded, [L] and [U] will also be banded and have the same band width as [A].

Let [L] [U] = [A]

$$\begin{bmatrix} 1 & & \\ l_2 & 1 & 0 \\ & l_3 & \\ & & \\ 0 & & l_n \quad 1 \end{bmatrix} \begin{bmatrix} u_1 & g_1 & & 0 \\ & u_2 & g_2 & \\ & & & \\ & 0 & & g_{n-1} \\ & & & u_n \end{bmatrix} = \begin{bmatrix} u_1 & g_1 & & \\ l_2u_1 & (l_2g_1+u_2) & g_2 & \\ & l_3u_2 & (l_3g_2+u_3) & g_3 \\ & & | & | \quad | \\ & & & | \quad | \end{bmatrix}$$

Equating the product with [A] above, it can be deduced that:

$$g_i = f_i$$

$$u_i = d_1$$

$$l_i = \frac{e_i}{u_{i-1}} \qquad i=2, \cdots, n$$

$$u_i = d_i - l_i f_{i-1} \qquad i=2, \cdots, n$$

Solve: [A] {X} = {B}

Forward Substitution:

$$\begin{bmatrix} 1 & 0 & 0 & 0 & 0 \\ l_2 & 1 & 0 & 0 & 0 \\ 0 & l_3 & 1 & 0 & 0 \\ & & & l_n & 1 \end{bmatrix} \begin{Bmatrix} y_1 \\ y_2 \\ \vdots \\ y_n \end{Bmatrix} = \begin{Bmatrix} b_1 \\ b_2 \\ \vdots \\ b_n \end{Bmatrix}$$

$y_1 = b_1$

$y_i = b_i - l_i y_{i-1} \qquad i=2, \ldots, n$

Backward Substitution:

$$\begin{bmatrix} u_1 & f_1 & & & \\ & u_2 & f_2 & & \\ & & u_3 & f_3 & \\ & & & u_4 & f_{n-1} \\ & & & & u_n \end{bmatrix} \begin{Bmatrix} x_1 \\ x_2 \\ \vdots \\ x_n \end{Bmatrix} = \begin{Bmatrix} y_1 \\ y_2 \\ \vdots \\ y_n \end{Bmatrix}$$

$$x_i = \frac{y_i - f_i x_{i+1}}{u_i} \qquad i = n-1,--,1$$

$$x_n = \frac{y_n}{u_n} \quad \frac{y_n}{u_n}$$

Exercise

Solve by Thomas Method:

$$\begin{bmatrix} 2 & -1 & & & \\ -1 & 2 & -1 & & 0 \\ & -1 & 2 & -1 & \\ 0 & & -1 & 2 & -1 \\ & & & -1 & 2 \end{bmatrix} \begin{Bmatrix} x_1 \\ x_2 \\ x_3 \\ x_4 \\ x_5 \end{Bmatrix} = \begin{Bmatrix} 8 \\ 0 \\ 0 \\ 0 \\ 2 \end{Bmatrix}$$

3.8 Gauss-Seidel Iterative Method

This method is generally used for sparse, diagonally-dominant matrices.

Consider:

1. $a_{11}x_1 + a_{12}x_2 + a_{13}x_3 = b_1$
2. $a_{21}x_1 + a_{22}x_2 + a_{23}x_3 = b_2$
3. $a_{31}x_1 + a_{32}x_2 + a_{33}x_3 = b_3$

Make an initial guess for x_2 and x_3 (in the absence of better information, set them to 0). Solve 1 for x_1:

$$x_1 = \frac{b_1 - a_{12} x_2 - a_{13} x_3}{a_{11}}$$

Using the calculated value for x_1 and the initial guess for x_3, solve 2 for x_2, thus:

$$x_2 = \frac{b_2 - a_{21} x_1 - a_{23} x_3}{a_{22}}$$

Then solve 3 for x_3, thus:

$$x_3 = \frac{b_3 - a_{31} x_1 - a_{32} x_2}{a_{33}}$$

Repeat the procedure until successive results agree. The general Gauss-Seidel formula is:

$$x_i = \frac{1}{a_{ii}} \left[b_i - \sum_{\substack{j=1 \\ j \neq i}}^{n} a_{ij} x_j \right] \quad i=1,2, \cdots ,n$$

where x_j on the right-hand side is always the most recent value. In this method, convergence is guaranteed if:

$$| a_{ii} | > \sum_{\substack{j=1 \\ i \neq 1}}^{n} | a_{ij} |$$

However, convergence may also be obtained if this condition is not satisfied, as long as the diagonal term is the largest number in the row:

$$| a_{ii} | > \left| \sum_{j \neq i} a_{ij} \right|$$

3.8.1 Convergence Criteria

Convergence criteria can either be *absolute* or *relative.*

Absolute:

$$| x_i^{k+1} - x_i^{(k)} | \leq \varepsilon \qquad (a \text{ specified limit})$$

This criterion is often used when the magnitude of the results and the desired accuracy (number of decimals) are known. Note that results may continue to change after the convergence criterion have been satisfied.

$$\left| \frac{x_i^{(k+1)} - x_i^{(k)}}{x_i^{(k+1)}} \right| \leq \varepsilon$$

This criterion tests the percentage change in each unknown. It may be used when the magnitude of results is unknown but may cause problems if some numbers are close to zero.

3.8.2 Point Relaxation

If convergence is monotonic, it could be accelerated by extrapolation. If it is oscillatory, convergence can be improved by damping the oscillations.

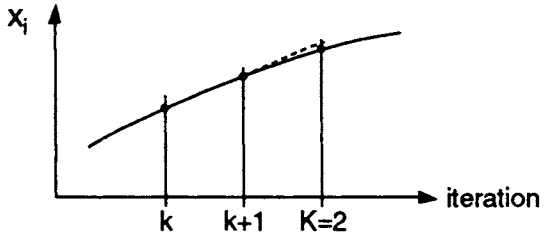

(a) Point relaxation

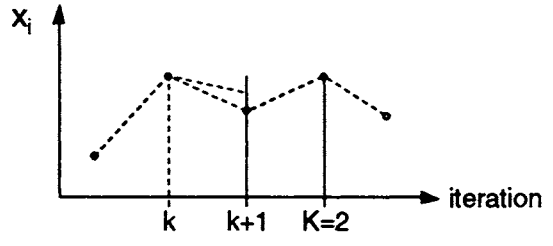

(b) Point relaxation

Convergence can be accelerated by extrapolation from $x_i^{(k+1)}$ or in the case of (b), convergence could be improved by damping the oscillations. This is done by modifying calculated values obtained by the iteration formula according to:

$$x_i^{(k+1)} - x_i^{(k)} + \lambda\ (x_i^{(k+1)} - x_i^{(k)})$$

The value of $x_i^{(k+1)}$ is understood to be that calculated by the iteration formula. This can also be written as:

$$x_i^{(k+1)} = \lambda\, x_i^{(k+1)} + (1 - \lambda)\, x_i^{(k)}$$

Thus the value used is the weighted average between the calculated value and the previous value, such that:

$0 < \lambda < 1$ underrelaxation (damping)
$\lambda = 1$ standard Gauss-Seidel iteration
$1 < \lambda < 2$ overrelaxation (acceleration)

3.8.3 Advantages and Disadvantages of Iterative Methods

Some of the advantages of iterative methods include the following:

- it is self-correcting
- round-off error does not accumulate
- it can be programmed to operate only on non-zero terms
- there is no matrix fill-in
- it is suitable for calculators and small computers

The major disadvantage of iterative methods is that they need fast convergence and good initial guess to be competitive with direct methods.

4. FINITE DIFFERENCES

4.1 Basic Principles

The basic objective of finite difference methods is to approximate the differential terms in the governing differential equations by corresponding different terms. The resulting difference

equation is then written at a finite number of points in the domain. This results in a set of algebraic equations which are easier to solve than the original partial differential equation.

The procedure is easily visualized in 1D. If, for example, u=u(x) is a continuous function, then:

$$\frac{du}{dx} = \lim_{\Delta x \to 0} \frac{\Delta u}{\Delta x}$$

or

$$\frac{du}{dx} = \frac{\Delta u}{\Delta x} = \varepsilon$$

where ε is an error term.

The error term can be evaluated by using a Taylor expansion for u(x+Δx) about x, as follows (See Fig. 9):

$$u(x+\Delta x) = u(x) + \Delta x\, u'(x) + \frac{(\Delta x)^2}{2!} u''(x) + \frac{(\Delta x)^3}{3!} u'''(x) + \cdots$$

which can be rearranged to yield:

$$u'(x) = \frac{u(x+\Delta x) - u(x)}{\Delta x} - \frac{\Delta x}{2} u''(x) - \cdots$$

where the terms beyond the first term on the right hand side represent the numerical error ε.

Since the error is dominated by the leading term (Δx/2)u″(x), ε is said to be of the order Δx or O(Δx). The above approximation of Δu/Δx is known as a *forward difference* approximation, which is first-order accurate.

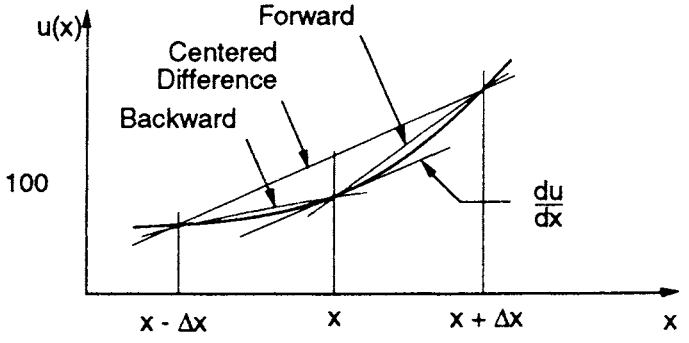

Figure 9: First-derivative approximations

A *backward difference* approximation is obtained by performing a similar expansion for u(x-Δx) about x. This results in:

$$u'(x) = \frac{u(x) - u(x-\Delta x)}{\Delta x} + \frac{\Delta x}{2} u''(x) - \cdots$$

which is also first-order accurate.

An approximation with a higher-order accuracy can be obtained by combining the forward and backward approximations, leading to:

$$u'(x) = \frac{u(x+\Delta x) - u(x-\Delta x)}{2\Delta x} - \frac{(\Delta x)^2}{3} u'''(x) + \cdots$$

where the leading error term is now of second order, or O $(\Delta x)^2$. This is known as a *central difference* approximation.

An approximation for the second derivative can be derived by adding the forward and

backward difference approximations to obtain:

$$u''(x) = \frac{u(x+\Delta x) - 2u(x) + u(x-\Delta x)}{(\Delta x)^2} - \frac{(\Delta x)^2}{12} u''''(x) + \cdots$$

which is also second-order accurate.

The above approximations are based on a uniform discretization Δx. Similar approximations can also be developed for non-uniform Δx, but the accuracy in that case will drop by one order.

4.2 Finite Difference Solution of 1D Flow Equation

The governing equation in 1D, with u as the basic unknown, and assuming uniform material, is:

$$\frac{\partial^2 u}{\partial x^2} = \frac{S}{K} \frac{\partial u}{\partial t}$$

We assume that the spatial domain extends between $0 \leq x \leq L$ and that the boundary and initial conditions are specified as:

$u(0,t) = u_0$

$u(L,t) = 0$

$u(x,0) = 0$

These boundary conditions are known as *first-type* or *Dirichlet* boundary conditions. The solution domain is discretized as shown in Fig. 10, where i,j designate the nodal numbers in the spatial and temporal directions, respectively.

A forward difference approximation to the governing equation is:

$$\frac{u_{i-1,j}-2u_{i,j}+u_{i+1,j}}{(\Delta x)^2} = \frac{S}{K}\,\frac{u_{i,j+1}-u_{i,j}}{\Delta t}$$

The equation involves the 4 nodes shown in Fig. 11, of which one is at the new time level j+1 while three are at the old time level j. Letting:

$$\rho = \frac{K}{S}\,\frac{\Delta t}{(\Delta x)^2}$$

the above difference equation can be rearranged to give:

$$u_{i,j+1} = (1-2\rho)u_{i,j} + \rho(u_{i-1,j} + u_{i+1,j})$$

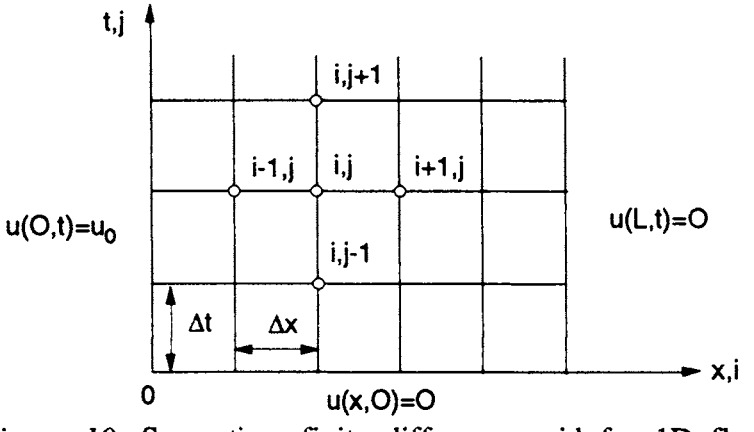

Figure 10: Space-time finite difference grid for 1D flow problem

Thus a value at a new time level j+1 can be calculated directly in terms of values at the old time level j. This is known as an *explicit* finite difference solution. For stability, the explicit

solution requires that $\rho \leq 1/2$. The solution is second-order accurate in space (for uniform Δx) and first-order accurate in time.

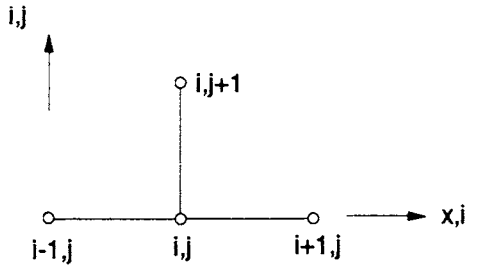

Figure 11: Nodal grouping for explicit difference solution

Alternatively, using a backward difference approximation for the time derivative, the governing equation can be approximated by:

$$\frac{u_{i-1,j} - 2u_{ij} + u_{i+1,j}}{(\Delta x)^2} = \frac{S}{K} \frac{u_{ij} - u_{i,j-1}}{\Delta t}$$

This equation now involves 3 nodes at the new time level j, plus one at the old time level j-1 (Fig. 12). It can be rearranged to give:

$$-u_{i-1,j} + (2 + \frac{1}{\rho})u_{i,j} - u_{i+1,j} = \frac{1}{\rho} u_{i,j-1}$$

Since there are 3 unknowns at the new time level j, the equation cannot be solved directly. By writing the equation at all nodes where u is unknown (this excludes the boundary nodes where u is specified), we obtain a set of simultaneous equations which can be solved.

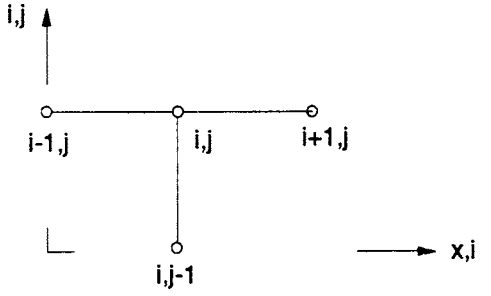

Figure 12: Nodal grouping for implicit difference solution

For example, for the grid shown in Fig. 10, which has 6 nodes in the spatial domain, and where the two boundary nodes carry specified values, we obtain 4 equations in 4 unknowns. These equations can be written in matrix form as follows:

$$\begin{bmatrix} (2+1/\rho) & -1 & & \\ -1 & (2+1/\rho) & -1 & \\ & -1 & (2+1/\rho) & -1 \\ & & -1 & (2+1/\rho) \end{bmatrix} \begin{Bmatrix} u_2 \\ u_3 \\ u_4 \\ u_5 \end{Bmatrix} = \begin{Bmatrix} (1/\rho)u_{2,j-1}+u_{1,j} \\ (1/\rho)u_{3,j-1} \\ 1/\rho)u_{4,j-1} \\ (1/\rho)u_{5,j-1}+u_{6j} \end{Bmatrix}$$

The right-hand side contains the values at the old time level j-1, plus the boundary values. The tridiagonal matrix equation can thus be solved at each time step using the results of the preceding time step. This solution is known as an implicit finite difference solution. The solution is second-order accurate in space and first-order accurate in time, and it is stable for any choice of Δt.

In order to achieve second-order accuracy also with respect to the time derivative, we can write the left-hand side of the finite difference equation as the average between the time levels

j and j-1. Thus the entire equation in effect represents the best approximation for a point located midway (centered) between the two time levels (Fig. 13). The algebraic equation then becomes:

$$-u_{i-1,j} + (2+\frac{2}{\rho})u_{ij} - u_{i+1,j} = u_{i-1,j-1} - (2-\frac{2}{\rho})u_{i,j-1} + u_{i+1,j-1}$$

where all the unknowns (the values of u at the new time level j) appear on the left-hand side and all the knowns on the right-hand side. The matrix equation is of the same form as that for the implicit solution. This is known as a *centered* finite difference solution, which has second-order accuracy in both space and time. It is also unconditionally stable.

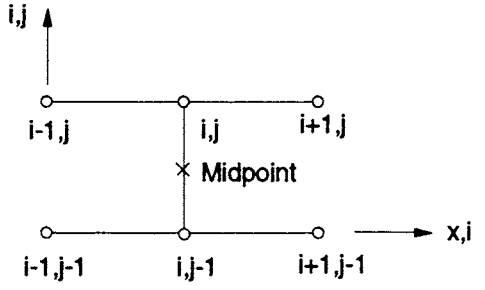

Figure 13: Nodal grouping for centered difference solution

In the above solutions, the boundary has been specified in terms of the unknown u at the boundary (*first-type* boundary condition). If instead a value of the flux q is specified at the boundary we speak of a *second-type* or *Neumann* boundary condition. In that case, we can equate this flux to the gradient of u at the boundary, using the Darcy equation. At the same time, we can approximate the boundary gradient by means of a centered difference approximation, using an extra node (0,j) placed outside the domain (Fig. 14). We obtain:

$$\frac{\partial u}{\partial x} = -\frac{q_n}{K} = \frac{u_{2,j} - u_{0,j}}{2\Delta x}$$

where n refers to the direction normal to the boundary. This yields:

$$u_{o,j} = -2\Delta x \frac{q_n}{K} - u_{2,j}$$

Since the value of u at the boundary is now unknown, we write a difference equation also for the boundary node (1,j), and we use the above equation to substitute for the term u_{0j} occurring in the difference equation. Using the implicit form, the difference equation for the boundary node becomes:

$$(2+\frac{1}{\rho})u_{1,j} - 2u_{2,j} = \frac{1}{\rho}u_{1,j-1} + 2\Delta x \frac{q_n}{K}$$

This equation would be added to the equations previously obtained for the implicit solution. Thus we have one additional equation and one additional unknown for each boundary node where the flux is specified. The above form preserves second-order accuracy in space.

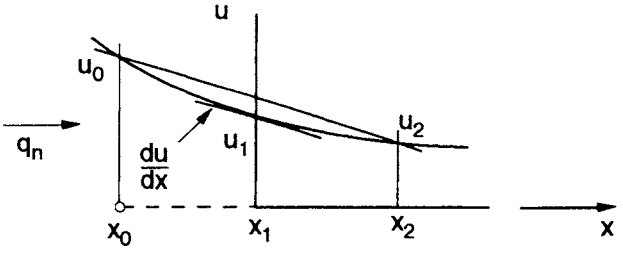

Figure 14: Second-type boundary conditon for 1D flow problem

Each of the above three solution types has its advantages and disadvantages. The explicit form is the easiest to program, but its stability constraint may require rather short time steps. The implicit form overcomes this constraint at the cost of some more elaborate programming. The centered form delivers the best accuracy, again at the cost of additional programming. In implicit or centered solutions of the flow problem, the length of the time step is arbitrary; a shorter time step, however, gives a better resolution of transient behaviour.

Figure 15 shows the transient behaviour of a typical 1D flow system, with u specified at each end, and a change imposed at the left end at the initial time. The solution is formulated in terms of dimensionless time:

$$T^* = \frac{Kt}{SL^2}$$

The spatial discretization is $\Delta x=0.05$. The exact analytical solution (Carslaw and Jaeger, 1946) is:

$$\frac{u(x,t)}{u_o} = \left\{1-\frac{x}{L}\right\} - \frac{2}{\pi}\sum_{n=1}^{\infty}\frac{1}{n}\sin\left\{\frac{n\pi x}{L}\right\}\exp\left\{\frac{-n^2\pi^2 Kt}{SL^2}\right\}$$

where the first term on the right-hand side is the steady-state solution and the summation term represents the transient response.

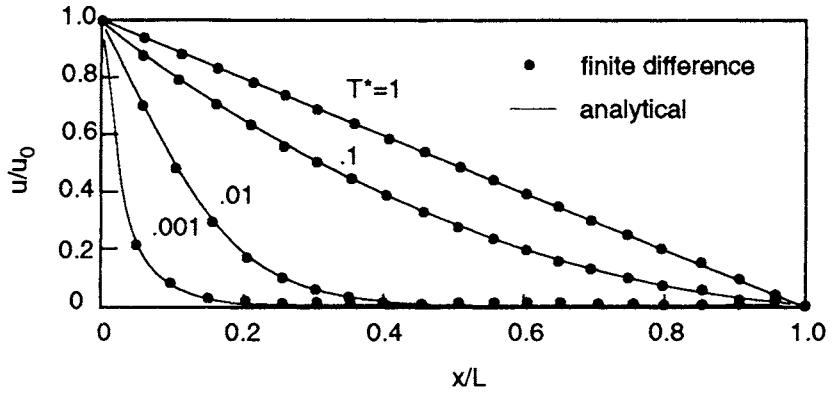

Figure 15: Transient behaviour of 1D flow system: Analytical and numerical solutions

The change imposed consists of setting $u/u_0=1$ at x=0. Profiles corresponding to T*=0.001, 0.01, 0.1, and 1.0 are shown in Fig. 15. The response generated by the imposed change gradually penetrates through the system, converging to a linear function at equilibrium. If a larger time step were selected, some of the early-time response, characterized by a steep gradient at the boundary, will be lost, but the solution will still converge to the correct equilibrium condition. It is also possible to go directly to the equilibrium condition in a single step by setting the specific storage to zero.

Finite difference solutions for 2D and 3D problems can also be formulated and numerous models based on this approach are in existence (eg FLOWPATH and MODFLOW). A case study is presented in Appendix 1 to demonstrate how a finite difference model is conceptualized, set up and applied to real situation.

4.3 Cape Cod Study

The case study presented in Appendix 1 was adapted from USGS open file reports 84-475 and 86-481 (de Lima and Olimpio, 1984 and Ragone, 1986 respectively). The study was conducted at Cape Cod, Massachusetts in the United States of America. Treated sewage had been discharged through infiltration beds into underlying sand and gravel aquifer since 1936 at an approximate rate of 0.46 Mgal/day. The contaminant plume that resulted from the discharge was estimated to be 11000 ft long, 3000 ft wide and 75 ft thick. The geology of the area consists of glacial deposits that are underlain by crystalline bedrock. The uppermost 90 to 140 ft consists of stratified sand and gravel which overlies silty sand and till. Average hydraulic conductivity of the aquifer materials was determined to be 380 ft/day and the average linear groundwater velocity was estimated as 1.5 ft/day. A numerical model was developed to provide insight to hydraulic processes at the site and predict the response of the system to different hydraulic stresses. Appendix 1 presents site characterization in cross section and plan view, conceptualization of the problem domain in terms of boundary conditions, discretization of the problem domain, and comparison of results of the calibrated model with the observed data.

5. FINITE ELEMENTS

5.1 Basic Principles

The main advantage of the finite element method is that domains of irregular geometry can be represented naturally. This advantage comes into play with 2D and 3D problems. Thus, although finite element solutions can be developed for any dimensionality, we will focus here on 2D domains. Regardless of the spatial dimensionality, the time dimension always has the same uniformity and is therefore usually handled with finite differences, even when the spatial dimensions are handled with finite elements. Comprehensive discussions of the finite element

method in groundwater hydrology may be found in texts such as Huyakorn and Pinder (1983).

In applying the finite element method, we start by dividing the domain into a number of elements (Fig. 16). Many element shapes are possible; in two dimensions, the most useful shape for groundwater problems is the linear triangle. The points where the element corners meet are the *nodes*.

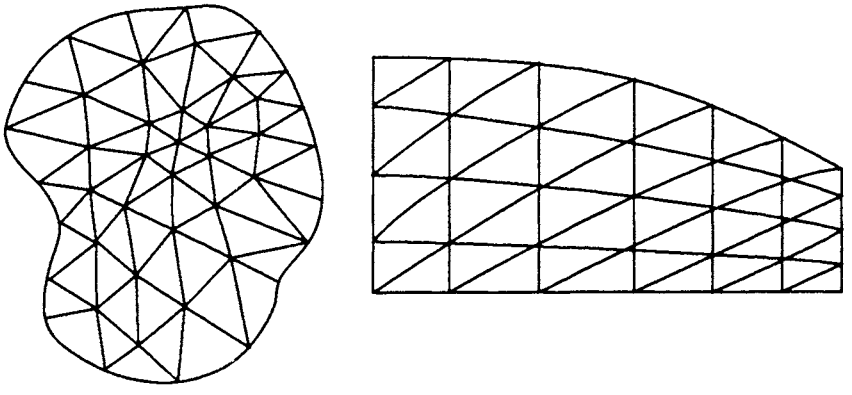

Figure 16: Typical finite element grids

The first step in the development of the finite element solution is to define an *interpolation function* that expresses the value of the unknown function u=u(x,y) in terms of its values u_j at the nodes (Fig. 17). The interpolation is accomplished by means of *basis functions*. For the linear triangle, these basis functions are inclined planes of the form shown in Fig. 18. There is one basis function for each of the 3 nodes on the element; each of these basis functions has a value of 1 at the node it represents, and a value of 0 at the other two nodes that lie on the same element.

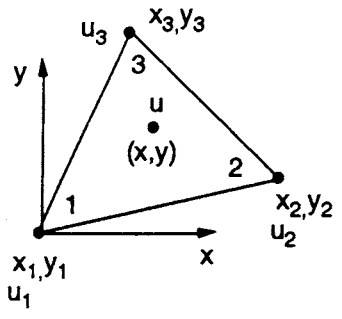

Figure 17: Typical linear triangle element

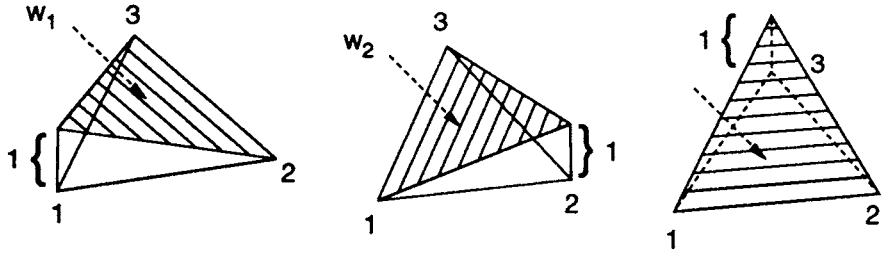

Figure 18: Basis functions for linear triangle

Since the basis functions are linear, the interpolation will be a piecewise linear approximation of u. We call the approximate function $\hat{u}=\hat{u}(x,y)$. The interpolation that expresses $\hat{u}$ in terms of u_j is:

$$\hat{u}(x,y) = \sum_{j=1}^{3} u_j w_j(x,y)$$

where $w_j(x,y)$ represents the basis functions. For the linear triangle, these are surfaces given by:

$$w_j(x,y) = \frac{1}{2\Delta}(a_j + b_j x + c_j y)$$

where the coefficients are obtained by cyclic permutation of the nodes i,j,k as follows (Zienkiewicz, 1977):

$$a_i = x_j y_k - x_k y_j$$

$$b_i = y_j - y_k$$

$$c_i = x_k - x_j$$

and where the determinant is defined as:

$$\det = 2\Delta = \begin{bmatrix} 1 & x_i & y_i \\ 1 & x_j & y_j \\ 1 & x_k & y_k \end{bmatrix}$$

with Δ being the area of the triangle. A property of the basis functions is that:

$$\sum_{j=1}^{3} w_j(x,y) = 1$$

everywhere within the element.

The second step in developing the finite element solution is the generation of the algebraic equations that will be solved for the unknown nodal values. To generate these equations, we use the *Weighted Residual Method* (Huyakorn and Pinder, 1983). Suppose we have a partial

differential equation of the form:

$$L(u) - f = 0$$

where L is a differential operator. An exact solution will be obtained if we substitute a trial solution in the form of:

$$u(x,y) = \lim_{n\to\infty} \sum_{j=1}^{n} u_j w_j(x,y)$$

where n is the number of nodes in the domain. If we limit the nodes to a finite number, as we must, the solution will be approximate and of the form:

$$u(x,y) \approx \hat{u}(x,y) = \sum_{j=1}^{n} u_j w_j(x,y)$$

where $\hat{u}$ designates an approximation of u. We can substitute the approximate solution into the original differential equation to obtain:

$$L(\hat{u}(x,y)) - f = R(x,y) \neq 0$$

where the non-zero residual function R(x,y) on the right-hand side is a consequence of the approximation.

According to the theory of weighted residuals, we can minimize the residual R(x,y) on the average over the domain by satisfying a set of weighted residual equations, which are:

$$\int_A R(x,y)\ w_i(x,y)dA = 0 \qquad i=1,2,\cdots,n$$

where A designates the solution domain, and $w_i(x,y)$ are a set of n weighting functions corresponding to the nodes (Fig. 19).

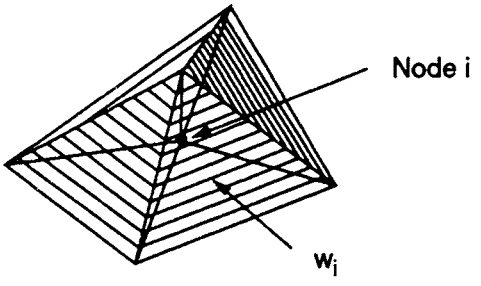

Figure 19: Linear weighting function

In the general weighted residual method, these *weighting functions* are independently chosen. In the *Galerkin Method*, on the other hand, which is a special variant of the weighted residual method, the weighting functions are chosen to be identical to the basis functions. This has the advantage of simplicity, and a further advantage in that the coefficient matrix for the flow equation becomes symmetrical. The Galerkin Method has been well proven in groundwater hydrology (Pinder and Frind, 1972) and we will here use it exclusively.

The numerical error in the Galerkin finite element method is *minimized globally*; that is, over the domain as a whole, the error is a minimum. As the number of nodes increases and the nodal distances decrease, the error decreases, and, in the limit as the number of nodes tends to infinity, the error tends to zero. Locally, the numerical error is of first order for non-uniform node spacing and of second order for uniform node spacing.

5.2 Finite Element Solution of 2D Flow Equation

The governing equation for flow in a heterogeneous isotropic medium, with the coordinate axes oriented along the principal directions of conductivity, is:

$$\frac{\partial}{\partial x}\left(K_{xx}\frac{\partial u}{\partial x}\right) + \frac{\partial}{\partial y}\left(K_{yy}\frac{\partial u}{\partial y}\right) - S_s\frac{\partial u}{\partial t} = 0$$

where u is the unknown potential. The boundary and initial conditions are of the form:

$$u=u_c \qquad on\ B_1 \quad (first\text{-}type)$$

$$-K_n\frac{\partial u}{\partial n} = q_n \quad on\ B_2 \quad (second\text{-}type)$$

$$u=u_0 \qquad at\ t=t_0$$

where B_1 and B_2 are parts of the boundary with $B = B_1 + B_2$ being the complete domain boundary, K_n is the effective hydraulic conductivity in the direction of the normal at the boundary, and t_0 is the initial time.

To develop the Galerkin finite element solution, we discretize the spatial domain with linear triangular elements and assume a trial solution of the form:

$$u(x,y) \approx \hat{u}(x,y) = \sum_{j=1}^{n} u_j w_j(x,y)$$

Upon substitution of the trial solution into the governing equation, a residual will be obtained which is:

$$R(x,y) = \frac{\partial}{\partial x}\left(K_{xx}\frac{\partial \hat{u}}{\partial x}\right) + \frac{\partial}{\partial y}\left(K_{yy}\frac{\partial \hat{u}}{\partial y}\right) - S_s\frac{\partial \hat{u}}{\partial t}$$

According to weighted residual theory, the residual will be minimized if a set of weighted residual equations is satisfied. The weighted residual will be minimized if a set of weighted residual equations is satisfied. The weighted residual equations are of the general form:

$$\int_A R(x,y)\ w_i(x,y)\ dxdy = 0 \qquad i = 1\ ,\ 2\ ,\ \cdots\ ,\ n$$

or specifically, for the case of the 2D flow equation:

$$\int_A \left\{ \frac{\partial}{\partial x}\left(K_{xx}\frac{\partial \hat{u}}{\partial x}\right) + \frac{\partial}{\partial y}\left(K_{yy}\frac{\partial \hat{u}}{\partial y}\right) - S_s\frac{\partial \hat{u}}{\partial t} \right\} w_i(x,y)\ dxdy = 0 \qquad i=1,2,\ \cdots\ ,\ n$$

The approximate functions u in the above equation are represented within each element by the interpolation function:

$$\hat{u}(x,y) = \sum_{j=1}^{3} u_j\ w_j(x,y)$$

which expresses $\hat{u}$ in terms of the unknown nodal values u_j.

The Galerkin procedure calls for the interpolation function to be substituted into the weighted residual equations. We note that, since the interpolation function is expressed in terms of the linear basis functions $w_j(x,y)$, evaluation of the second derivatives in the weighted residual equations will cause the equations to vanish. To overcome this problem, we first transform the second-derivative terms by applying Green's theorem (Hildebrand, 1965). The result is:

$$\int_A \left\{ K_{xx}\frac{\partial w_i}{\partial x}\frac{\partial \hat{u}}{\partial x} + K_{yy}\frac{\partial w_i}{\partial y}\frac{\partial \hat{u}}{\partial y} \right\} dxdy$$

$$+ \int_B \left\{ K_{xx}\frac{\partial \hat{u}}{\partial x}\ l_x + K_{yy}\frac{\partial \hat{u}}{\partial y}\ l_y \right\} w_i(x,y)\ db$$

$$+ \int_A S_s \frac{\partial \hat{u}}{\partial t} w_i(x,y)\, dxdy = 0 \qquad i=1,2, \cdots, n$$

where l_x, l_y are the direction cosines of the inward normal at the boundary, and db is an increment of the boundary. The inward rather than the outward normal is chosen in order to be consistent with the mass conservation convention which specifies that mass added to the system is positive.

We can now substitute the interpolation function for the variable u. The nodal values u_j contained in the interpolation function, being point values, can be taken outside the integral. Also, since the basis functions, which must be integrated, are defined individually for the elements, we can break up the entire integral into elemental contributions which are summed over all the elements. Furthermore, the boundary integral in the above equation represents the second-type (flux) boundary condition $q_n=-K_n\partial u/\partial n$, which allows us to replace the term {.} by the boundary flux $\{-q_n\}$. The boundary integral is known as the *natural boundary condition* since it is generated naturally by the weighted residual finite element formulation.

Finally, we let the time derivative be approximated by:

$$\frac{\partial \hat{u}}{\partial t} = \frac{\partial}{\partial t}\left(\sum_{j=1}^{n} u_j w_j(x,y)\right)$$

The weighted residual equations thus become:

$$\sum_{j=1}^{n} u_j \sum_{e} \int_{A^e} \left\{ K_{xx} \frac{\partial w_i}{\partial x} \frac{\partial w_j}{\partial x} + K_{yy} \frac{\partial w_i}{\partial y} \frac{\partial u_j}{\partial y} \right\} dxdy$$

$$- \sum_{e} \int_{B^e} q_n w_i db + \sum_{j=1}^{n} \frac{\partial u_j}{\partial t} \sum_{e} \int_{A^e} S_s \, w_i w_j \, dxdy = 0 \qquad i=1,2, \cdots, n$$

where A^e represents the element area, and B^e represents the side of an element lying on the boundary. The above n equations can be written in summation notation as:

$$\sum_{j=1}^{n} u_j M_{ij}^{K} + \sum_{j=1}^{n} \frac{\partial u_j}{\partial t} M_{ij}^{S} - F_i^{B} = 0 \qquad i=1,2, \cdots, n$$

or in matrix notation as:

$$[M^K]\{u\} + [M^S] \left\{ \frac{\partial u}{\partial t} \right\} - \{F^B\} = 0$$

where $[M^K]$ is the conductance matrix, $[M^S]$ is the storage matrix, and $\{F^B\}$ is the boundary flux vector. The coefficient matrices are now entirely in terms of material parameters and geometric terms which express the element geometry through the basis functions. The procedure for evaluation of the matrices is to first generate the elemental coefficient matrices and then to assemble these into the corresponding global matrices. The elemental matrices corresponding to the specialized equations addressed here are given in Sections 5.4, 5.5, and 5.6.

The time derivative can be approximated by a forward difference approximation of the form:

$$\frac{\partial u}{\partial t} = \frac{u_{k+1} - u_k}{\Delta t}$$

where k designates the time level. In order to obtain optimum accuracy and unconditional stability, we can place the spatial terms in the equation at a point in time where the time derivative approximation has the lowest error. In most cases this is the midpoint between the old and the new time levels, or $t_k + \Delta t/2$ (centered difference approximation). However, we can also choose a general time weighting of the form $t_k + \eta\Delta t$, where $0 \leq \eta \leq 1$. The spatial

terms will then be weighted in time according to:

$$\eta\ u_{k+1} + (1-\eta)u_k$$

On the basis of a general time weighting, the matrix equation becomes:

$$\left\{ \eta[M^K] + \frac{1}{\Delta t}[M^S] \right\} \{ u \}_{k+1} = \left\{ -(1-\eta)[M^K] + \frac{1}{\Delta t}[M^S] \right\} \{ u \}_k + \eta\{ F^B \}_{k+1} + (1-\eta)\{F^B\}_k$$

where $\eta = 1$ gives an implicit-in-time solution and $\Delta=1/2$ gives a centered-in-time solution.

To account for the first-type boundary condition, the matrix equation is partitioned according to nodes at which u is unknown and nodes at which u is known. The partitioning is as follows:

$$\left[\begin{array}{c|c} M_{ff} & M_{fc} \\ \hline M_{cf} & M_{cc} \end{array}\right] \left\{\begin{array}{c} u_f \\ \hline u_c \end{array}\right\} = \left\{\begin{array}{c} F_f \\ \hline F_c \end{array}\right\}$$

where M and F stand for the complete coefficient matrix (left-hand side) and forcing vector (right-hand side) of the finite element matrix equation, respectively, and where the subscripts f and c designate free nodes (u unknown) and constrained nodes (u specified), respectively.

The partitioned equation is multiplied out to give:

$$[M_{ff}] \{ u_f \} + [M_{fc}] \{ uc \} = \{ F_f \}$$

$$[M_{cf}] \{ u_f \} + [M_{cc}] \{ u_c \} = \{ F_c \}$$

Only the first of these two equations is needed for the solution. The second equation is used if the fluxes at the first-type boundary are required, for example, in mass balance calculations. The second term in the first equation, which represents the link between the first-type boundary nodes and the interior nodes of the domain, contains known terms only and is moved to the right-hand side. The equation to be solved thus becomes:

$$[M_{ff}] \{ u_f \} = \{ F_f \} - [M_{fc}] \{ u_c \}$$

where the right-hand side now contains all known quantities, which include the solution at the preceding time step, values at the first-type boundary, and fluxes at the second-type boundary.

The above matrix equation, which is typical for flow problems and purely diffusive problems, has symmetric coefficient matrices. The usual method of solution is the Cholesky method, which takes advantage of matrix symmetry. For the 1D form, the Thomas method is commonly used. For very large systems, the preconditioned conjugate gradient method (Schmid and Braess, 1988) is now becoming increasingly popular.

After solution of the matrix equations, the specific discharge in each element can be calculated by substituting the potentials into the Darcy equation (Section 2.1). The elemental interpolation function is used to express the potential function in term of the nodal values u_j produced by the matrix solution. For the case where the coordinate axes coincide with the principal directions of conductivity, the components of specific discharge in 2D become:

$$q_x = -\frac{K_{xx}}{2\Delta} \sum_{j=1}^{3} u_j b_j$$

$$q_y = -\frac{K_{yy}}{2\Delta} \sum_{j=1}^{3} u_j c_j$$

where b_j,c_j are the basis function coefficients. The groundwater velocities are then given by $v_i=q_i/\theta$. Since the basis function coefficients, which result from the differentiation of the linear basis function, are constant over each element, the velocity components will be element-wise constant, and discontinuous from one element to the next.

Matrix equations similar to the above can be developed for the various specialized equations for flow and transport. The finite element solutions for the three types of equations given in Section 2 are developed below.

5.3 Anisotropy and Heterogeneity

The above development is valid for isotropic material or anisotropic material with the coordinate axis coinciding with the principal directions of anisotropy. For the more general case, where the coordinate axes do not coincide with the principal directions (Fig. 20), we can choose one of two options. The first is to include the cross-derivative terms in the development of the solution. The second option is to rotate the coordinate axes into the principal directions. The second option is computationally more efficient, since the terms in the finite element equation are kept to a minimum. This option should be used where the principal directions are invariant, and where the rotation is easily accomplished, as for example in 2D flow problems.

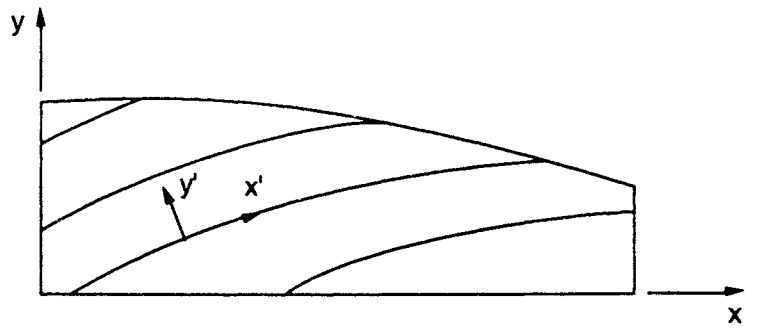

Figure 20: General anisotropic

The rotation is performed on the nodal coordinates on a node-by-node basis, according to (Fig. 21):

$$\begin{Bmatrix} x' \\ y' \end{Bmatrix} = \begin{bmatrix} \cos\beta & \sin\beta \\ -\sin\beta & \cos\beta \end{bmatrix} \begin{Bmatrix} x \\ y \end{Bmatrix}$$

where x′, y′ are the coordinates of point x,y in the principal direction coordinate system, and β is the angle between the cartesian axes and the principal axes. The finite element formulation permits each element to have its own individual angle of rotation. This is a significant advantage for cross-sectional systems with complex stratification.

The calculated potentials, being scalar quantities, are independent of the rotation. However, the velocities, being vector quantities, must be rotated back to cartesian coordinates if the velocity calculation was done in rotated coordinates (see preceding section). The back rotation

is:

$$\begin{Bmatrix} v_x \\ v_y \end{Bmatrix} = \begin{bmatrix} \cos\beta & -\sin\beta \\ \sin\beta & \cos\beta \end{bmatrix} \begin{Bmatrix} v'_x \\ v'_y \end{Bmatrix}$$

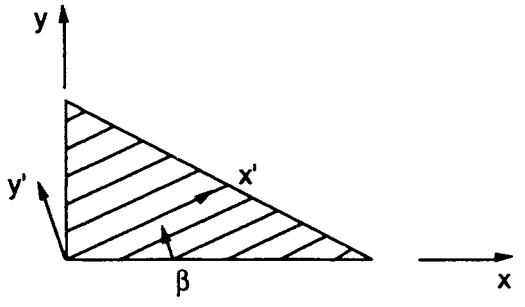

Figure 21: Rotation of axes

The problem of anisotropy also arises in the solution of the transport equation (Section 5.6). In this case, the principal directions are the directions parallel and perpendicular to the flow. Unfortunately, these directions are in general not invariant, since they depend on the flow boundary conditions. The standard procedure in transport modelling is, therefore, to use cartesian coordinates and to include the cross-derivative terms. One conceptual dilemma in this approach is that the cross derivative terms in the dispersion tensor ($D_{xy'}$ D_{yx}) are usually defined according to the classical approach, which is now recognized to be valid only at the local scale. Lacking practical alternatives, however, most models also apply the classical definition to the field scale. This is defensible on the basis that the dominant direction of contaminant migration in most aquifers is horizontal.

In situations where depth-dependent chemical or biochemical reactions occur, the vertical positioning of the plume may be of importance. In such cases, the cartesian form may not

give sufficient accuracy in the solution of the transport equation. This problem can be overcome by solving the transport equation in principal coordinates (see for example Frind *et al.*, 1990). The finite element grid for the transport solution is, in that case, defined by the flownet (see Section 4.5), which is generated by the solution of the potential and streamfunction equations. In this approach, the flow velocities are not needed in the solution of the transport equation, since the advective displacement is defined by the streamfunction solution.

The finite element formulation also accommodates material heterogeneity in a unique way. Heterogeneity is reflected in the governing equations in that the material properties, i.e. K_{ij} and D_{ij}, are functions of space and are therefore included as part of the argument of the differential operator. This would normally result in terms of the form $\partial K_{ij}/\partial x_j$ or $\partial D_{ij}/\partial x$ (see Section 5.3). These terms, however, do not appear in the finite element equation. This is due to the transformation of the differential terms by Green's Theorem, resulting in a boundary integral term and an area integral term in which the material property is no longer an argument of the differential operator. The boundary integral term vanishes in the interior of the grid because the fluxes crossing the inter-element boundaries cancel each other. The end result of this is that the finite element equations are fully valid for heterogeneous systems without derivatives of the material property functions.

5.4 Confined/Unconfined Aquifer Equations

The governing equations for flow in confined or unconfined aquifers are given in Section 2.3. The basic assumptions are that flow in the aquifer is predominantly horizontal, and that the aquifer is separated from neighbouring flow systems by aquitards whose permeability is substantially lower than that of the aquifer. A confined aquifer receives recharge mainly by leakage through the aquitards from above or below, while an unconfined aquifer receives recharge through infiltration from above. In addition, both can be recharged at the lateral boundaries, or by injection.

We assume that the coordinate axes coincide with the principal directions of transmissivity. Since the flow solution is fairly insensitive with respect to the time derivative approximation, we use backward differences in time. The finite element equation for both confined and unconfined aquifers then takes the form:

$$\left([M^K] + [M^L] + \frac{1}{\Delta t}[M^S]\right)\{\phi\}_{k+1} = \frac{1}{\Delta t}[M^S]\{\phi\}_k + \{F^R\} + \{F^B\} + \{F^Q\}$$

where k is the time level, $[M^K]$ is the conductance matrix, $[M^L]$ represents the leakage flux, $[M^S]$ is the storage matrix, and $\{F^R\}$, $\{F^B\}$, $\{F^Q\}$ represent the areal recharge flux, the boundary recharge flux, and the source/sink recharge flux, respectively.

For a grid consisting of linear triangular elements, the elemental components of the above matrices are defined as follows:

$$[M^K]^e = \frac{T_{xx}}{4\Delta}\begin{bmatrix} b_1b_1 & b_1b_2 & b_1b_3 \\ b_2b_1 & b_2b_2 & b_2b_3 \\ b_3b_1 & b_3b_2 & b_3b_3 \end{bmatrix} + \frac{T_{yy}}{4\Delta}\begin{bmatrix} c_1c_1 & c_1c_2 & c_1c_3 \\ c_2c_1 & c_2c_2 & c_2c_3 \\ c_3c_1 & c_3c_2 & c_3c_3 \end{bmatrix}$$

$$[M^L]^e = \left(\frac{K'_1}{b'_1} + \frac{K'_2}{b'_2}\right)\frac{\Delta}{12}\begin{bmatrix} 2 & 1 & 1 \\ 1 & 2 & 1 \\ 1 & 1 & 2 \end{bmatrix}$$

$$[M^S]^e = \frac{\Delta}{12}\begin{bmatrix} 2 & 1 & 1 \\ 1 & 2 & 1 \\ 1 & 1 & 2 \end{bmatrix}$$

$$\{F^R\}^e = \left(\frac{K'_1}{b'_1}h_1 + \frac{K'_2}{b'_2}h_2 + q_R\right)\frac{\Delta}{3}\begin{Bmatrix}1\\1\\1\end{Bmatrix}$$

$$\{F^B\}^e = q_n\frac{L^e}{2}\begin{Bmatrix}1\\1\end{Bmatrix}$$

where b_j, c_j are the basis function coefficients, Δ is the element area, K'_1, K'_2, b'_1, b'_2 represent the hydraulic conductivity and thickness of the upper and lower aquitards, respectively; h_1, h_2 are the heads in the adjoining aquifers that contribute leakage flux; q_R is the recharge at the watertable; q_n is the influx at the lateral (second-type) boundaries, and L^e is the length of the elements at the boundary. The source/sink vector $\{F^Q\}$ contains simply the well recharge or discharge at the appropriate node, with recharge being positive and discharge being negative.

In the case of a confined aquifer, the solution is linear and proceeds in a time-marching manner, starting with the specified initial condition. The unconfined aquifer solution, on the other hand, is nonlinear on account of the parameter T=Kb, in which the saturated thickness b=h-B is a function of the unknown watertable head h. The solution is therefore iterative. The iterative procedure consists of substituting the calculated heads back into the equation and resolving the system. The iteration usually converges rapidly, provided the change in the saturated thickness is small relative to the thickness itself. If the change during a time step is large, or if dewatering is imminent, numerical problems can occur. The usual remedy is to reduce the time step. Special techniques must be incorporated if dewatering occurs.

A groundwater system consisting of several aquifers separated by aquitards can be represented by coupling areal models together. A multi-aquifer model of this type has been developed by Rudolph and Sudicky (1990).

5.5 Potential/Streamfunction Equations

The governing equations in a cross-sectional flow system in terms of potentials and streamfunctions are given in Section 2.4. The basic assumption is that flow is entirely within the plane of the section. Since the flow system is taken to be at steady state, the equations have no storage term. However, changes in the flow system in time, for example due to changing recharge, can be accommodated by means of successive instantaneous steady states. Although this approach neglects the storage mechanism of the system, the equilibrium solution is fully valid.

We will assume that the coordinate axes coincide with the principal directions of hydraulic conductivity. The finite element equations for the potentials and streamfunctions are:

$$[M^{\phi}]\{\phi\} = \{F^{\phi}\}$$

$$[M^{\psi}]\{\Psi\} = \{F^{\psi}\}$$

For a grid consisting of linear triangles, the coefficient matrices are:

$$[M^{\phi}]^e = \frac{K_{xx}}{4\Delta}\begin{bmatrix} b_1b_1 & b_1b_2 & b_1b_3 \\ b_2b_1 & b_2b_2 & b_2b_3 \\ b_3b_1 & b_3b_2 & b_3b_3 \end{bmatrix} + \frac{K_{yy}}{4\Delta}\begin{bmatrix} c_1c_1 & c_1c_2 & c_1c_3 \\ c_2c_1 & c_2c_2 & c_2c_3 \\ c_3c_1 & c_3c_2 & c_3c_3 \end{bmatrix}$$

$$[M^{\psi}]^e = \frac{1}{4\Delta K_{yy}}\begin{bmatrix} b_1b_1 & b_1b_2 & b_1b_3 \\ b_2b_1 & b_2b_2 & b_2b_3 \\ b_3b_1 & b_3b_2 & b_3b_3 \end{bmatrix} + \frac{1}{4\Delta K_{xx}}\begin{bmatrix} c_1c_1 & c_1c_2 & c_1c_3 \\ c_2c_1 & c_2c_2 & c_2c_3 \\ c_3c_1 & c_3c_2 & c_3c_3 \end{bmatrix}$$

$$\{F^{\phi}\}^e = q_n \frac{L^e}{2}\begin{Bmatrix} 1 \\ 1 \end{Bmatrix}$$

$$\{F^{\psi}\}^{e} = \frac{-\Delta\phi^{e}}{2}\begin{Bmatrix}1\\1\end{Bmatrix}$$

where L^e is the length of the element on the boundary, and $-\Delta\phi = \phi^i - \phi_{i+1}$ is the head change over the element having nodes i and i+1 on the boundary (Fig. 23). Upon assembly, the nodal values F_i^{ϕ} express the equivalent nodal recharge at the second-type potential boundary, which is the boundary flux multiplied by one-half the element length on either side of node i (Fig. 22). Likewise, the assembled nodal values F_i^{ψ} express one-half the negative head difference between the neighbouring nodes on either side of node i, or $(\phi_{i-1} - \phi_{i+1})/2$ (Fig. 23).

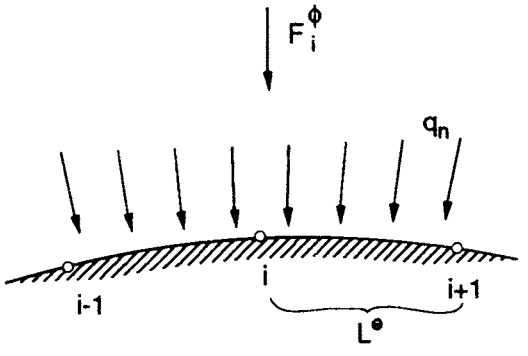

Figure 22: Second-type boundary condition for potential

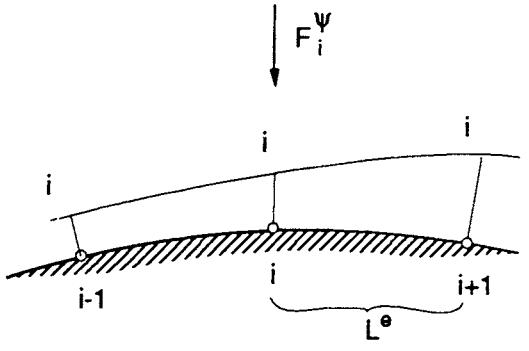

Figure 23: Section-type boundary condition for streamfunctions

First-type boundary conditions on either ϕ or ψ are accounted for in the finite element equations by partitioning the equations and moving the linking terms to the right-hand side. Thus the final coefficient matrix will contain only terms corresponding to nodes where the basic variable is unknown.

The potential/streamfunction equations can also be solved for the case where the position of the watertable (the upper boundary of the grid) is unknown. The boundary condition on ϕ will in that case be defined in terms of the recharge flux at the watertable. The condition to be satisfied is that at the watertable, the hydraulic head must equal the elevation head:

$$\phi_w = y_w$$

since the pressure component of the hydraulic head is taken to be relative to atmospheric pressure. The solution procedure for the nonlinear case starts with an assumed watertable position. The calculated head at the watertable is then compared with the elevation head, and the watertable is adjusted (up or down) accordingly. The solution is repeated until

convergence is obtained. The iterations usually converge rapidly, provided the aquifer near the watertable contains no major discontinuities.

After solution of the matrix equations for potentials and streamfunctions, the velocities can be calculated either from the potentials (see Section 4.2) or from the streamfunctions (see Section 2.4). In the latter case, we can make use of the fact that the interval in the values of the streamfunctions that bound a streamtube equals the discharge in the streamtube. Therefore, the groundwater velocity in the direction of a streamline is given by:

$$v_s = \frac{q_s}{\theta} = \frac{\Delta\psi}{\theta\Delta p}$$

where $\Delta\psi$ is the streamfunction interval, and Δp is the width of the corresponding streamtube. Since both the streamfunction and the streamtube width are continuous functions, the velocity calculated by the above procedure will be continuous between elements.

Figure 24 shows a typical finite element grid for a cross-sectional flow system. The boundary condition at the watertable is a uniform recharge of 15 cm/year, the left and bottom boundaries are impermeable, and the right boundary is an outflow boundary. The material is isotropic. The simulation starts with an initially rectangular grid, and the watertable is iteratively adjusted until a gradient that is consistent with the given recharge is obtained.

The flownet produced by the potential/streamfunction model is shown in Fig. 25 (note the vertical scale exaggeration). In (a), a uniform hydraulic conductivity of 10^{-6} m/sec is used, while in (b), the same system is modified by placement of a lens of 10^{-4} m/sec in the middle of the flow system. The high-conductive lens is seen to be highly effective in focusing the flowlines. In addition, it also reduces the watertable gradient above the lens, as well as the total watertable rise, which is 2.2 m for case (a) and 1.7 m for case (b).

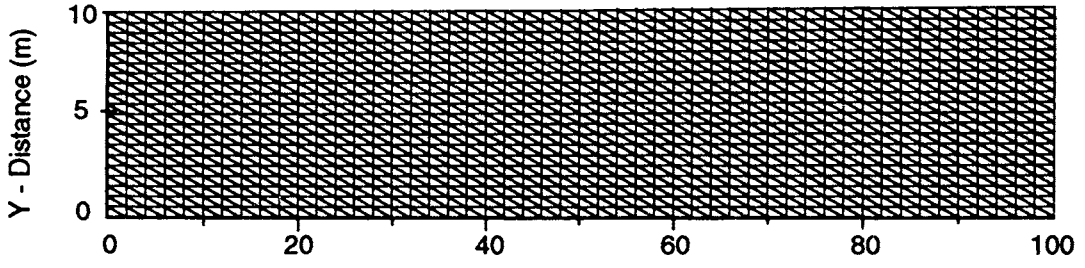

Figure 24: Finite element grid for cross-sectional flow system

5.6 Transport Equation

The governing equation for advective-dispersive transport with linear sorption and first-order decay is given in Section 2.5. The equation is valid in one, two, and three dimensions. The velocity field required for solution of the transport equation can be determined either by application of the general Darcy equation to the flow solution (see Sections 2.1 and 4.2), or by direct use of a streamfunction solution (see Section 4.5 above). The former approach is valid for both cartesian and principal coordinates, while the latter approach is used only when the transport equation is formulated in principal coordinates.

With either approach, the velocities will be element-wise constant and therefore discontinuous between elements. In the finite element solution of the transport equation,

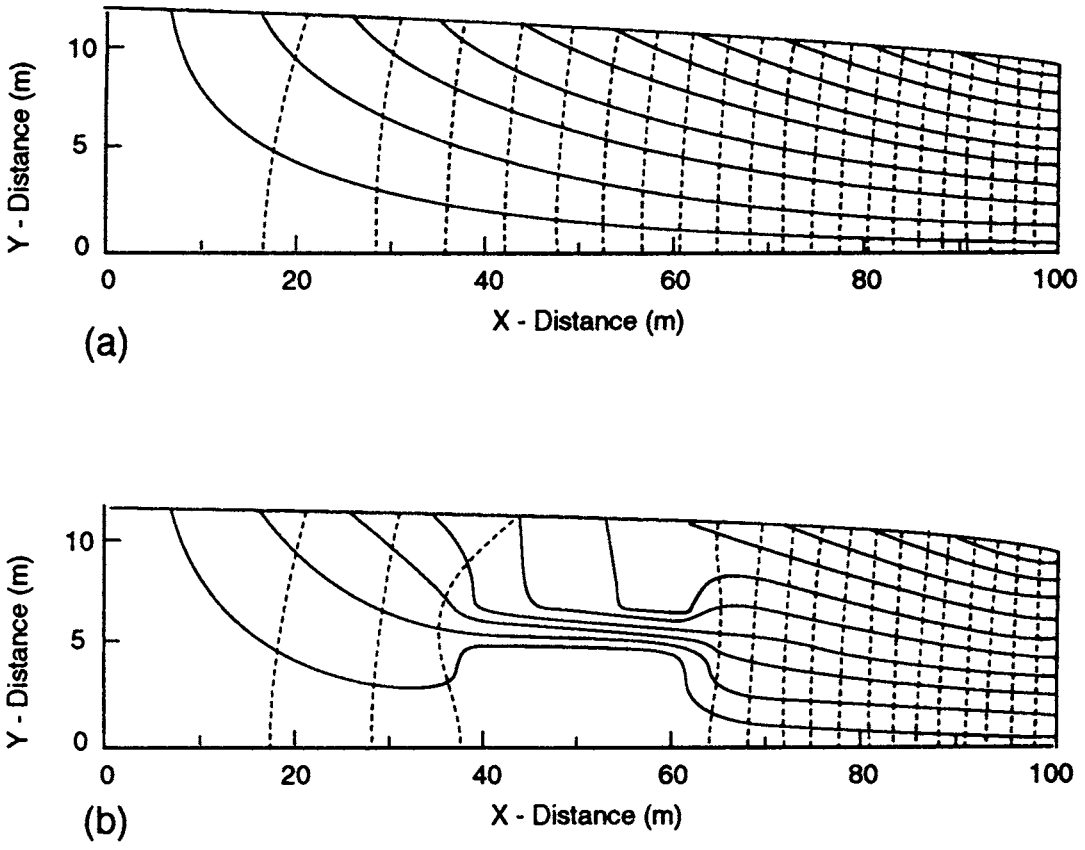

Figure 25: Flownet for cross-sectional flow system: (a) uniform material, $K=10^{-6}$ m/sec, (b) same material, except lens of $K=10^{-4}$ m/sec at center of system

this discontinuity is acceptable since the elemental parameters are integrated over the elements and the error due to the discontinuity is thereby minimized. In other approaches for the

solution of the transport equation, such as particle tracking, the discontinuity in the velocity field may not be acceptable.

We will here focus on two spatial dimensions and we will base the finite element solution on a general cartesian formulation which does not require coincidence between the coordinate axes and the principal directions. Since the numerical solution of the transport equation is sensitive with respect to time weighting, we use a general time-weighted approximation. In the absence of other information, however, a centred time weighting scheme usually gives the best accuracy in transport simulations. The finite element equation is:

$$\left\{\eta[M] + \frac{1}{\Delta t}[M^T]\right\}\{c\}_{k+1} = \left\{-(1-\eta)[M] + \frac{1}{\Delta t}[M^T]\right\}\{c\}_k + \{F^B\}$$

where η is the time weighting factor. The coefficient matrix [M] is made up of contributions as follows:

$$[M] = [M^D] + [M^V] + [M^\lambda] + [M^B]$$

where the matrices making up [M] are the dispersion, advection, decay, and boundary matrices, respectively, $[M^T]$ is the mass storage matrix, and $\{F^B\}$ is the mass flux boundary term. Both $[M^B]$ and $\{F^B\}$ arise from the third-type boundary condition. The elemental contributions to the above matrices, for linear triangles in a 2D domain, are as follows:

$$[M^D]^e = \frac{D_{xx}}{4\Delta}\begin{bmatrix} b_1b_1 & b_1b_2 & b_1b_3 \\ b_2b_1 & b_2b_2 & b_2b_3 \\ b_3b_1 & b_3b_2 & b_3b_3 \end{bmatrix} + \frac{D_{xy}}{4\Delta}\begin{bmatrix} b_1c_1 & b_1c_2 & b_1c_3 \\ b_2c_1 & b_2c_2 & b_2c_3 \\ b_3c_1 & b_3c_2 & b_3c_3 \end{bmatrix}$$

$$+ \frac{D_{yx}}{4\Delta}\begin{bmatrix} c_1b_1 & c_1b_2 & c_1b_3 \\ c_1b_1 & c_2b_2 & c_2b_3 \\ c_3b_1 & c_3b_2 & c_3b_3 \end{bmatrix} + \frac{D_{yy}}{4\Delta}\begin{bmatrix} c_1c_1 & c_1c_2 & c_1c_3 \\ c_2c_1 & c_2c_2 & c_2c_3 \\ c_3c_1 & c_3c_2 & c_3c_3 \end{bmatrix}$$

where D_{ij} are the components of the dispersion tensor, v_i are the velocity components, R is the

$$[M^V]^e = \frac{v_x}{6}\begin{bmatrix} b_1 & b_2 & b_3 \\ b_1 & b_2 & b_3 \\ b_1 & b_2 & b_3 \end{bmatrix} + \frac{v_y}{6}\begin{bmatrix} c_1 & c_2 & c_3 \\ c_1 & c_2 & c_3 \\ c_1 & c_2 & c_3 \end{bmatrix}$$

$$[M^\lambda]^e = \frac{R\lambda\Delta}{12}\begin{bmatrix} 2 & 1 & 1 \\ 1 & 2 & 1 \\ 1 & 1 & 2 \end{bmatrix}$$

$$[M^B]^e = \frac{L^e}{6}(v_x l_x + v_y l_y)\begin{bmatrix} 2 & 1 \\ 1 & 2 \end{bmatrix}$$

$$[M^T]^e = \frac{R\Delta}{12}\begin{bmatrix} 2 & 1 & 1 \\ 1 & 2 & 1 \\ 1 & 1 & 2 \end{bmatrix}$$

$$\{F^B\}^e = \frac{q_0 c_0}{\theta}\frac{L^e}{2}\begin{Bmatrix} 1 \\ 1 \end{Bmatrix}$$

retardation coefficient, q_0 is the recharge flux, c_0 is the solute concentration in the recharge flux, L^e is the length of the element side on the boundary, and l_x, l_y are the direction cosines of the inward normal at the boundary.

The above form of the mass storage matrix $[M^T]$ is known as the *consistent* form because the finite element interpolation is applied consistently to each term of the governing equation including the time derivative term. As an alternative, the *lumped* form can be obtained by adding the terms in each row of $[M^T]$ and placing the value on the diagonal. In each case, the sum of all the matrix terms must equal the total volume of the element. The consistent form gives slightly better accuracy in most applications, while the lumped form gives better convergence in some highly nonlinear problems.

A further contribution to the matrix equation is derived from the free exit boundary condition (Frind, 1988) which should be used whenever a contaminant plume reaches a domain boundary. This boundary condition does not require any known boundary values. The incorporation of the free exit boundary effectively moves the downstream boundary to infinity.

In contrast to the flow equation, the transport equation leads to an unsymmetric finite element matrix equation on account of the advective component. Standard transport models, therefore, use mostly the Gauss technique for the solution of the matrix equations. Alternatively, a special technique (Leismann and Frind, 1989) can be applied to make the transport matrix symmetrical; this facilitates solution by a highly efficient symmetrical conjugate gradient technique (Schmid and Braess, 1988).

The numerical solution of the transport equation proceeds in a stepwise manner starting with the given initial condition. If the flow system is at steady state, the flow solution is executed only once; if the flow system is transient, the flow solution must be coupled to the transport solution and executed at each time step.

Various nonlinearities can occur in the solution of the transport equation. For example, in the case of biological decay where the process depends on the availability of the reactants, the decay coefficient will be a function of the concentration of the various constituents. The mobile constituents will be represented by individual transport equations, while the immobile ones will be represented by appropriate mass balance relationships. During each time step, the solution procedure will iterate over all the transport equations while adjusting the decay coefficients until convergence occurs.

5.7 Numerical Dispersion and Numerical Constraints

Numerical dispersion is a term used to describe the numerical error that can arise in the solution of the transport equation. Its main cause is the presence of the advective term in the equation. Numerical dispersion can take the form of a smeared concentration profile, or it can cause oscillations of the profile resulting in negative concentrations or concentrations exceeding the source concentration.

In nonreactive transport, a moderate amount of numerical dispersion may be acceptable. In reactive transport, however, reactions taking place at some point in the aquifer depend on the concentration of the individual reactants at that point. Numerical inaccuracies can have profound effects on the results, as well as on the overall validity of the simulation. The control of numerical dispersion is therefore particularly vital in the simulation of reactive transport. Constraints on the numerical parameters that control numerical dispersion have been developed (Daus *et al.*, 1985).

Numerical dispersion is controlled by three factors: the spatial discretization, the time step, and the choice of the time weighting. The spatial discretization is constrained by the grid Peclet number criterion which is:

$$Pe = \frac{|\, v \,|\, \Delta L}{|\, D \,|} \leq 2$$

where $|v| = |q|/\theta$ is the magnitude of the velocity vector, $|D|$ is the effective dispersion coefficient in the direction of the velocity vector, and ΔL is the length of the element in the direction of flow. Letting $|D| = \alpha_L |v|$, the above relationship yields the constraint:

$$\Delta L \leq 2\alpha_L$$

which controls the grid spacing in the flow direction.

In practical situations, the requirement $P_e \leq 2$ cannot be easily satisfied everywhere. Fortunately, the solution is quite robust so that the occasional element exceeding the constraint (up to, say, Pe $\leq$ 4) will rarely cause difficulties. The Peclet criterion should, however, be satisfied on the average over the grid as a whole. In the direction transverse to the flow vector, the grid spacing is usually guided by the source configuration and by the expected transverse spreading behaviour, that is, a small transverse grid spacing should be chosen when the transverse dispersivity is small.

The time step is constrained by the grid Courant criterion, which is:

$$Cr = \frac{|\, v \,|\, \Delta t}{R\Delta L} \leq \frac{Pe}{2}$$

Letting Pe = 2, the time step Δt becomes:

$$\Delta t \leq \frac{R\Delta L}{|\, v \,|}$$

which physically means that a particle migrating at velocity |v| must not travel farther during one time step than the length of one element. This constraint should be satisfied for each element in the grid.

With respect to time weighting, the Taylor series expansion reveals that a centred scheme gives a higher accuracy (second-order) than either an explicit or an implicit scheme. Weighting more toward the implicit side will generally tend to dampen any oscillations that may be present, at the expense of additional smearing. Since this additional smearing has the appearance of physical dispersion due to a larger dispersivity, the results may be misleading and the use of implicit time weighting in solving the transport equation is therefore not

recommended. Overall, it has been found that reliable accuracy with essentially no numerical dispersion is obtained with a centred time weighting scheme and with the spatial and temporal discretization chosen in accordance with the grid Peclet and Courant constraints.

A further constraint on the time step arises on account of the mass loss due to decay (Luckner and Schestakow, 1986). This constraint is:

$$\Delta t \leq \frac{1}{\lambda}$$

which expresses the fact that the mass lost from any one element during a time step cannot be greater than the mass present in the element at the beginning of the time step. Exceeding this constraint will lead to negative concentrations, which, in the case of reactive systems, would cause the process to break down. Therefore this constraint must be rigorously observed.

Some of the numerical characteristics discussed above are illustrated in Figures 26, 27, and 28, which depict the solution of the 1D advection-dispersion equation under various conditions. The physical parameters are v=0.167 m/day and α=1.0 m. The boundary condition at the left is either of the first type with c/c_0=1.0 or the third type with q_0c_0/θ=0.167 m/day. The analytical solution for the first-type boundary condition, also known as the *Ogata-Banks* solution (Bear, 1979) is:

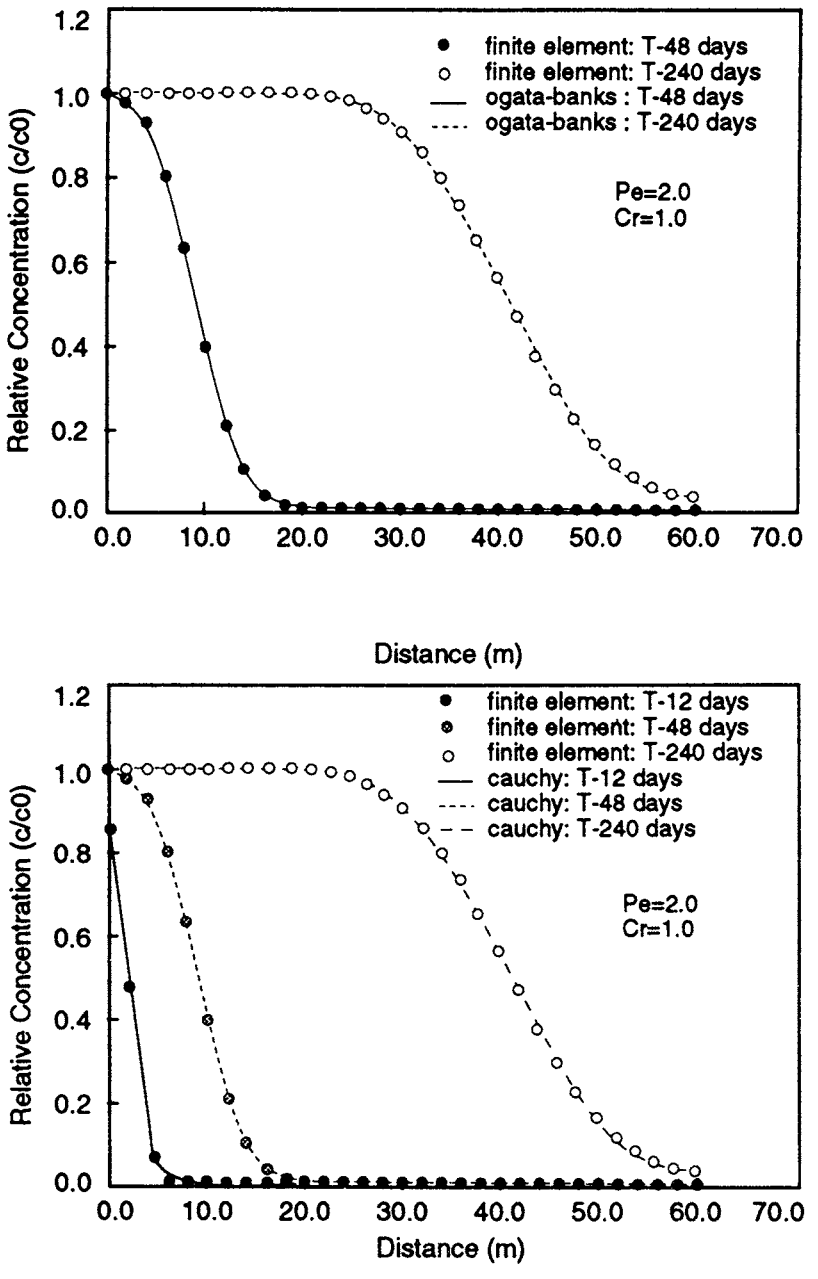

Figure 26: 1D advection-dispersion solution, numerical vs. analytical

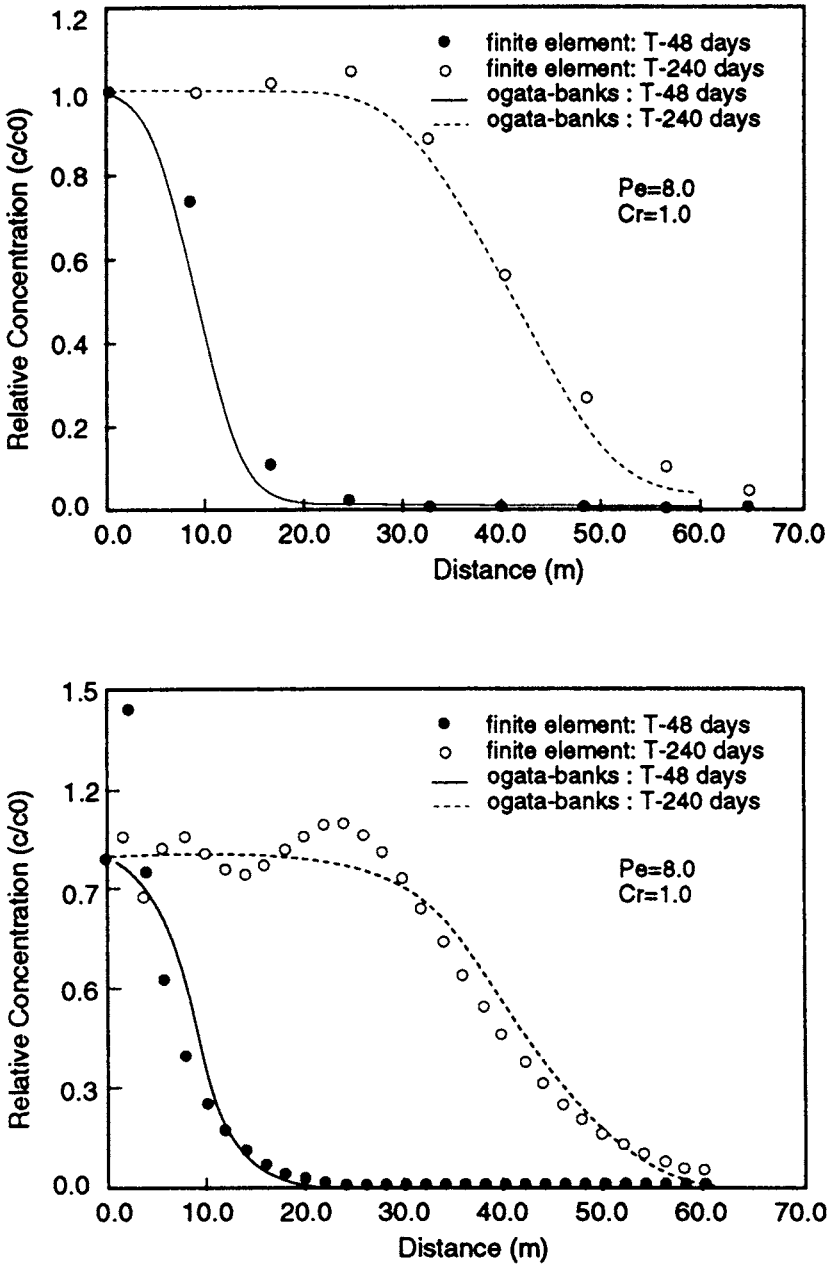

Figure 27: 1D advection-dispersion solution, numerical vs. analytical

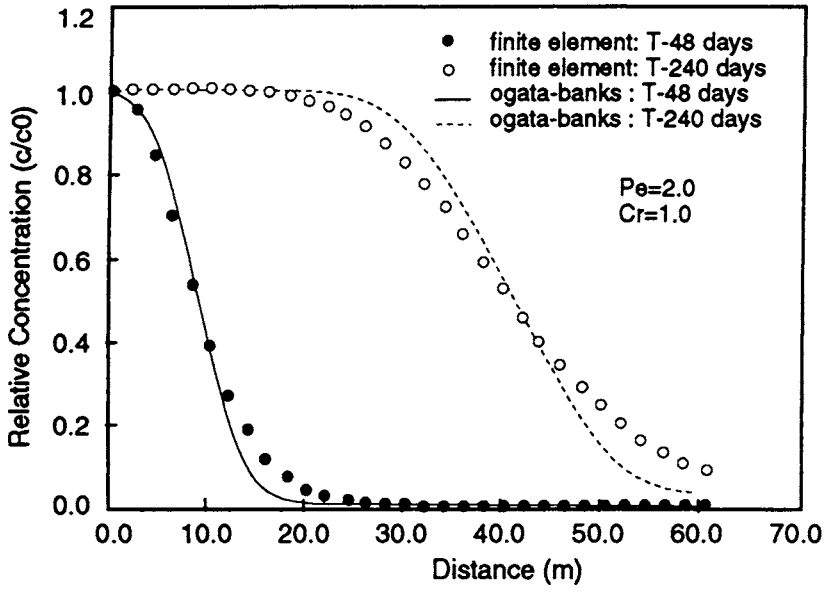

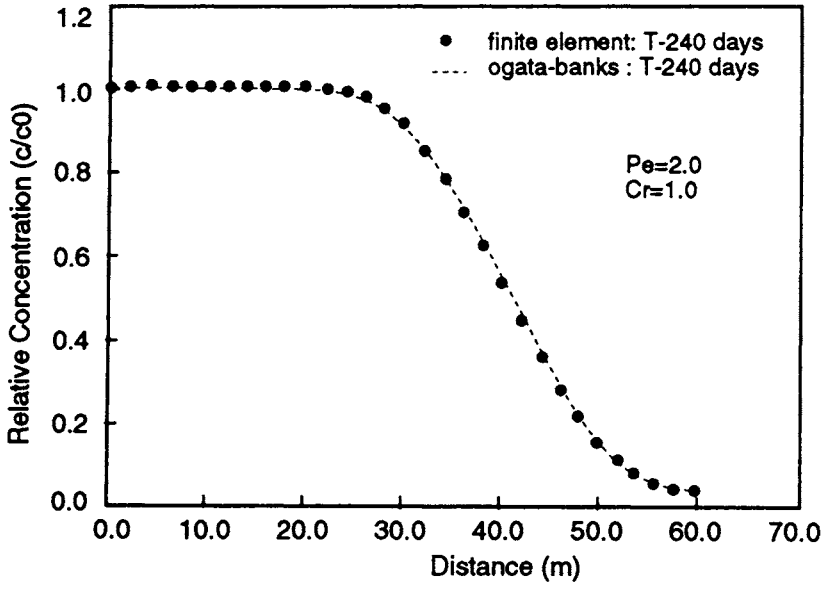

Figure 28: 1D advection-dispersion solution, numerical vs. analytical

$$\frac{c(x,t)}{c_0} = \frac{1}{2}\left[erfc\left\{\frac{x-vt}{2\sqrt{Dt}}\right\} + \exp\left\{\frac{vx}{D}\right\} erfc\left\{\frac{x+vt}{2\sqrt{Dt}}\right\}\right]$$

where the complementary error function erfc{.} is defined as:

$$erfc(u) = \frac{2}{\sqrt{\pi}} \int_u^\infty e^{-\xi^2} d\xi$$

The first term in the above solution gives the symmetric advection-dispersion profile, while the second term gives the effect of the first-type boundary which becomes smaller with increasing distance from the boundary.

The corresponding solution for the third-type boundary condition (Bear, 1979) is:

$$\frac{c(x,t)}{c_0} = \frac{1}{2}\left[erfc\left\{\frac{x-vt}{2\sqrt{Dt}}\right\} - \exp\left\{\frac{vx}{D}\right\} erfc\left\{\frac{x+vt}{2\sqrt{Dt}}\right\}\left\{1+\frac{vx+v^2t}{D}\right\}\right] + \frac{v\sqrt{t}}{\sqrt{\pi D}} \exp\left\{-\frac{(x-vt)^2}{4Dt}\right\}$$

Figure 26 is a comparison of the two types of boundary conditions. With the first-type boundary, the solution starts immediately at c/c_0=1.0, while with the third-type boundary, it starts at c/c_0=0 and gradually builds up to c/c_0=1.0. As a result, the mass input is greater during the early time period for the first-type boundary case, which has a constant mass input. Also the point where c/c_0=0.5 coincides with the point x=vt in the third-type boundary case, but is slightly ahead in the first-type boundary case. The two profiles approach each other with increasing time. Since the recommended spatial and temporal discretization is used and the time weighting is centred, the numerical solution closely agrees with the analytical solution

in both cases.

Figure 27 shows the effect of exceeding the discretization constraints. In Figure 27a, the grid spacing is four times the recommended value according to the Peclet constraint, the result is significant overshoot and smearing of the profile. In Figure 27b, the time step exceeds the value recommended by the Courant constraint by a factor of four; this also generates fairly large oscillations.

In Fig. 28a, an implicit (backward) time-weighting is used instead of a centred time weighting. This causes a marked smearing of the profile (compare with Fig. 26a). Figure 28b shows the effect of using a lumped mass storage matrix; the accuracy obtained with this formulation is comparable to that obtained with the consistent mass matrix (compare again with Fig. 26a).

5.8 Case Studies

There are numerous studies where models that are based on finite element methods have been used to predict groundwater flow and movement of contaminants in aquifers. The case study presented in Appendix 2 (Ophori and Farvolden, 1985) describes how a numerical model was used to evaluate the use of a hydraulic trap for preventing collector well contamination in the Forwell aquifer, Ontario, Canada. The source of contamination was described as an oil reclamation plant which operated over a period of approximately two decades. Contamination from the lagoons used for sludge waste disposal migrated through the aquifer, contaminating an estimated volume of 30,000 m^3 of groundwater.

The study describes extensive literature search and detailed pumping and recovery tests to characterize the aquifer. Hydraulic parameters obtained during the literature search and field tests were used as input into the numerical model developed to simulate groundwater flow near steady state field conditions. Triangular finite elements were used in the study, with finer mesh in the vicinity of the pumping wells. The model was calibrated by adjusting inferred

boundaries until the water levels predicted by the model were similar to observed data. The calibrated model was then used to determine the effect of a hydraulic trap in the form of a purge well which was intended to provide protection against contamination from the collector well.

Another study is presented in Appendix 3 where finite elements method was used to investigate a concept that would ordinarily be difficult to demonstrate. A 1D saturated-unsaturated flow model was applied to the transient drainage of water through a two-layer vertical column of porous media. The objective was to demonstrate the hydraulic principles involved in the use of fine-grained materials as protective covers for reactive mine tailings. The objective of installing the covers is to keep the materials at high moisture content thereby reducing the influx of oxygen into the reactive tailings. In the study provided in Appendix 3, emphasis was placed on the choice of materials which have appropriate physical properties to achieve the set objectives because of the dependence of observed response of the two-layer system on the retention characteristics of the component materials. The study further demonstrates how models could be used for the purpose of system design.

6. PARTICLE TRACKING METHODS

Particle tracking methods offer a valuable alternative to finite difference and finite element methods for simulating contaminant transport. In particle tracking, the distribution of a solute in the groundwater is represented by a finite number of particles, where each particle carried either a certain concentration or a certain fraction of the total mass. The particles are moved through the domain according to the velocity field, and their behaviour is observed. The status of the system at a given time can be deduced from the distribution of the particles. The accuracy and smoothness of the solution will depend on the number of particles used.

One of the main advantages of particle tracking is that the Peclet constraint on the grid spacing does not apply and that the type of numerical dispersion that is controlled by this

constraint does not occur. The method is therefore well-suited for advection-dominated problems, where the Peclet constraint would dictate a very fine spacial discretization if finite difference or finite element methods were applied. Freedom from the Peclet constraint, however, does not mean that the spatial discretization can be indiscriminately large since the accuracy of the final solution still depends on the grid resolution.

Before solving the transport equation by either finite differences, finite elements, or particle tracking, the velocity field must first be determined. This is usually accomplished by numerically differentiating the hydraulic heads obtained from the numerical solution of the flow equation. A major difference between finite elements and particle tracking lies in the manner in which the flow velocities are used in the transport calculations: In finite elements, velocities are used in an integrated form, while in particle tracking, they are used directly for advecting the particles. For this reason, element-wise discontinuous velocities are not acceptable in particle tracking. Sophisticated interpolation procedures are therefore used in order to obtain a continuous velocity field (Kinzelbach, 1986). The relative ease of implementation of these interpolation procedures when using rectangular grids leads to a preference for finite difference methods for the calculation of the heads in most particle tracking schemes.

A disadvantage of particle tracking is that nonlinear chemical or biochemical processes are not easily incorporated. The optimal use of particle tracking methods is thus in hydraulically-oriented situations, such as pump-and-treat remediation measures for groundwater contamination, or the delineation of groundwater protection zones. In purging situations, the key question to be addressed often concerns the optimal strategy for the hydraulic removal of a contaminant plume from the aquifer. Dispersion is of secondary importance in such cases.

6.1 The Method of Characteristics

One of the most popular transport codes today is the Method of Characteristics (MOC) code developed by Konikow and Bredehoeft (1978). To understand the method, the transport

process can be conveniently visualized by considering a single particle. The particle is carried along by the moving water and it experiences dispersion, sorption, and decay along the way. These processes are all linear and they can therefore be considered separately and superimposed. The particle is considered to be representative of some control volume and it is accordingly tagged with an initial concentration equivalent to the average concentration of that control volume. The particle moves along *pathlines* (the characteristic curves) in the velocity field (Fig. 29).

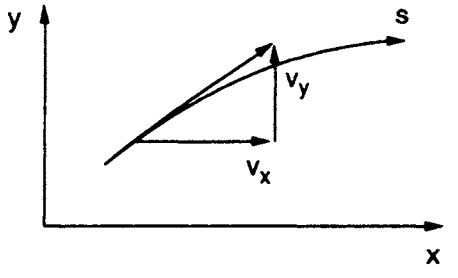

Figure 29: Pathline in 2D flow field

In two dimensions, the rate of change of concentration in the moving particle is given by the *substantial derivative*:

$$\frac{dc}{dt} = \frac{\partial c}{\partial t} + \frac{\partial c}{\partial x}\frac{dx}{dt} + \frac{\partial c}{\partial y}\frac{dy}{dt}$$

where the first term on the right-hand side represents the changes experienced by the moving particle and the remaining terms represent the changes due to the motion of the particle. The *characteristic equations* are:

$$\frac{dx}{dt} = v_x$$

and

$$\frac{dy}{dt} = v_y$$

where v_x,v_y represent the velocity components. The above equations are known as the incompressible form of the *Euler equations*. In the absence of sources or sinks and no dispersion or decay, we have:

$$\frac{\partial c}{\partial t} = v_x\frac{\partial c}{\partial x} + v_y\frac{\partial c}{\partial y} = 0$$

so that:

$$\frac{dc}{dt} = 0$$

Therefore, the concentration of the moving particle will remain the same in the non-dispersive and non-reactive case. The displacement of the particle up to time t is expressed exactly by integrating along the pathline equation:

$$x(t)=x_0 + \int_{t_0}^{t} v_x(x(\tau),y(\tau))d\tau$$

$$y(t) = y_0 + \int_{t_0}^{t} v_y(x(\tau),y(\tau))d\tau$$

where x_0, y_0, t_0 are the starting point and time, and τ is the integration variable. In the numerical solution, the finite displacement during the time interval from t to t+Δt is

determined by performing an equivalent but approximate numerical integration (Fig. 30):

$$x(t+\Delta t) = x(t) + v_x(x(t),y(t))\Delta t$$

$$y(t+\Delta t) = y(t) + v_y(x(t),y(t))\Delta t$$

Since the velocity at the starting point is used here, the calculation represents an explicit (upstream) approximation, which is first-order accurate. Alternatively, center-weighted procedures can be used that iteratively calculate the advective displacement in terms of the average of the velocities at the old and new positions, giving second-order accuracy.

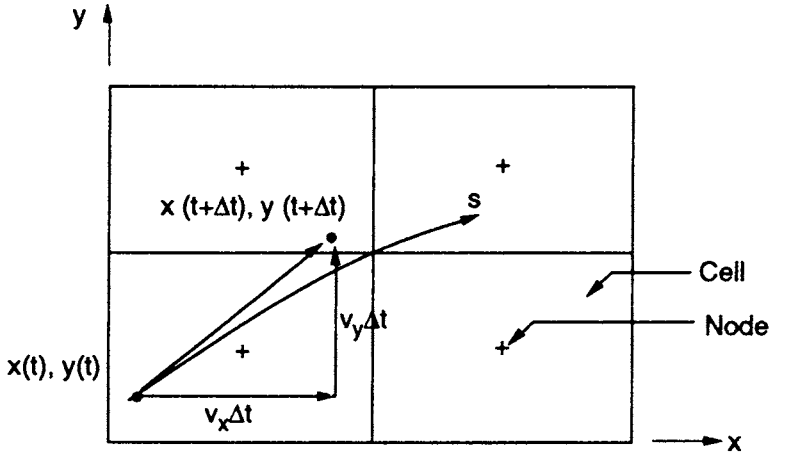

Figure 30: Advective displacement of a particle

The processes of dispersion, decay, and retardation can be considered separately in the MOC. If dispersion were to occur in addition to advection, the term expressing the change of concentration of the moving particle (see substantial derivative equation) will become:

$$\frac{\partial c}{\partial t} = \frac{\partial}{\partial x_i}\left(D_{ij}\frac{\partial c}{\partial x_j}\right)$$

which is the pure-dispersion equation for the moving particle.

Since dispersion is a process that redistributes mass, the solution of the above equation requires consideration of all particles together. The solution is analogous to the procedure discussed in Section 3.2. For example, for a uniformly-spaced grid where the coordinate axes coincide with the principal directions of the dispersion tensor, the explicit calculation will yield a dispersive change over the time step Δt at particle location i,j (Fig. 31) given by:

$$\Delta c_{i,j} = c(t+\Delta t)_{i,j} - c(t)_{i,j} = \Delta t\, D_{xx}\left\{\frac{c_{i-1,j} - 2c_{i,j} + c_{i+1,j}}{(\Delta x)^2}\right\}_t + \Delta t D_{yy}\left\{\frac{c_{i,j-1} - 2c_{i,j} + c_{i,j+1}}{(\Delta y)^2}\right\}_t$$

where the right-hand side is entirely in terms of the concentrations at the old time level. A more general procedure valid for an arbitrary coordinate orientation and variable coefficients, which requires 9 nodal points for the calculation of $\Delta c_{i,j}$, is discussed by Kinzelbach (1986). In order to obtain the regular grid pattern required for the dispersive calculation, the particles must be reassigned (with suitable concentration adjustments) to the cell centers prior to the dispersive calculation.

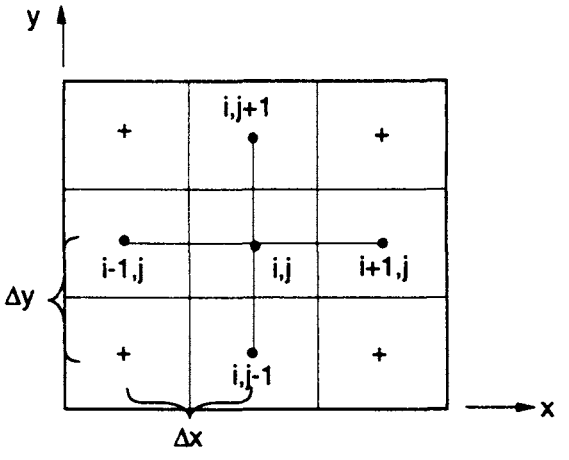

Figure 31: Particle pattern for explicit calculation of dispersive transport component

The above explicit calculation is subject to the stability constraint:

$$\Delta t \left(\frac{D_{xx}}{(\Delta x)^2} + \frac{D_{yy}}{(\Delta y)^2} \right) \leq \frac{1}{2}$$

Alternatively, an implicit solution procedure can be used which avoids the stability constraint. Konikow and Bredehoeft (1978) use the explicit procedure.

Decay is a process that operates on each particle individually. The change experienced by the moving particle is in that case given by:

$$\frac{\partial c}{\partial t} = -\lambda c$$

and the finite change Δc over the time step Δt is accordingly:

$$\Delta c = c(t+\Delta t) - c(t) = -\lambda c(t)\Delta t$$

The change calculated for each particle is added to the existing particle concentration.

Linear sorption can be incorporated easily by dividing the velocity v and the dispersion coefficient D by the retardation coefficient (R), which is given by:

$$R = 1 + \frac{\rho_b}{\theta} K_d$$

The effect of this process will be a slowing down of the advective advance and the spreading.

Observance of the grid Courant constraint is necessary in all particle tracking procedures in order to limit particle migration to no more than one cell length per time step. If this constraint were exceeded, particles would literally jump across intervening cells, and the information resident in those cells would remain unused. This constraint is independent of the stability constraint that applies to the explicit solution of the dispersive transport component. Although a formal constraint on the grid spacing, analogous to the Peclet constraint, does not exist in particle tracking methods, the grid spacing nevertheless controls the resolution of the velocity field, and hence the accuracy of the simulation. Therefore, a reasonably fine cell spacing should be used in areas of large gradient changes. If dispersion is included, particles must be distributed throughout the domain, including areas that initially have zero concentration, to allow for the spreading of the plume.

6.2 Capture Zones and Plume Purging

The travel time T of a particle along its pathline can be computed easily by accumulating the time steps:

$$T = \sum_k \Delta t_k$$

By releasing particles along a contaminant front and recording their position at specified time levels, the advective advance of a front can be displayed at different times.

A useful concept in groundwater protection is the *capture zone* of a well, which is defined as the zone within which all water is eventually captured by the well. A capture zone can be generated by starting a number of particles around the periphery of the well and tracking them in the reverse flow direction. The capture zone is time-dependent and it will continue to expand until the withdrawal at the well is balanced by recharge from the surface, from neighbouring aquifers, or from the boundaries. If the well is a water supply well, the capture zone will define the zone that is sensitive to contamination and that may be designated as a *groundwater protection zone*. Figure 32 shows typical time-related capture zones associated with a single pumping well in a uniform flow field for 3 different points in time.

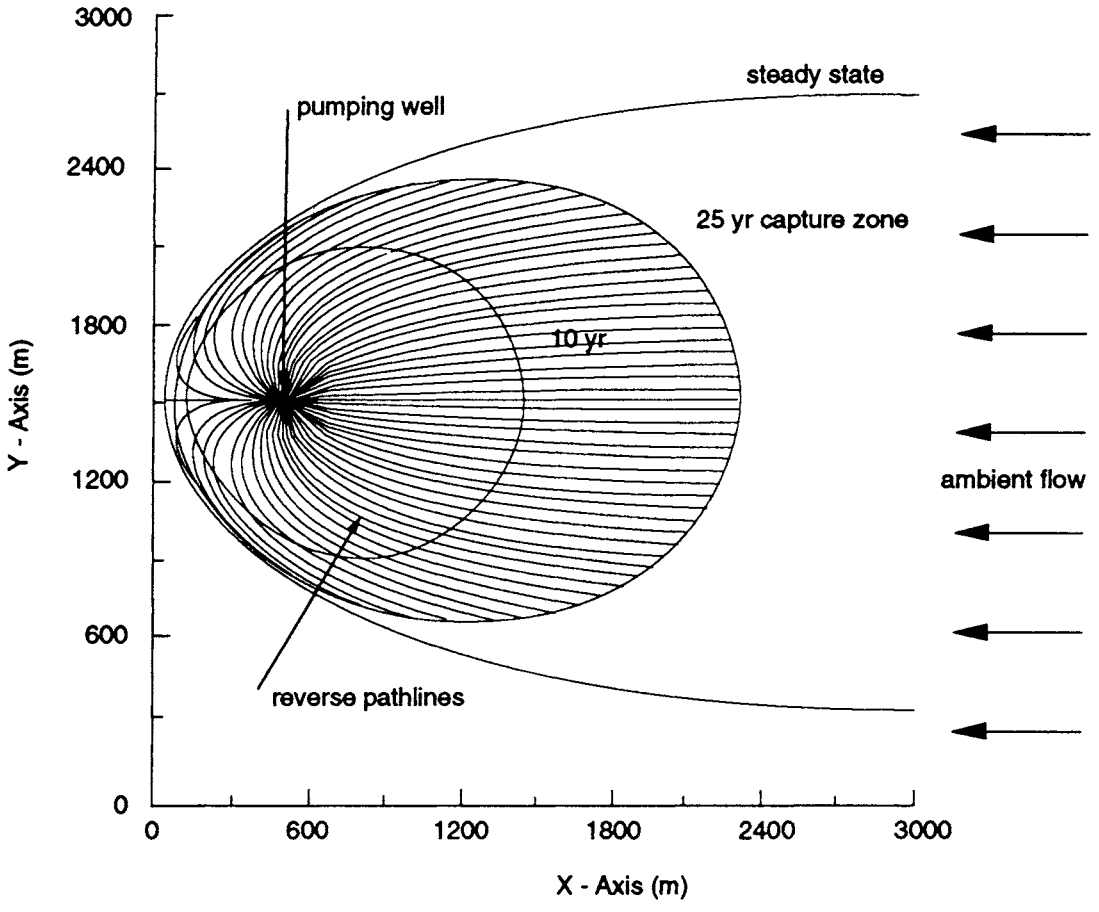

Figure 32: Pathlines and capture zones in a uniform flow field

The capture zone concept is also useful in the context of hydraulic purging of groundwater contamination. If the extent of contamination is known, the purge well can be placed in such

a way that its capture zone encompasses the plume. The purging operation can then be simulated by tracking the particles representing the boundary of the capture zone back to the well. Questions such as the optimal location of the purge well or wells, and the time required for plume removal, are usually of prime interest in the planning of the operation.

In the case of plume purging, the plume will be in a condition of maximal dispersal prior to purging. The additional dispersion occurring during the purge operation is therefore of little interest and the dispersive transport component can be justifiably neglected. Linear adsorption/desorption as well as first-order decay may be of interest and can be included. Overall, however, the most important transport component in such situations is the advective component. The MOC, in its advective mode, is therefore well suited for handling such situations.

One aspect that may play a role in plume purging is the fact that contaminant mass can be retained in low-conductivity zones within a heterogeneous aquifer. Thus a significant portion of the mass may still be in the aquifer even though the hydraulic remediation would indicate complete removal of the plume. This is known as the *dual porosity* phenomenon, which, unfortunately, is not easily incorporated into the MOC.

6.3 The Random Walk Method

The Random Walk Method (Prickett *et al.*, 1981) differs from the MOC in that each particle represents a fixed mass, so that the sum of all particle masses equals the total mass in the system. Particles are displaced advectively and dispersively. For simplicity, we will here consider a 1D system. In this case, the advective-dispersive displacement of a particle with respect to its initial position is given by (Fig. 33):

$$v = vt + \rho\sqrt{2Dt}$$

where $\rho \sim N(0,1)$ is a normally-distributed random variable with mean = 0 and standard deviation = 1, and where $D = \alpha v$. The random variable ρ is obtained from a random number generator.

The time stepping scheme for the 1D problem therefore becomes:

$$x(t+\Delta t) = x(t) + v\Delta t + \rho\sqrt{2\alpha v\Delta t}$$

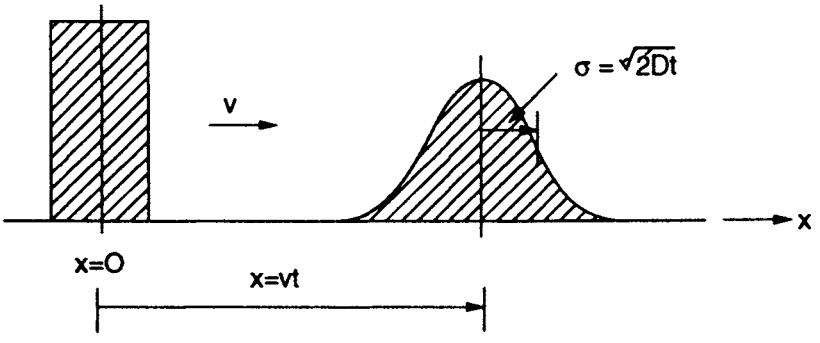

Figure 33: Advective-dispersive displacement in Random Walk Method

This is again an explicit procedure having first-order accuracy. The corresponding 2D formulation is similar.

A problem arises here (Kinzelbach, 1986) in that the advective-dispersive displacement calculated by the above equation represents a solution not to the advection-dispersion equation:

$$\frac{\partial c}{\partial t} + \frac{\partial (vc)}{\partial x} - \frac{\partial}{\partial x}\left(D\frac{\partial c}{\partial x}\right) = 0$$

but to the slightly different equation:

$$\frac{\partial c}{\partial t} + \frac{\partial (vc)}{\partial x} - \frac{\partial^2 (Dc)}{\partial x^2} = 0$$

In order to amend this discrepancy, a correction is added to the velocity term giving:

$$v^*(x,t) = v(x,t) + \frac{\partial D(x,t)}{\partial x}$$

The correction $\partial D/\partial x$ is applied whenever the dispersion coefficient $D=\alpha v$ varies on account of either a variable velocity or a variable dispersivity or both. The corrected velocity v^* is used in the calculation of the advective displacement.

A scale-dependent dispersivity can be incorporated in the random walk method by utilizing some suitable function that would take on the value of the local dispersivity at the source, and that would increase asymptotically to the field value over a travel distance of about 40 to 50 correlation lengths of the statistically homogeneous medium. Linear sorption and first-order decay can also be incorporated in the same way as in the MOC.

The number of particles required in the Random Walk Method is controlled primarily by the requirement to have a sufficient number of particles left in low-concentration zones (the fringes of the plume) for the calculation of concentrations. Thus the anticipated dispersion, retardation, and decay mechanisms must be considered when selecting particle populations.

7. REFERENCES

Akindunni, F.F. 1987. Effect of the capillary fringe on unconfined aquifer response to pumping: Numerical simulations. Ph.D. thesis, Earth Sciences Department, University of Waterloo.

Akindunni, F.F. and R.W. Gillham. 1992. Unsaturated and Saturated Flow in Response to Pumping of an Unconfined Aquifer: Numerical Investigation of Delayed Drainage. *Ground Water (In Press).*

Akindunni, F.F., R.W. Gillham and R.V. Nicholson. 1991. Numerical simulations to investigate moisture-retention characteristics in the design of oxygen-limiting covers for reactive mine tailings. *Canadian Geotechnical Journal*, Vol. 28, 446-451.

Bear, J., 1979. *Hydraulics of Groundwater.* McGraw-Hill, New York, N.Y.

Bear, J. and A. Verruijt. 1987. *Modeling Groundwater Flow and Pollution.* D. Reidel Publishing Company.

Carslaw, H.S., and J.C. Jaeger, 1946. *Conduction of Heat in Solids.* Oxford University Press, Oxford, U.K.

Daus, A.D., E.O. Frind and E.A. Sudicky, 1985. Comparative error analysis on finite element formulations of the advection-dispersion equation. *Advances in Water Resources,* Vol. 8 (June), 86-95.

de Lima V.A. and J.C. Olimpio, 1984. Hydrogeology and simulation of groundwater flow at a superfund-site wells G and H, Woburn, Massachussets; USGS Open File Report 84-475.

Freeze, R.A., and J.A. Cherry, 1979. *Groundwater.* Prentice-Hall, Englewood Cliffs, N.J.

Frind, E.O., 1979. Exact aquitard response functions for multiple aquifer mechanics. *Advances in Water Resources,* Vol. 2 (June), 77-82.

Frind, E.O., 1988. Solution of the advection-dispersion equation with free exit boundary. *Numerical Methods for Partial Differential Equations,* Vol. 4, 301-314.

Frind, E.O.,W.H.M. Duynisveld, O. Strebel, and J. Boettcher, 1990. Modelling of multi-component transport with microbial transformation in groundwater: The Fuhrberg Case. *Water Resour. Res.,* 26(8), 1707-1719.

Frind, E.O. and G.B. Matanga, 1985. The dual formulation of flow for contaminant transport modeling: 1. Review of theory and accuracy aspects. *Water Resour. Res.,* 21(2), 159-169.

Frind, E.O., G.B. Matanga and J.A. Cherry, 1985. The dual formulation of flow for contaminant transport modeling: 2. The Borden Aquifer. *Water Resour. Res.,* 21(2), 170-182.

Frind, E.O. and J.W.H. Molson, 1989. On the relevance of the transport parameters in predictive modelling of groundwater contamination. In *Groundwater Management: Quality and Quantity,* IAHS Publ. No. 188, (Eds. A. Sahuquillo, et al.), 331-347.

Frind, E.O., E.A. Sudicky, and S.L. Schellenberg, 1987. Micro-scale modelling in the study of plume evolution in heterogeneous media. *Stochastic Hydrology and Hydraulics,* 1(4), pp. 263-279.

Gelhar, L.W., and C.L. Axness, 1983. Three-dimensional stochastic analysis of macrodispersion in aquifers. *Water Resour. Res.,* 19(1), 161-180.

Hildebrand, F.B., 1965. *Advanced Calculus for Applications.* Prentice-Hall, Englewood Cliffs, N.J.

Huyakorn, P.S., and G.F.Pinder, 1983. *Computational Methods in Subsurface Flow.* Academic Press, Orlando, Fla.

Kinzelbach, W., 1986. *Groundwater Modelling.* Elsevier, Amsterdam.

Konikow, L.F., and J.D.Bredehoeft, 1978. Computer model of two-dimensional solute transport and dispersion in groundwater. Techniques of Water Resources Investigations, U.S. Geological Survey, 7(C2), U.S. Govt. Printing Office, Washington, D.C.

Leismann, H.M., and E.O. Frind, 1989. A symmetric-matrix time integration scheme for the efficient solution of advection-dispersion problems. *Water Resour. Res.*, 25(6), 1133-1139.

Luckner, L., and W.M. Schestakow, 1986. *Migrations prozesse im Boden- und Grundwasserbereich.* VEB Deutscher Verlag fuer Grundstoffindustrie, Leipzig.

Molson, J., E.O. Frind and E.A. Sudicky. Use of Groundwater Flow and Transport Models, in "*Contaminated Site Handbook*", (In Preparation).

Nwankwor, G.I., R.W. Gillham, G. van der Kamp and F.F. Akindunni. 1992. Unsaturated and Saturated Flow in Response to Pumping of an Unconfined Aquifer: Field Evidence of Delayed Drainage. *Ground Water (In Press).*

Ophori, D.U. and R.N. Farvolden. 1985. A hydraulic trap for preventing collector well contamination: A case study. *Ground Water*, Vol . 23, pp 600-610.

Pinder, G.F., and E.O. Frind, 1972. Application of Galerkin's procedure to aquifer analysis, *Water Resour. Res.* 8(1) 108-120.

Prickett, T.A., T.G. Naymik, and C.G. Lonnquist, 1981. A "random walk" solute transport model for selected groundwater quality evaluations. Illinois State Water Survey, Bulletin 65.

Ragone, S.E., 1986 (editor). USGS program on toxic waste-groundwater contamination, Proceedings of the second technical meeting, Cape Cod, Massachusetts. USGS Open File Report 86-481.

Rudolph, D.L., and E.A. Sudicky, 1990. Simulation of groundwater flow in coupled multiaquifer systems: Performance of a quasi three-dimensional technique in the steady state case. *Canadian Geotechnical Journal*, Vol. 27, 590-600.

Schmid, G., and D. Braess, 1988. Comparison of fast equation solvers for groundwater flow problems. In *Groundwater Flow and Quality Modelling*, NATO ASI Series C, Vol. 224, (Eds. E. Custodio et al.) 173-188. D. Reidel, Dordrecht.

Sudicky, E.A., 1986. A natural gradient tracer experiment on solute transport in a sand aquifer: Spatial variability of hydraulic conductivity and its role in the dispersion process. Water Resour. Res., 22(13), 2069-2082.

Sudicky, E.A., J.A. Cherry and E.O. Frind, 1983. Migration of contaminants in groundwater at a landfill: A case study. 4. A natural gradient tracer test. Journal of Hydrology, Vol. 63, Nos. 1-2, 81-108.

Tsang, Chin-Fu. 1991. The Modeling Process and Model Validation. *Groundwater.* 29(6):825-831.

Wang, H.F. and M.P. Anderson. 1982. *Introduction to Groundwater Modeling Finite Difference and Finite Element Methods*. W.H. Freeman and Company.

Wexler, E.J., 1989. Analytical Solutions for One-, Two-, and Three-Dimensional Solute Transport in Groundwater Systems with Uniform Flow. U.S. Geological Survey, Rep. 89-56. Tallahassee, Fla.

Zienkiewicz, O.C., 1971. *The Finite Element Method in Engineering Science*. McGraw-Hill, London.

8. GLOSSARY

Adsorption. The assimilation of fluid (gas, vapour, or dissolved matter) by the surface of a solid.

Advection. The process by which solutes are transported by the bulk motion of the flowing groundwater.

Air Stripping. A process of mass transfer by which a substance in groundwater is transferred to solution in a gas, usually air.

Alluvium. A general term used for clay, silt, sand, gravel, or other unconsolidated material deposited during comparatively recent geologic time by a stream or other body of running water as a sorted or semisorted sediment in the bed of the stream or on its floodplain or delta, or as a cone or fan at the base of a mountain slope.

Anisotropic. Having some physical property (eg hydraulic conductivity) that varies with direction of measurement.

Aquiclude. A saturated geologic unit that does not transmit water freely to a well or spring under ordinary hydraulic gradients.

Aquifer. A saturated geologic unit that can transmit economical quantities of groundwater to wells and springs under ordinary hydraulic gradients.

Aquifer Test. A test involving the withdrawal of measured quantities of water from or addition of water to a well and the measurement of resulting changes in head in the aquifer both during and after the period of discharge or addition.

Aquitard. A geologic unit through which virtually no groundwater moves.

Bedrock. A general term used for the rock, usually solid, that underlies soil or other unconsolidated material.

Capillary Fringe. The saturated zone at the bottom of the vadose zone where groundwater exists under negative pressure, having been drawn upward by capillary force.

Coefficient of Permeability. See Hydraulic Conductivity.

Coefficient of Storage. The volume of water an aquifer releases from or takes into storage per unit surface area of the aquifer per unit change in hydraulic head.

Coefficient of Transmissivity. See Transmissivity.

Cone of Depression. A depression in the groundwater table or potentiometric surface that develops around a well from which water is being withdrawn.

Confined Aquifer. A saturated geologic unit in which the groundwater is isolated from the atmosphere at the point of discharge by impermeable geologic formations and generally contains groundwater that exists at a pressure greater than atmospheric.

Contamination. The degradation of natural water quality as a result of human activities. There is no implication of any specific limits, since the degree of permissible contamination depends upon the intended end use, or uses, of the water.

Darcy's Law. A derived equation for the flow of fluids relating volumetric fluid flux to hydraulic gradients. It is based on the assumption that the flow is laminar and that inertia can be neglected.

Dispersion. The spreading and mixing of chemical constituents in groundwater caused by diffusion and mechanical mixing due to microscopic variations in velocities within and between pores.

Drawdown. The distance between the static water level and the surface of the cone of depression.

Effluent. A waste liquid discharge from a manufacturing or treatment process, in its natural state or partially or completely treated, that discharges into the environment.

Equipotential Line. A line along which the pressure head of groundwater in an aquifer is the same. Fluid flow is perpendicular to these lines in the direction of decreasing hydraulic head.

Evapotranspiration. Loss of water from a land area through transpiration of plants and evaporation from the soil.

Flow Lines. Lines indicating the direction followed by groundwater toward points of discharge. Flow lines are perpendicular to equipotential lines.

Groundwater Table. The surface where pressure head is zero in a saturated geologic unit. It is approximated by the top surface of an unconfined aquifer.

Head. Energy contained in a water mass, produced by elevation, pressure, or velocity.

Head Loss. That part of head energy which is lost because of friction as water flows.

Heterogeneous. Nonuniform in structure or composition throughout.

Homogeneous. Uniform in structure or composition throughout.

Hydraulic Conductivity. The rate of flow of a unit volume of groundwater through a unit cross sectional area and under a unit hydraulic gradient, at the prevailing temperature.

Hydraulic Gradient. The rate of change in hydraulic head per unit change of distance of groundwater flow measured along a given direction.

Hydraulic Head. Energy per unit weight of groundwater, produced by elevation and pressure.

Hydrogeologic. Those factors that deal with subsurface waters and related geologic aspects of surface waters.

Intrinsic Permeability. See Permeability.

Isotropic. Having physical properties that are the same in all directions.

Laminar Flow. Water flow in which the stream lines remain distinct and in which the flow direction at every point remains unchanged with time. It is characteristic of the natural movement of groundwater.

Landfill. A general term indicating a location where refuse, dirt from excavations, household garbage, etc. are disposed.

Leachate. The liquid that has percolated through solid waste and dissolved soluble components.

Limestone. A sedimentary rock consisting mainly of calcium carbonate which exists primarily in the form of the mineral calcite.

Molecular Diffusion. Dispersion of a chemical caused by the kinetic activity of the ionic or molecular constituents.

Observation Well. A well drilled in a selected location for the purpose of observing parameters such as water levels and pressure changes.

Overburden. The loose soil, silt, sand, gravel, or other unconsolidated material overlying bedrock, either transported or formed in place.

Partial Penetration. When the intake portion of the well is less than the full thickness of the aquifer.

Perched Water. Unconfined groundwater separated from an underlying main body of groundwater by an unsaturated zone.

Percolate. The act of water seeping or filtering through the soil without a definite channel.

Permeability. The property or capacity of a porous rock, sediment, or soil for transmitting a fluid; it is a measure of the relative ease of fluid flow under unequal pressure.

Pollution. A term used when the contamination concentration levels restrict the potential use of groundwater.

Porosity. The percentage of the bulk volume of a rock or soil that is occupied by interstices, whether isolated or connected.

Potentiometric Surface. An imaginary surface representing the hydraulic head of groundwater in a confined aquifer that is defined by the level to which water will rise in a well that is installed in the aquifer.

Pumping Test. A test involving water level measurements as groundwater is withdrawn from a well. It is conducted to determine aquifer or well characteristics.

Recharge. The process of adding water to the zone of saturation or the amount of water thus added.

Specific Yield. The volume of water an unconfined aquifer releases from storage per unit surface area of the aquifer per unit decline of watertable.

Static Water Level. The level of water in a well that is not being affected by withdrawal of groundwater.

Storage Coefficient. See Coefficient of Storage.

Storativity. See Coefficient of Storage.

Till. Predominantly unsorted and unstratified drift, generally unconsolidated, deposited directly by and underneath a glacier without subsequent reworking by meltwater, and consisting of a heterogeneous mixture of clay, silt, sand, gravel, and boulders ranging widely in size and shape.

Tortuosity. A term used to describe the sinuosity of the actual flow path in a porous medium. It is evaluated as the ratio of the length of the flow path to the length of the sample.

Transmissibility. See Transmissivity.

Transmissivity. The rate at which groundwater is transmitted through a unit width of an aquifer under a unit hydraulic gradient.

Transpiration. The process by which water absorbed by plants, usually through the roots, is evaporated into the atmosphere from the plant surface.

Turbulent Flow. Water flow in which the flow lines are confused and heterogeneously mixed.

Unconfined Aquifer. An aquifer where the water table is exposed to the atmosphere through openings in the overlying materials.

Vadose Zone. The zone containing water under pressure less than that of the atmosphere. This zone is limited above by the ground surface and below by the water table.

Viscosity. The property of a substance to offer internal resistance to flow. Specifically, the ratio of the shear stress to the rate of shear strain.

Water Table. The surface (ie. surface of zero pressure head) at which the pressure is equal to that of the atmosphere.

APPENDICES

APPENDIX 1

NUMERICAL SIMULATION OF GROUNDWATER FLOW

AT A SUPERFUND SITE:

CAPE COD STUDY

Cape Cod Study[1]

Background

- site studied as part USGS program
- treated sewage through infiltration beds to aquifer since 1936 - 0.46 Mgal/d
- plume 11,000 ft long, 3000 ft wide and 75 ft thick
- chloride, detergents, boron, and 100 organic compounds (e.g., trichloroethene, tetrachloroethene dichlorobenzene)

Objectives in Modeling

- early stage - to understand processes and predict system response
- our use - to understand how models set up and applied

[1]Adapted from USGS Open-File Rep. 84-475; 86-481

Geology

- glacial deposits overlying crystalline bedrock
- uppermost 90-140 ft stratified sand and gravel overlies silty sand and till

Hydrogeology

- hydraulic conductivity - 380 ft/d
- estimated, average groundwater velocity 1.5 ft/d

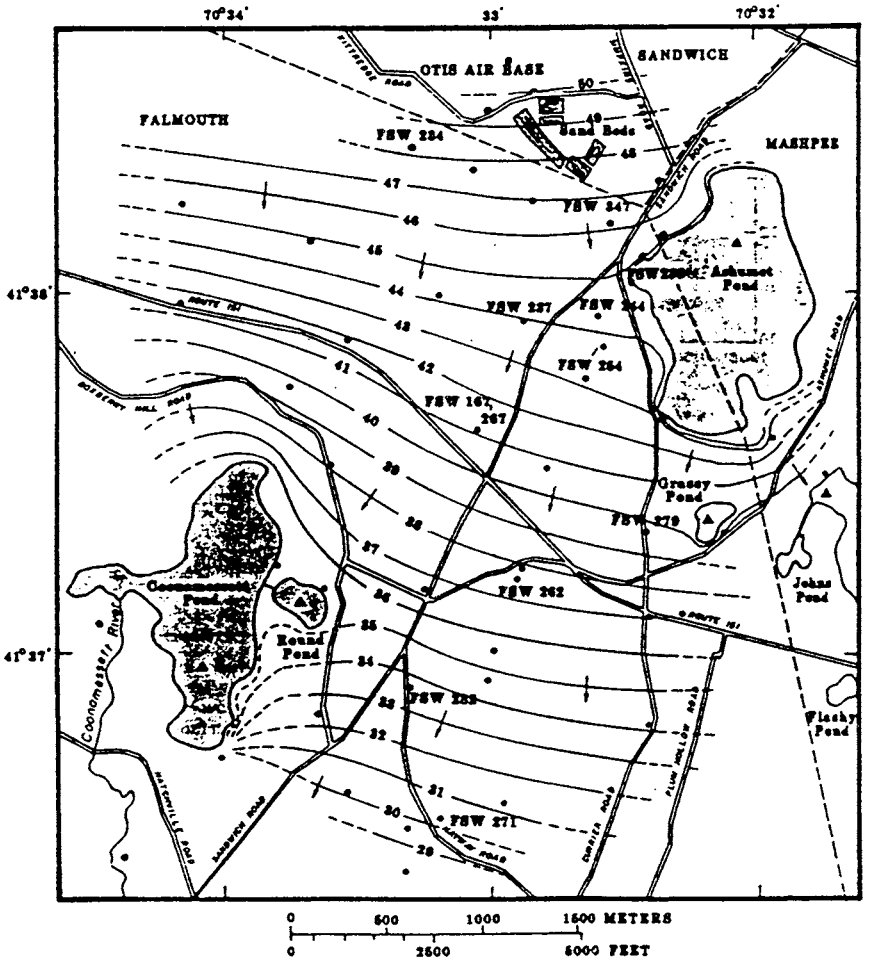

35 --- WATER-TABLE CONTOUR, NOVEMBER, 1979—Shows altitude of water table. Contour interval 1 foot. Datum is sea level. Arrows show direction of ground-water movement. Contours dashed where inferred.

FSW 234 • WATER-LEVEL OBSERVATION WELL—Number is well designation used in tables 2 and 4.

▲ POND AT WHICH WATER LEVEL WAS MEASURED

Plume Geometry

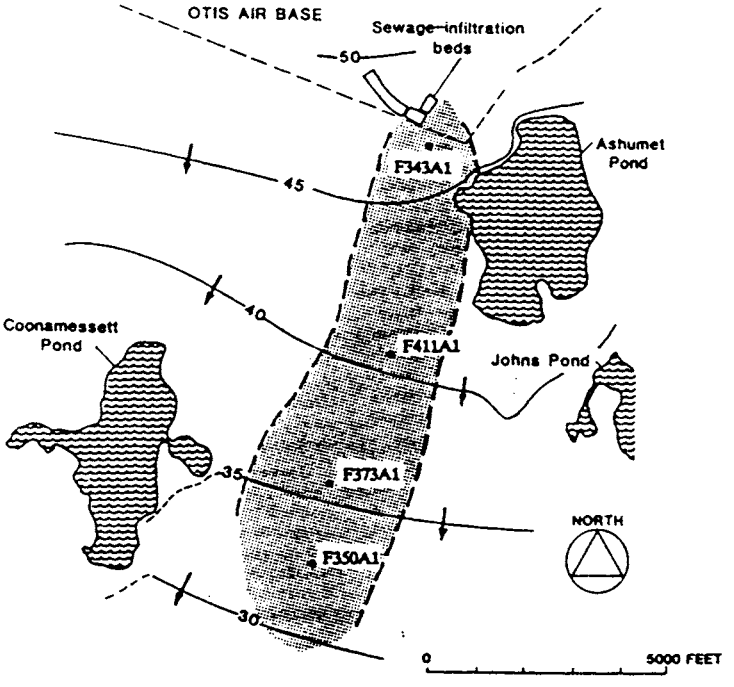

EXPLANATION

GENERAL AREA OF PLUME OF SEWAGE-CONTAMINATED GROUND WATER, AUGUST 1985—Area delineated by field observations of elevated specific conductance and foaming caused by detergents

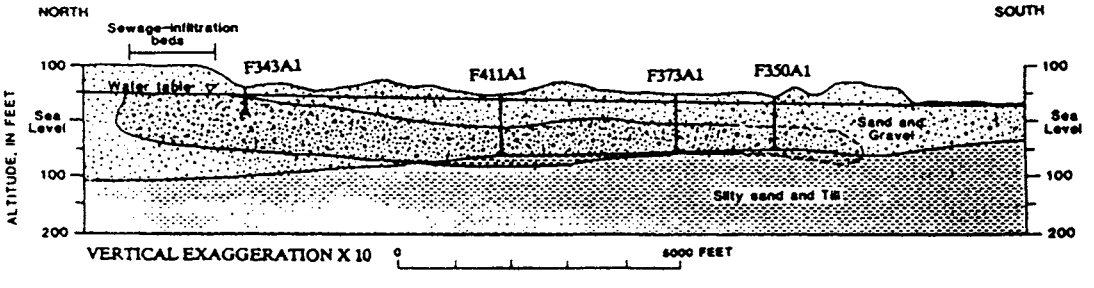

Critical Steps in Developing a Model

- processes involved?
- equations to describe these processes?
- region shape -

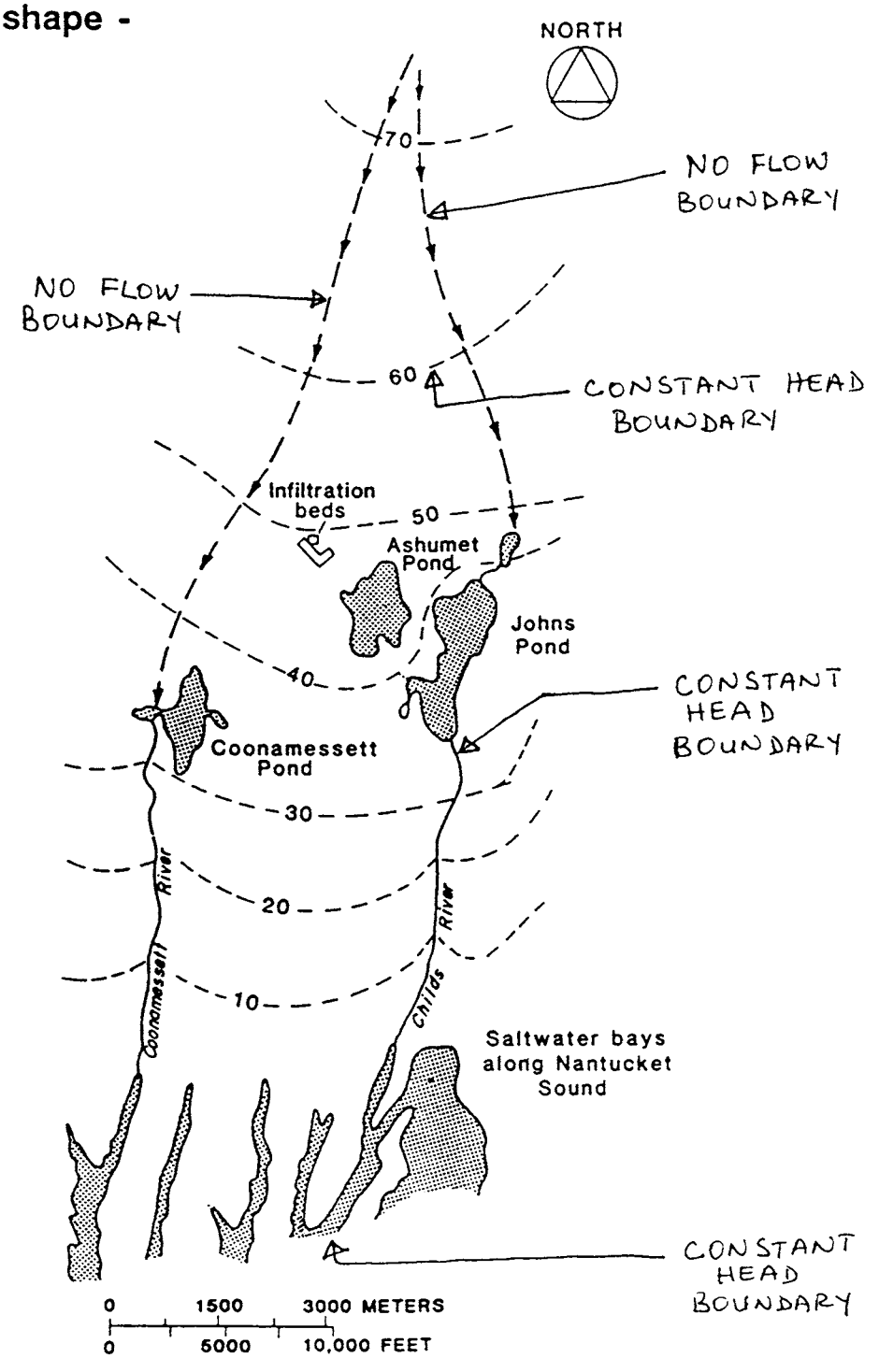

Flow Model

- discretization and boundary conditions

- parameter values - preliminary estimates from field data and guesses refined in calibration

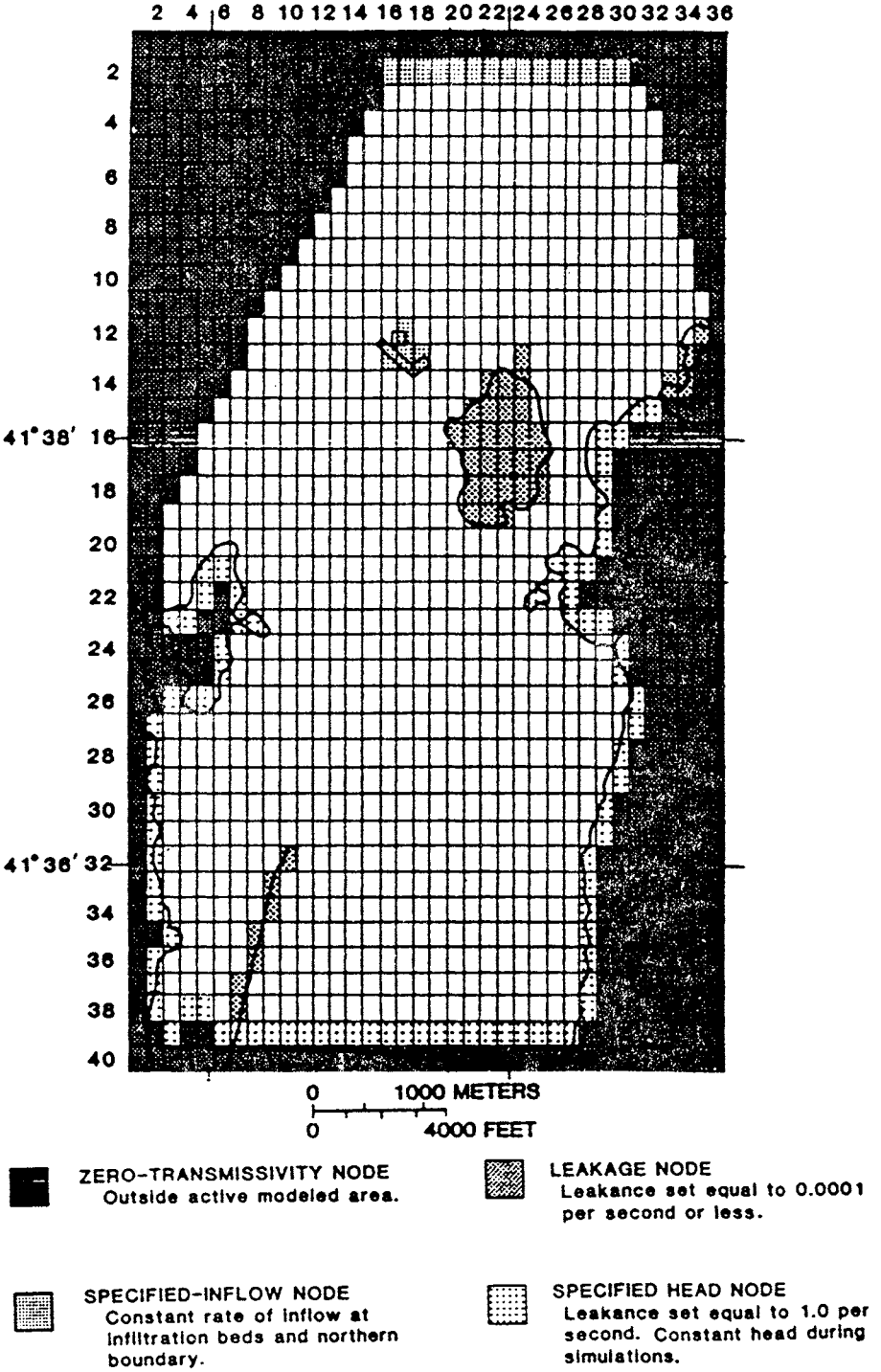

Observed and Computed Water Table

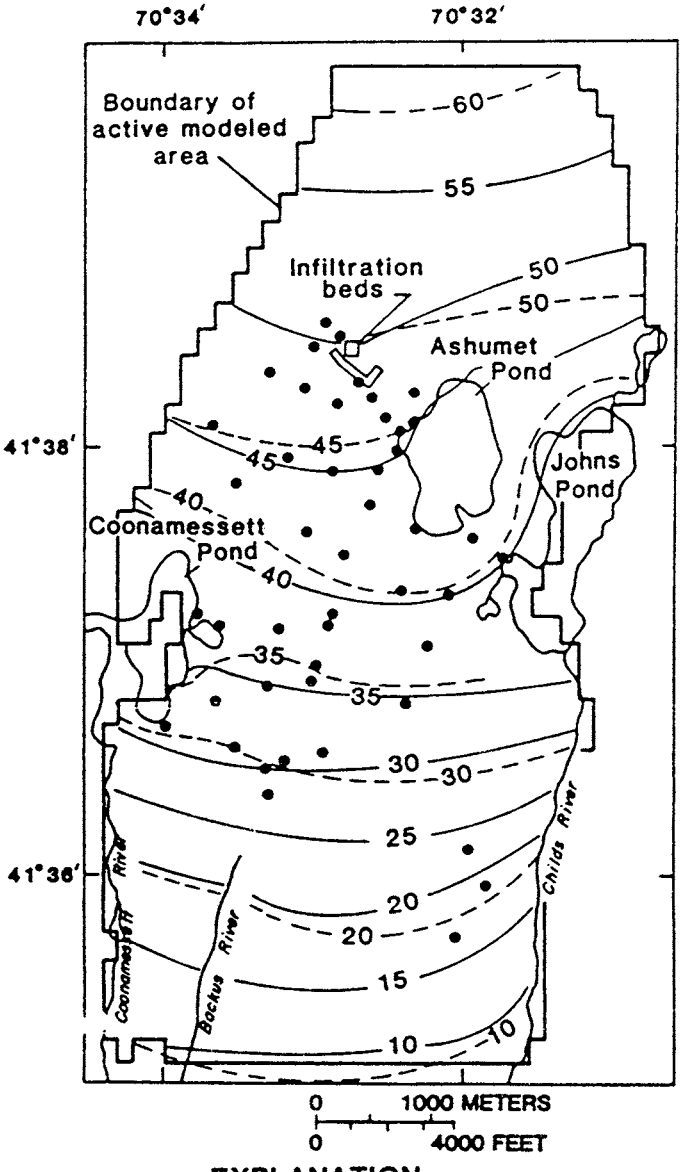

EXPLANATION

---40--- WATER-TABLE CONTOUR, NOVEMBER 1979--
Shows altitude of water table. Contour interval 5, 10 feet. Datum is sea level.

——40—— COMPUTED WATER-TABLE CONTOUR, FLOW-MODEL CALIBRATION--
Shows altitude of simulated water table. Contour interval 5 feet. Datum is sea level.

• WATER-LEVEL OBSERVATION WELL--
Site where computed and observed water levels compared during calibration.

APPENDIX 2

HYDRAULIC TRAP FOR PREVENTING COLLECTOR WELL CONTAMINATION: FORWELL CASE STUDY

(Ref: Ground Water, v. 23(5), pp. 600-610, 1985)

A Hydraulic Trap for Preventing Collector Well Contamination: A Case Study

by Duke U. Ophori[a] and Robert N. Farvolden[b]

ABSTRACT

A hydraulic trap in the form of a purge well is proposed for the Forwell collector well K-71. The trap, which will protect well K-71 from contamination by contaminants migrating downgradient from the old Breslube waste disposal site, is based on a qualitative flow net obtained from a finite-element model of the Forwell Aquifer. The trap constitutes pumping at the position of observation well OW 9-80 at a continuous rate of at least 6.1×10^{-3} m^3/s. The uniqueness of the trap lies in its simplicity and relatively low cost.

INTRODUCTION

The Forwell induced infiltration well field supplies about 6,818.4 m^3/day of water to the cities of Kitchener-Waterloo, Ontario, something less than 10% of the total demand. On the basis of recommendations by the Grand River Induced Infiltration Committee (GRIIC) reports (1976 and 1977), several developmental processes have been undertaken to improve production by two "30.48-meter" horizontal collectors (K-70 and K-71) presently inducing infiltration from the Grand River. Also, canals have been dug around each collector to enhance infiltration and stabilize the cone of influence. The waste disposal site of the old Breslube petroleum refinery plant, which lies to the east of the well field, is a potential threat to the quality of water pumped from the collectors.

The waste disposal site is located at the highest topographic elevations in the area. The water level in the Forwell Aquifer is also highest around the disposal site, and slopes toward the collectors and the Grand River. Under these conditions, contaminants which escape into the aquifer from the disposal site could be expected to migrate toward the collectors and the Grand River under natural ground-water flow. Furthermore, the rate of contaminant migration might be enhanced by production from the collectors.

The topography of the Forwell site and the water-level configuration of the Forwell Aquifer are shown in a stratigraphic cross section of the site in a later section.

Drawdown cones of influence associated with induced infiltration well fields are commonly stabilized by infiltration from nearby rivers after long continued pumping. In the highly permeable river-connected Forwell Aquifer, stabilization was rapidly approached and in conjunction with a digital model of the aquifer has been advantageously employed in the design of the hydraulic trap in this study.

SITE DESCRIPTION

Location

The site is located about 4,828 m east of Kitchener, Ontario, Canada, approximately 2,414 m south of the Highway 7 bridge over the Grand River near Breslau and about 1,609 m southeast of the bridge (Figure 1). It is accessible by a laneway from regional road 17 at a point about 805 m south of the railway tracks in Breslau.

Geology

Chapman and Putnam (1966) described the Waterloo Hills physiographic region of which the Forwell site is part, and Karrow (1968, 1971, 1974) has done considerable detailed work in this area since then. Figure 2 shows the surficial glacial

[a]Department of Geology, University of Alberta, Edmonton, Alberta T6G 2E3, Canada (on study leave from Department of Geology, University of Port Harcourt, Port Harcourt, Nigeria).

[b]Institute for Groundwater Research, Department of Earth Sciences, University of Waterloo, Waterloo, Ontario N2L 2G1, Canada.

Received October 1984, revised January 1985, accepted April 1985.

Discussion open until March 1, 1986.

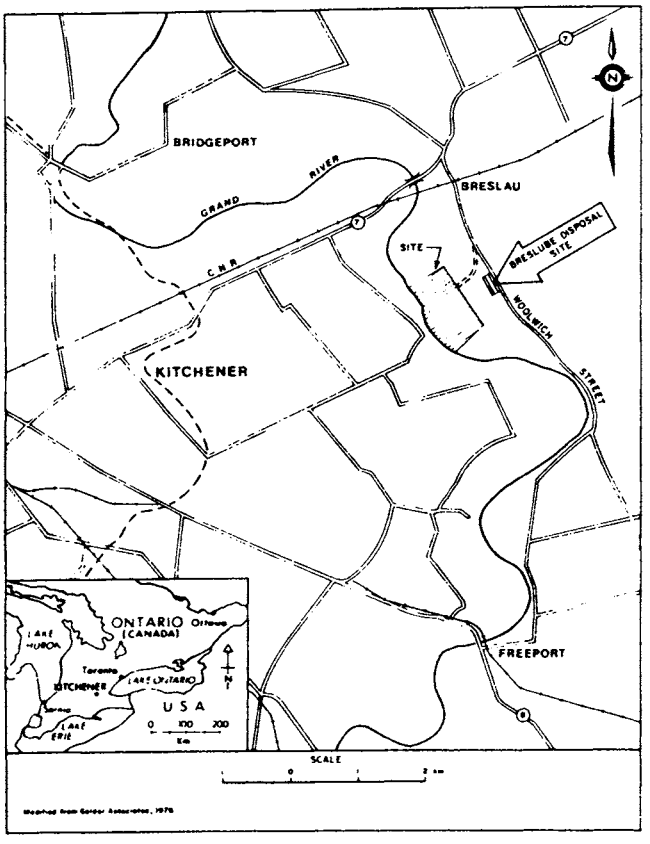

Fig. 1. Location map.

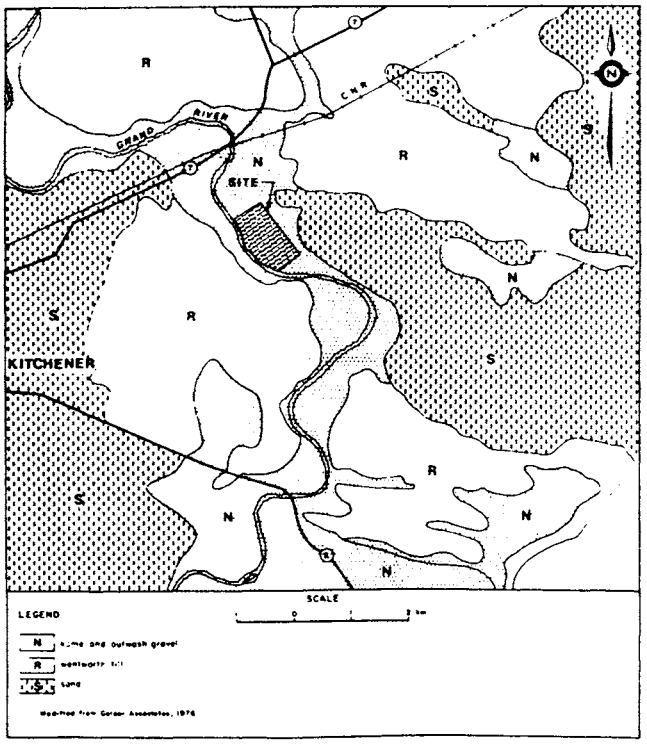

Fig. 2. Surficial geology

and postglacial deposits in the vicinity of the site. The surface is composed of sandy till ridges and hills of kames or kame moraines with outwash sand occupying the intervening hollows. The site itself lies in a major outwash channel in which the modern Grand River flows. The outwash deposits are predominantly uniform sand and gravel, occasionally silty. In the study area, the Grand River has an average gradient of 0.0013 (Karrow, 1968). The relatively low-gradient, broad-sweeping meanders and extensive floodplains indicate that the river is quite mature at the site. The glacial drift which varies in thickness from 9.1 to 24.4 m in the floodplains and up to 91.4 m in the uplands, consists of various interbedded till units, glaciolacustrine deposits and outwash deposits (Karrow, 1961; 1968; 1971). Numerous and extensive coarse gravel and sand deposits occur along the Grand River spillway. At present, the Grand River appears to be depositing gravelly materials along many of its meanders (Baechler, 1974).

The study site is underlain by gently dipping Silurian sedimentary rocks. Thus, bedrock consists of the Salina and Guelph Formations, comprising mainly dolomite and limestone. In addition, the Salina Formation contains interbedded shales and some gypsum as secondary fillings in pores (Hewitt and Freeman, 1972). The relationship between the various deposits at the Forwell site is illustrated in Figure 2a. The position of this geologic cross section is shown in Figure 3.

Hydrogeology

General

The hydrogeology of the site is based mainly on a number of domestic water wells and test wells installed by International Water Supply Ltd. (IWS) between 1948 and the present, reports by Golder Associates Ltd. (GA) and Hydrology Consultants Ltd. (HC), and the GRIIC.

As a result of sand and gravel mining operations, the surface of the site is hummocky. Several deep pits contain ponded water at varying elevations which evidently infiltrates to deeper zones. South of the site, a creek draining the glacial till upland to the east of the site runs into the Grand River. The influent nature of the creek is caused by the hydraulic gradient resulting from the lower hydraulic head in the aquifer than that of the surficial water (GA, 1976). This influent stream which infiltrated 53,019.9 m^3/day of water into the lower aquifer in the past (GA, 1976), is presently contained downstream along its course.

In general, four basic stratigraphic units have

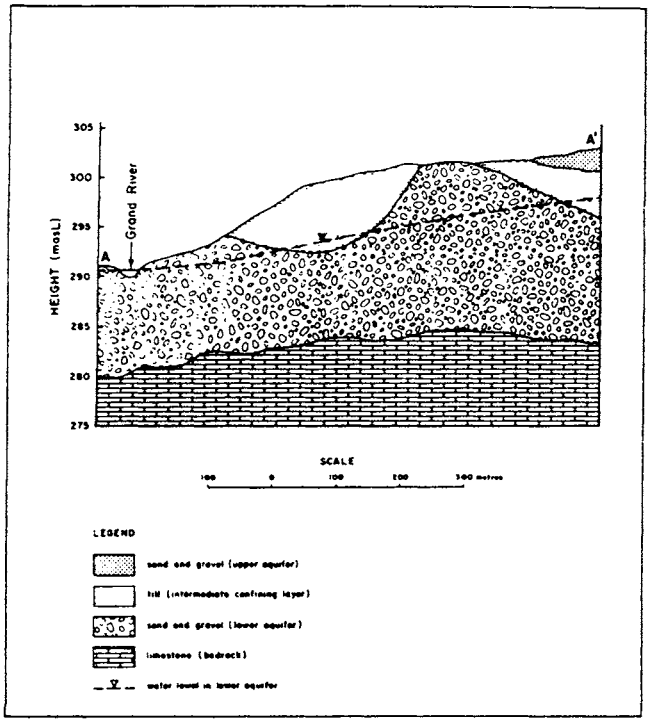

Fig. 2a. Stratigraphic cross section of the Forwell site.

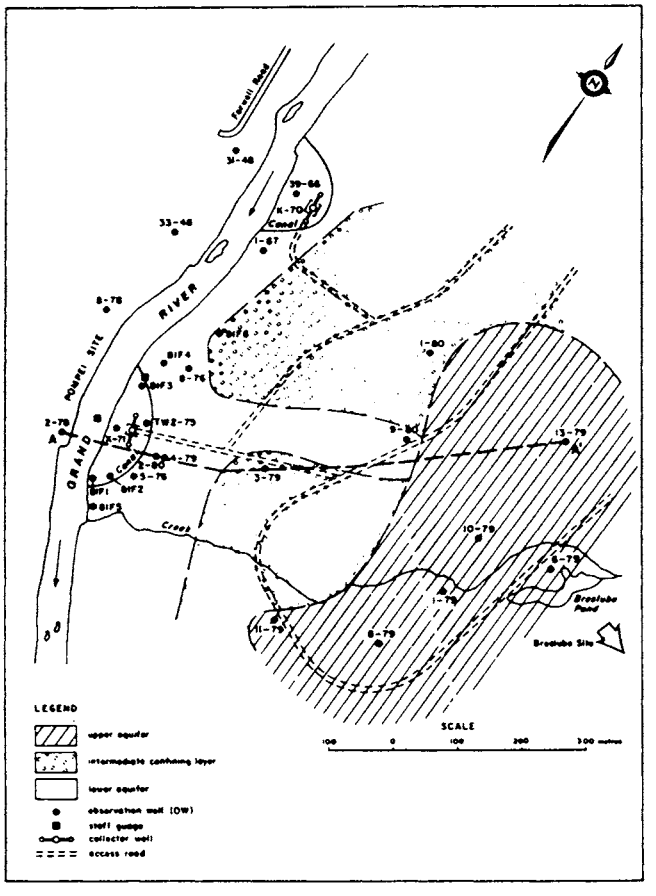

Fig. 3. Outcrop map of hydrostratigraphic units and installations for October 1981 pumping test.

been identified in the study area: (1) upper aquifer, (2) intermediate confining layer, (3) lower aquifer, (4) bedrock. Their surficial outcrop relationships are illustrated in Figure 3.

Upper Aquifer

The Upper Aquifer which occurs in the eastern portion of the site has been removed by erosion from some portions where it existed originally. The aquifer varies from silty sand in the west to clean sand and gravel in the east, with up to 3.1 m of saturated thickness under both confined and unconfined conditions due to perching caused by the underlying semiconfining beds. Based on soil description, hydraulic conductivity varies from 1.2×10^{-5} m/s for the silty sand up to 4.0×10^{-4} m/s for the clean sand and gravel near the Breslube disposal lagoons (IWS, 1980). The general direction of movement of water in this zone is toward the Grand River and the unit does not form a major ground-water zone (GA, 1976).

Intermediate Confining Layer

But for a strip on the eastern margin of the Grand River and a narrow zone extending from the river northeastwards, the intermediate confining layer occurs throughout the site. Locally, it attains a thickness of up to 13.7 m. This till layer has a higher silt and sand content in the eastern half of the site than the central portion and some layers of lacustrine clay occur locally. Utilizing grain-size distribution curves and the Hazen approximations, permeabilities of the confining layer range from 10^{-10} to 6×10^{-5} m/s (GA, 1976). High infiltration rates through the confining layer are a result of the relatively large hydraulic gradient across the layer, especially where the permeability is relatively high.

Consequently, the confining beds are capable of transmitting all of the precipitation that reaches them (GA, 1976).

Lower Aquifer

The bouldery and stony nature of the lower aquifer has limited most of the boreholes to relatively shallow penetration of the aquifer. Of the ten boreholes completed to the bedrock at the Forwell site and the adjacent Pompei site on the west side of the Grand River, only one borehole (TW 2-75) reportedly encountered glacial till between the lower aquifer and the bedrock, indicating that the lower till is local. Using evidence from the borehole data and the bedrock topography map of Miller *et al.* (1979), an average thickness of 15.3 m was estimated for the lower

aquifer. The aquifer materials have been variously described by different workers. A general consensus is that the aquifer consists mainly of sand and gravel, everywhere silty and bouldery. Occasionally, the materials are clayey (IWS, 1979), cemented (IWS, 1966) or clean (IWS, 1966; GA, 1976; GRIIC, 1976). Data on available samples agree with this description. The silty sand and gravels are moderately permeable at about 10^{-6} m/s while cleaner sections have permeabilities of 10^{-4} m/s (GA, 1976).

The lower aquifer is the major water-bearing unit at the Forwell site and the one referred to as the Forwell Aquifer in this study. In the absence of pumping, ground-water movement in the aquifer is toward the Grand River. Aquifer conditions vary from confined artesian in the east to unconfined water table near the Grand River (IWS, 1980). This aquifer is hydraulically connected to the Grand River (GRIIC, 1976).

Bedrock

The map by Miller *et al.* (1979) shows the topography of the westward gently-sloping bedrock surface. The bedrock consists of dolomite and shale of the Silurian Salina Formation which, over most parts of this location, underlies the lower aquifer. The Salina Formation is known to contain very hard and sulphate-laden water. The direction of ground-water movement is likely similar to that in the lower aquifer (GA, 1976).

METHOD OF STUDY

The study was carried out in four stages. The first stage involved an extensive literature review of earlier reports on the Forwell site and its immediate confines. All available data relating to the site were assembled and examined. These data included results of previous test drilling and geophysical surveys along the Grand River carried out by IWS, borehole data from the exploratory drilling program by the GRIIC, and data from other studies. Chemical and water-level data since 1979 were also supplied by the Regional Municipality of Waterloo. Results of two pumping tests by previous investigators were evaluated. The first test was conducted by the GRIIC in 1975. A test well located near the present K-71 was pumped for 119 hours at a constant rate of 1.4×10^{-2} m^3/s. A total of six observation wells situated at various distances from the test well and river were monitored. In the second pumping test of July 1976, the same test well was pumped for 460 hours at the rate of 1.7×10^{-2} m^3/s and 11 observation wells were monitored. The Thiem steady-state method of analysis defined an average transmissivity of 2.9×10^{-3} m^2/s for the Forwell Aquifer. Gevaert (1979) reported a storativity value of 0.08, radius of influence of 213 m; distance from pumped well to effective recharge boundary of 106 m, percentage of water diverted from the river as 77 and an infiltration rate of 4.9×10^{-7} m/s at the site. Further details of the pumping test analyses may be obtained from GRIIC (1976) and Gevaert (1979). A careful study of the observation well hydrographs for both tests reveals that near-steady-state conditions were obtained at the site after two days of pumping.

As part of this study, additional data from more test holes and piezometers were necessary to define the cone of influence adequately, at the second stage. A total of six water-table piezometers were installed with a truck-mounted CME 55 drill rig, using both solid- and hollow-stem augers. These piezometers were restricted to the area around K-71 as it was hoped that definition of the cone of influence of pumping of K-71 would be sufficient to yield the desired results. All installations for the October 1981 pumping test are shown in Figure 3.

To provide a response in the aquifer that can be attributed to a specific pumping rate, well K-71 pumping at a rate of 2.8×10^{-2} m^3/s was shut down and allowed to recover from October 14-17, 1981. The recovery data for two observation wells, like those of the earlier pumping tests, suggest that near-steady-state conditions are approached after about two days (Ophori, 1982). The recovery test was followed by a three-day pumping test during which well K-71 was pumped at a constant rate of 1.7×10^{-2} m^3/s. This rate was considered high enough to produce the necessary response in the system as well as to facilitate comparison between earlier and present results in the area around K-71. Ten observation wells were monitored and measurements were taken before and after the pumping test in 15 other wells from October 17-20, 1981 (Figure 3). Typical observation well hydrographs (Figure 4) show that most of the drawdown occurred in the first ten hours; thereafter, drawdown was slow but continuous. At about 45 hours, drawdown became negligible with time but water levels were influenced by a rise in river stage approximately six hours later. It is obvious that near-steady-state conditions were approached after 48 hours of pumping.

In Figure 5, the water-table configuration after 48 hours of pumping in October 1981 is compared with that of August 1981. The August

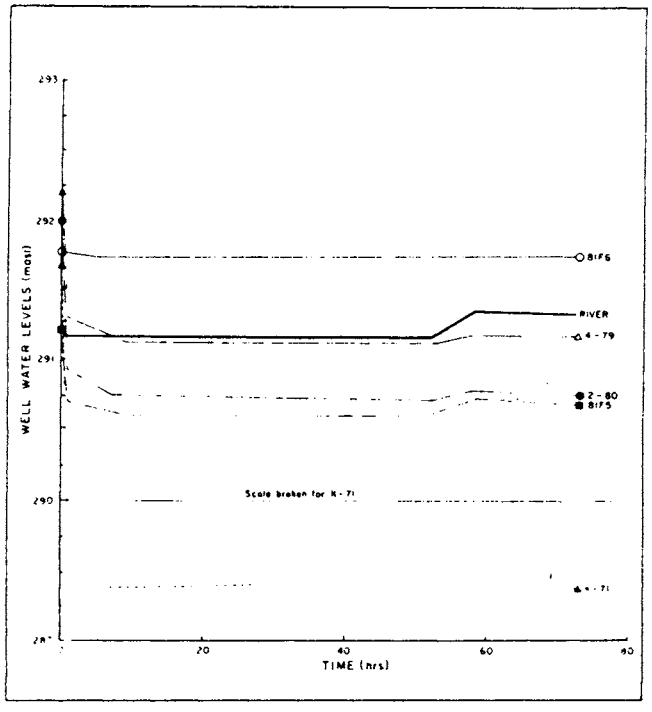

Fig. 4. Hydrographs of typical observation wells.

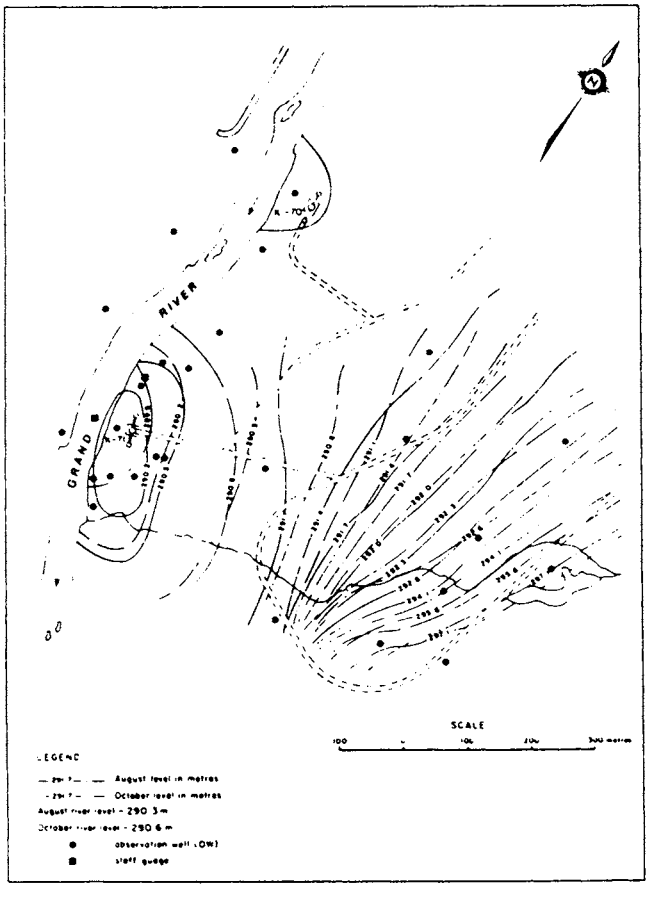

Fig. 5. Comparison of August and October 1981 steady-state water levels.

configuration was prepared from water-level data supplied by the Regional Municipality of Waterloo after one month of continuous pumping at the normal average production rate of 2.8×10^{-2} m^3/s. Within the cone of influence, there is a 0.3 m rise in ground-water levels from August to October. A careful observation reveals that this 0.3 m difference is closely related to river-stage fluctuation from August to October 1981. This favorable comparison of water levels is a further evidence that near-equilibrium conditions prevailed at the end of the pumping test, and predictions based on this test would be valid with little or no error. An attempt to analyze the recovery data by the Theis recovery method as described by Kruseman and de Ridder (1970) yielded transmissivity values much higher than expected for the aquifer. Nonetheless, the recovery test gave a useful guide to expected drawdown and pumping period necessary to establish near-steady-state conditions. A knowledge of this limiting period was important in order to avoid errors in interruption that might be misleading in setting up the normal pumping schedule at this site. A reliable set of data for transient conditions was difficult due to complex boundary conditions. The Thiem steady-state method as outlined in Kruseman and de Ridder (1970) was used to evaluate the aquifer transmissivity. The method is valid for an aquifer system with a recharge boundary, provided piezometers considered are in a line parallel and not too close to the recharge boundary (Walton and Ackroyd, 1966). An average transmissivity value of 3.0×10^{-3} m^2/s was calculated by this method. A second transmissivity value of 3.7×10^{-3} m^2/s was estimated for the aquifer, using the method of Rorabaugh (1956). These transmissivity values fall within the range of transmissivities reported by GRIIC (1976) and Gevaert (1979). Detailed explanation of these methods and further analysis of the data is presented in Ophori (1982).

At the third stage, the hydrologic and hydraulic parameters obtained from the earlier stages of the study were incorporated in the development of a model to simulate the actual ground-water flow when near-steady-state conditions prevailed. Boundaries were inferred and adjusted to obtain realistic results.

Finally, at the fourth stage, the model was used to determine the effect of a hydraulic trap in the form of a purge well which would provide protection against contamination from the Breslube site.

MODEL DESCRIPTION AND CALIBRATION

The general partial differential equation that approximately governs the flow of water in a two-dimensional isotropic aquifer is

$$\frac{\partial}{\partial x}\left(T\frac{\partial h}{\partial x}\right)+\frac{\partial}{\partial y}\left(T\frac{\partial h}{\partial y}\right)-S\frac{\partial h}{\partial t}-Q-\frac{K}{b}(h-ha)=0 \quad \ldots\ldots (1)$$

where

T is the transmissivity of the aquifer, L^2T^{-1};

h is the hydraulic head in the aquifer, L;

S is the storage coefficient of the aquifer, dimensionless;

Q is the flux of a source or sink, L^3T^{-1};

x and y are the space coordinates, L;

K is the vertical hydraulic conductivity of a confining layer, LT^{-1};

b is the thickness of a confining layer, L; and

ha is the hydraulic head in the adjacent aquifer, L.

The mathematical model used to approximate (1) was that from the Pinder and Frind (1972) finite-element solution of the differential equation for transient flow in plan view. This solution used the Galerkin procedure to generate the approximating integral equations and evaluated them with iso-parametric quadrilateral elements by numerical integration. For a complete explanation of this method, the reader is referred to the paper by Pinder and Frind (1972). Although the method assumes a confined aquifer, it can be applied to an unconfined aquifer in which drawdown is small in comparison to the saturated thickness (Muskat, 1937; Kazmann, 1946; Lohman, 1972). Moreover, the Forwell Aquifer exhibits both confined and unconfined conditions (IWS, 1980).

In the present study, the domain was approximated by finite triangular elements which requires a modification of the original program of Pinder and Frind (1972). The grid had 110 nodes and 191 elements with a maximum bandwidth of 23. Small triangular elements were used near the pumping well, and the size increased with distance (Figure 6).

The image-well theory was incorporated into the model to simplify the complex boundary conditions imposed on the system by the Grand River and canal around K-71. Furthermore, it was hoped that the theory would reduce the computing cost of developing the model by eliminating the number of runs that would be required to obtain reliable flux into the system at the river and canal nodes. Figure 7 shows the observed drawdown cone at the end of the pumping test. But for the immediate vicinity of the pumping well, the cone is highly asymmetrical and resembles that expected for a single recharge boundary on the river side of the pumping well. Consequently, the entire

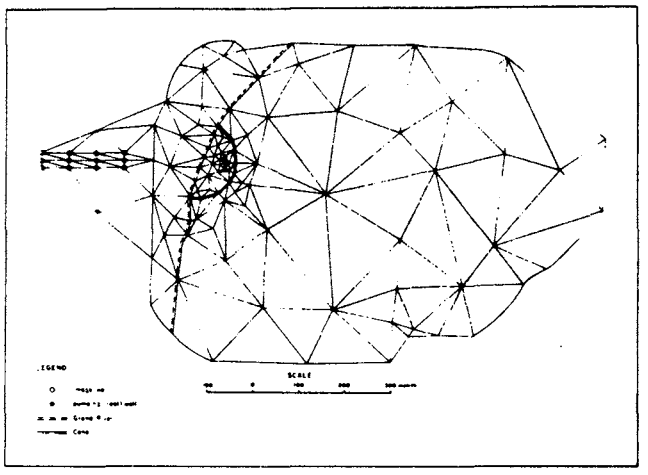

Fig. 6. Finite-element grid.

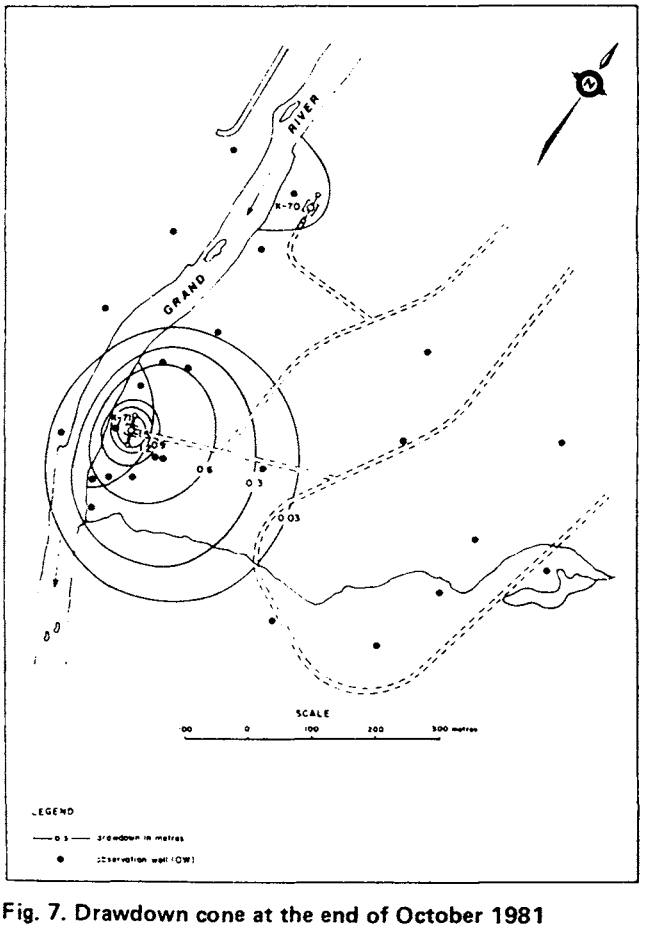

Fig. 7. Drawdown cone at the end of October 1981 pumping test.

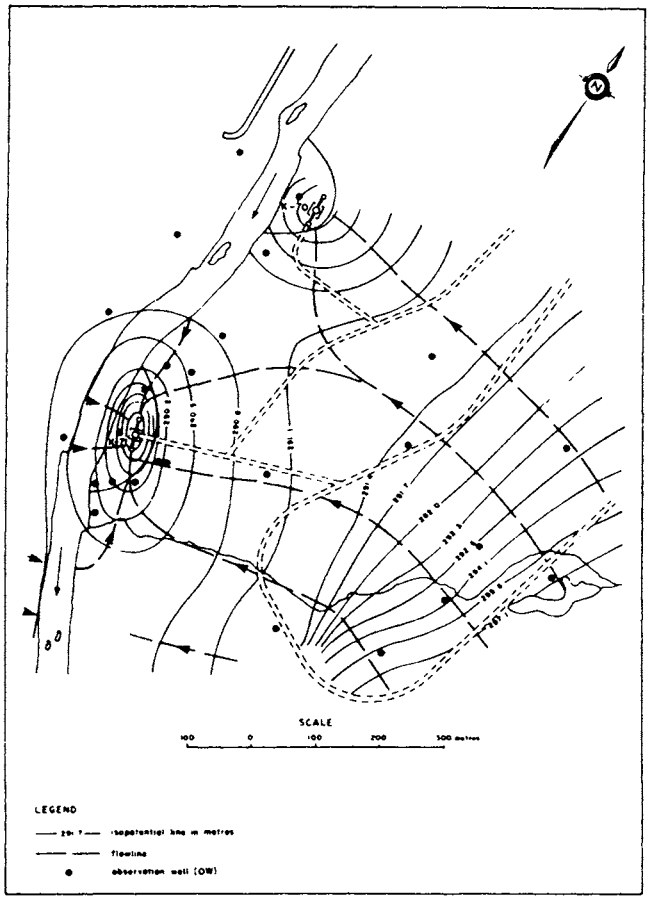

Fig. 8. Simulated steady-state flow net.

channel system was approximated by a single recharge boundary which was replaced by a line source and finally by image wells as suggested in Rorabaugh (1956). To simulate the long horizontal screen, the collector well (K-71) was modeled by three real wells equally spaced and each pumping at one-third the test pumping rate of K-71 (1.7×10^{-2} m^3/s). Three equivalent recharging "image wells" were placed at a distance "a" beyond the line source. This approach is a simplified form of those described by Ferris (1959), Walton and Walker (1961), Walton and Schaefer (1956), and Walton (1970).

To further simplify the problem, the system was started as hydrostatic and the water-level datum was chosen to be zero.

As data were insufficient to describe the areal extent of the aquifer rigorously, the north boundary of the model was fixed by the ground-water divide which separates the flow fields of K-70 and K-71. This divide was confirmed by field measurements of ground-water levels due to pumping of each of K-70 and K-71. The other boundaries were located far enough from the pumping center so that no-flux conditions could be assumed. The west boundary was adjusted to accommodate the image wells at a distance "2a" from the real wells with which they produce the effect of the line source midway between them. The lower calculated transmissivity of 3.0×10^{-3} m^2/s seemed more reliable, and together with a storativity value of 0.08 adapted from Gevaert (1979), were used in the model.

The model was calibrated with the aid of the information above and a computer program which solves equation (1). An attempt was made to simulate the observed near-steady-state drawdown cone and hence head distribution in the aquifer. This procedure is based on the assumption that a particular head distribution is the result of a unique set of aquifer boundaries and properties.

Several runs were processed varying the positions of the image wells. In each case, the transient model described earlier was run till near-steady-state conditions prevailed—that is, after long-continued pumping. Best results were simulated with the image wells at a distance "2a" of 304 m from the real wells. The resulting near-steady-state flow net (Figure 8) compares favorably with the observed flow net (Figure 9) indicating that the model closely describes the hydrogeologic condi-

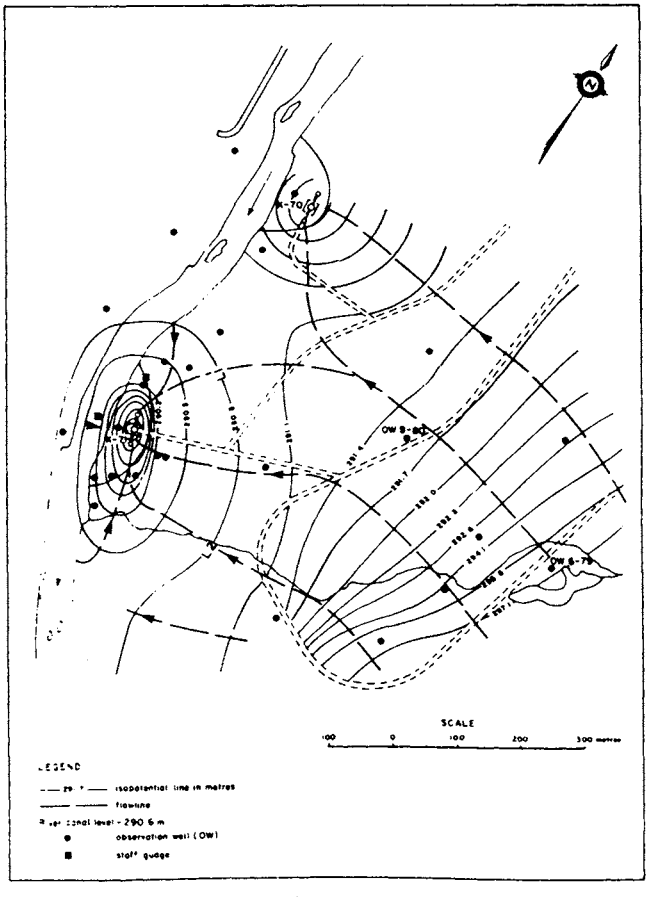

Fig. 9. Observed steady-state flow net.

tions at the Forwell site. The slight variation in the 290.5 m isopotential line may be caused by local variation in the aquifer parameters. An approximate distance of 152 m to effective recharge boundary is inferred by these results. This value is in agreement with those calculated earlier at the site (Gevaert, 1979; Ophori, 1982). As a similar interpretation seems feasible for K-70, it is concluded that for the pumping rates considered in this study, the Forwell Aquifer behaves as though it has boundaries beyond the cone of influence of pumping on one side and has a perfect recharge line source on the other side, 152 m west of K-71.

POLLUTION HAZARDS

The Breslube oil reclamation plant (Figure 1) which operated from the early 1960's until the late 1970's used lagoons to dispose of the oily acid sludge waste and waste water high in phenols derived from reclamation processes. Some test pits were excavated through contaminated silty sand fill, silt, and sand and gravel saturated up to 3.1 m with a black oily substance (International Water Consultants (IWC), 1980; GA, 1976).

The contamination from the lagoon has migrated into the upper aquifer, grossly contaminating an estimated 40,470 m^2, representing about 27,276 to 36,368 m^3 of contaminated water (IWC, 1980). Water from this layer is typically odorous and grey when initially discharged and contains phenol concentrations from 7,000 to 22,000 ppb along with other parameters in the well characterization group (IWC, 1980). Heavy metals were either not detected or were present in low concentration, suggesting that they are held in the soil close to the lagoon.

Phenol concentrations of up to 11,000 ppb and 8,000 ppb have been measured in ponds and streams recharged by the lagoons and which then drain to the Grand River downstream from K-71 (Figure 9a). Analyses by the Regional Municipality of Waterloo over several years show that the level of phenols in observation wells fluctuates widely with highest values associated with low-flow conditions. High-phenol concentrations measured in the aquifer water below the intermediate confining layer at OW 6-79 (IWC, 1980) indicate that contaminants have passed through this layer in less than 20 years. The transit time is significantly less than would be expected if the overall permeability of the confining layer was as determined in the laboratory (IWC, 1980), suggesting that the layer has higher in-situ permeability including secondary permeability.

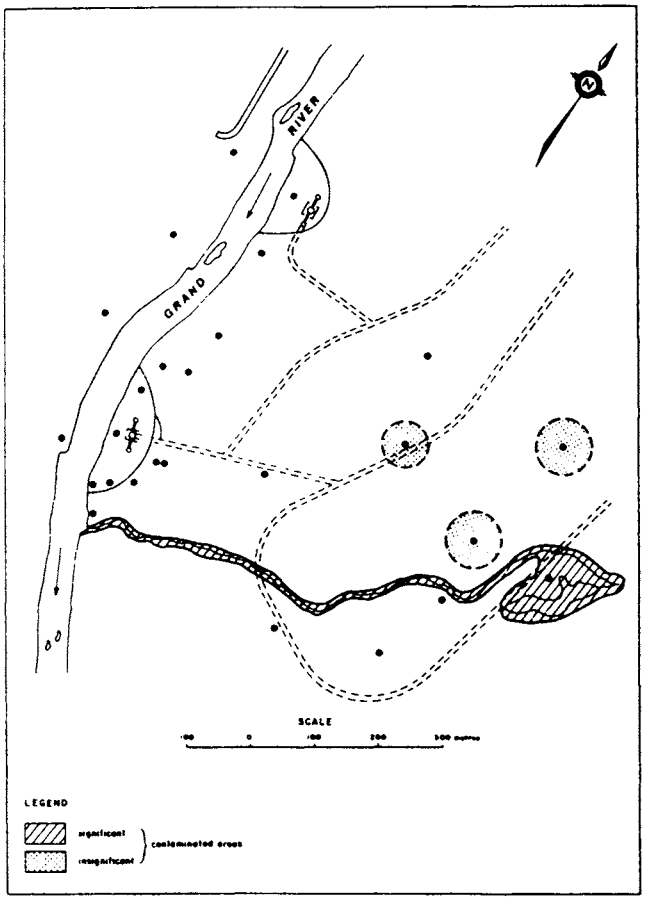

Fig. 9a. Distribution of contaminants.

Contamination is less in the lower aquifer, and consists of soluble compounds with a maximum concentration of 90 ppb. Three centers of relatively high-contaminant concentration have been located (IWC, 1980).

1. At OW 6-79 immediately west of the lagoon. It was estimated that it would take about 2.5 years to flow from the area of the lagoons to the collectors;

2. Between the lagoons and the collector wells and centered on OW 13-79 with estimated migration time to the collectors of 1.5 years; and

3. Near K-71 and the stream resulting from creek leakage especially where the intermediate confining layer is absent. There is already a low level of phenol present in the area of K-71, at least in the upper portion of the aquifer.

Following these results, three corrective measures for the lower and eight for the upper aquifers were suggested by IWC (1980). The suggested measures for the lower aquifer include: (a) the containment of the creek, which conveys contaminated water from the pond to the Grand River, in a corrugated metal pipe; (b) installation of a purge well or wells northwest of OW 9-80,

Table 1. Chemical Data of July, August, and September 1981 (ppm) (Supplied by Reg. Mun. of Waterloo)

LOCATION	DATE	HARDNESS	ALKALINITY	IRON	CHLORIDE	PH	CONDUCTIVITY	SULPHATE	PHENOLS (ppb)
1-67	July 20	224	213	31	57	8.4	539	48	<1
5-76	July 20	396	830	66	19	7.3	730	87	<1
8-76	July 20	324	610	78	4	7.4	550	39	<1
1-79	July 20	384	293	35	34	7.3	760	102	<1
3-79	July 20	404	712	138	26	7.7	750	112	<1
4-79	July 20	364	503	60	20	7.6	619	77	<1
6-79	July 20	700	2060	165	106	7.2	2100	480	2
8-79	July 20	360	1550	325	7	7.5	541	92	<1
10-79	July 20	258	317	13	11	7.3	520	42	<1
11-79	July 20	280	1400	270	6	7.4	520	29	<1
13-79	July 20	392	266	34	23	7.3	750	150	<1
1-80	July 20	404	464	120	5	7.3	650	35	<1
2-80	July 20	336	306	29	17	7.3	620	59	<1
9-80	July 20	352	994	53	2	7.4	621	32	<1
K-70	July 14	272	216	<.01	22	7.6	530	57	<1
K-71	July 14	332	246	<.01	24	7.5	650	76	<1
1-67	Aug. 12	232	189	17	27	7.3	490	40	<1
5-76	Aug. 12	444	615	34	26	7.1	750	84	<1
8-76	Aug. 12	344	485	27	5	7.4	570	40	<1
1-79	Aug. 12	392	280	39	36	7.3	760	114	<1
3-79	Aug. 12	432	344	49	21	7.3	800	120	<1
4-79	Aug. 12	396	296	16	24	7.3	720	78	<1
6-79	Aug. 12	920	1190	103	108	7.2	2050	490	<1
8-79	Aug. 12	336	1650	244	30	7.5	570	120	1
10-79	Aug. 12	328	411	20	14	7.1	580	55	1
11-79	Aug. 12	324	634	101	7	7.5	500	45	2
13-79	Aug. 12	408	241	12	24	7.4	740	130	<1
1-80	Aug. 12	392	355	48	4	7.2	630	28	<1
2-80	Aug. 12	352	260	13	18	7.3	500	52	<1
9-80	Aug. 12	408	579	46	2	7.3	630	29	<1
K-70	Aug. 12	---	---	--	--	---	---	--	<1
K-71	Aug. 12	---	---	--	--	---	---	--	<1
1-67	Sep. 16	214	192	20	25	8.0	485	40	1
5-76	Sep. 16	358	548	39	--	--	--	69	1
8-76	Sep. 16	328	437	20	5	8.0	620	40	<1
1-79	Sep. 16	354	954	231	35	7.7	810	125	1
3-79	Sep. 16	410	354	87	26	7.7	790	125	1
4-79	Sep. 16	376	304	24	25	7.6	760	86	<1
6-79	Sep. 16	460	1130	116	111	7.2	2250	495	7
8-79	Sep. 16	278	840	194	7	7.4	600	103	1
10-79	Sep. 16	256	340	14	12	7.1	600	42	2
11-79	Sep. 16	260	1280	90	12	7.5	560	42	2
13-79	Sep. 16	364	238	11	22	8.1	770	145	<1
1-80	Sep. 16	362	352	88	4	7.6	640	31	<1
2-80	Sep. 16	356	293	6	19	7.6	620	56	3
9-80	Sep. 16	288	440	23	2	7.8	580	34	<1
K-70	Sep. 16	268	210	.02	22	8.3	530	49	<1
K-71	Sep. 16	304	237	<.01	23	7.8	600	65	<1

southwest of OW 13-79, and possibly east of K-71 with yields of about 3.8×10^{-3} m^3/s; and (c) the possibility of intercepting ground-water flow from the east by means of deepened recharge canals around the collectors. Option (a) has been successfully implemented, (c) has been attempted and found not feasible for reasons outlined in IWC (1980), and (b) is discussed in the following paragraphs.

Table 1 shows chemical data for July, August, and September 1981 of the Forwell site, supplied by the Regional Municipality of Waterloo. These data indicate phenol concentrations below 1 ppb around OW 13-79, suggesting that this area has not continuously survived as a potential contaminant source to the collectors. Generally, phenol concentrations are within treatable limits in the short term, and induced water at collector wells falls within the Ministry of Environment's permissible criteria for public drinking-water supplies. Present data also indicate that substantial phenol concentrations have not arrived at the collectors as expected from the times of arrival estimated by IWC (1980). This may be due to attenuation as well as early implementation of some of the corrective measures suggested by IWC (1980). Furthermore, the cone of influence of K-71 (Figure 7) is restricted and does not significantly

affect the contaminated centers. This would mean that contaminant migration from the centers is controlled by the naturally slow ground-water movement.

In the long term, however, as seepage from the upper aquifer through the intermediate confining layer advances, arrival of high-phenol concentrations at the collectors is anticipated especially from the lagoon area (around OW 6-79). The need for a protective measure is therefore apparent.

THE HYDRAULIC TRAP

On the basis of the anticipated pollution, a hydraulic trap is designed in the form of a purge well at OW 9-80. The trap employs the principles of flow net construction (Walton, 1970; Freeze and Cherry, 1979). The trap location was chosen for the following reasons: (1) recommendation by IWC (1980); (2) flowlines from the contaminated ponds around OW 6-79 pass through this zone to the collectors (Figure 9); (3) the authors observed that discharged water from OW 9-80 was odorous and grey during a sampling session by staff of the Regional Municipality of Waterloo, signifying some level of contamination at this point. The trap could be located east of OW 9-80, but any contaminants already downgradient would be free from the trap and could be expected to reach K-71 eventually.

To complete the trap design, pumping in the aquifer model described earlier was replaced by three real wells at the collector, each pumping at one-third the normal rate of operation at K-71. The equivalent "image wells" were placed at 304 m to the west as earlier suggested by the model. The model was then run several times with varying discharge rates at OW 9-80. Starting with a discharge rate of 7.6×10^{-4} m^3/s and increasing in steps of 7.6×10^{-4} m^3/s, a limiting rate of 6.1×10^{-3} m^3/s was found to produce the drawdown cone necessary to divert all flowlines from the center of contamination into a sink (Figure 10). This waste water may be discharged into the Grand River downstream from K-71. Should the need arise, a lower capacity purge well may be sited northeast of OW 1-80 and west of OW 13-79. At least one more observation well is needed in this area for this design. Since the influent lower reach of the creek is presently contained by engineering works, the proposed trap at OW 9-80 would be sufficient to the south of the site. In terms of efficiency, cost, and practicability, this corrective measure is considered the most suitable of all the measures proposed by IWC (1980).

SUMMARY

The ground-water system in the vicinity of the old Breslube disposal site, which lies to the east of the Forwell collector-well K-71 was simulated using a two-dimensional finite-element model. The model was calibrated with the aid of a near-steady-state drawdown cone which resulted from a field pumping test. In order to simplify the problem significantly, and to obtain realistic results simultaneously, the image-well theory was incorporated into the model.

The calibrated model showed that the Forwell Aquifer behaves as though it has boundaries beyond the cone of influence of pumping on one side and has a perfect recharge line source on the other side, 152 m west of K-71.

The predictive simulation which followed indicated that a pumping well in the position of OW 9-80 with a constant discharge rate of at least 6.1×10^{-3} m^3/s, would divert all of the water moving from the contamination source for onward discharge to the Grand River downstream from K-71.

As the proposed trap would be operated on

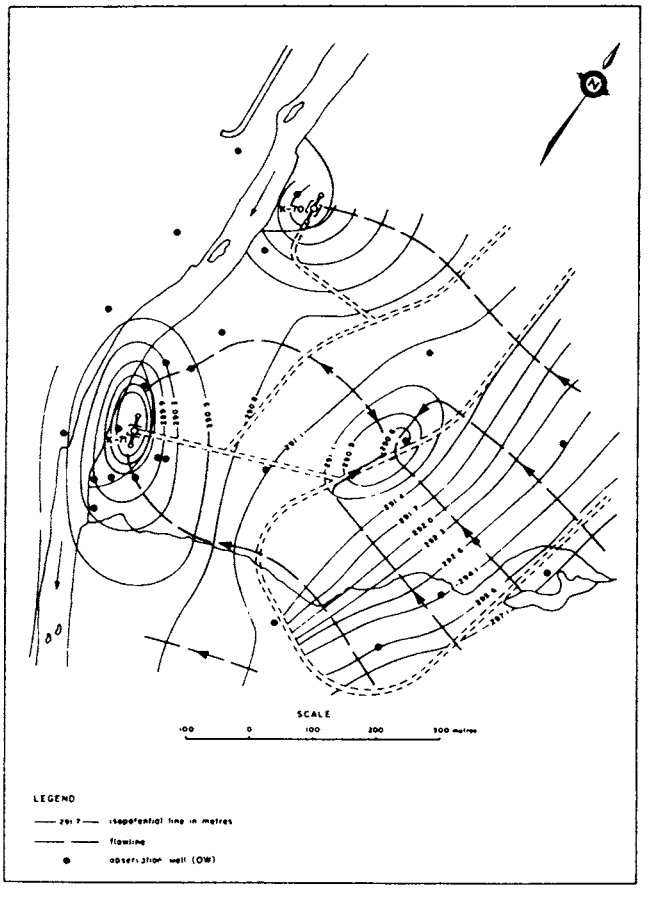

Fig. 10. Flow net with hydraulic trap.

purely physical rather than chemical principles, it is viewed as a relatively simple and inexpensive, yet important, tool to protect the Forwell collector well from contamination.

ACKNOWLEDGMENT

The criticisms and suggestions of Dr. R. W. Gillham of the Department of Earth Sciences, University of Waterloo, Ontario, are gratefully acknowledged. We owe special thanks to John Pawley, John Michalofsky, and Stan Schneider, all of the Regional Municipality of Waterloo, who allowed free access to information.

This study was funded by the Regional Municipality of Waterloo.

REFERENCES

Baechler, F. 1974. The effect of metro Kitchener as an urban area on the sediment load and regime of the Grand River. M.Sc. Thesis, University of Waterloo, Ontario.

Chapman, L. J. and D. F. Putnam. 1966. The Physiography of Southern Ontario (2nd edition). Ontario Res. Foundation, University of Toronto Press, Toronto, Ontario.

Ferris, J. G. 1959. Ground Water. In C. O. Wisler and E. F. Brater (editions). John Wiley and Sons, Inc., New York.

Freeze, R. A. and J. A. Cherry. 1979. Groundwater. Prentice-Hall, Englewood Cliffs, N.J. 604 pp.

Gevaert, D. 1979. Location and evaluation of induced infiltration sites near the Grand River in the Kitchener-Waterloo area. M.Sc. Thesis, University of Waterloo, Waterloo, Ontario.

Golder, H. Q. and Associates Ltd. and Hydrology Consultants Ltd. 1976. Hydrogeological/geotechnical study, proposed landfill site, (Forwell site), Breslau, Ontario. Regional Municipality of Waterloo, Ontario.

Grand River Induced Infiltration Committee Reports. 1976 and 1977. Regional Municipality of Waterloo, Ontario.

Hewitt, D. F. and E. B. Freeman. 1972. Rocks and minerals of Ontario. Ont. Dept. of Mines, Geol. Circular 13.

International Water Consultants Ltd. 1980. Groundwater investigation, well K-70 and K-71 area. Regional Municipality of Waterloo, Ontario.

International Water Supply Ltd. 1966. Report on test drilling and geophysical surveys along the Grand River. Regional Municipality of Waterloo, Ontario.

International Water Supply Ltd. 1979. Performance tests of collectors. Regional Municipality of Waterloo, Ontario.

International Water Supply Ltd. 1980. Groundwater investigation, Forwell area. Regional Municipality of Waterloo, Ontario.

Karrow, P. F. 1961. Pleistocene geology of the Galt map area. Ont. Dept. of Mines, Geol. Circular 9.

Karrow, P. F. 1968. Pleistocene geology of the Guelph area. Ont. Dept. of Mines, Geol. Rept. 61.

Karrow, P. F. 1971. Quaternary geology of the Stratford-Conestogo area, Ont. Geol. Surv. Can., Paper 70-34.

Karrow, P. F. 1974. Till stratigraphy in parts of southwestern Ontario. Geol. Soc. of Amer. Bull. v. 85, pp. 761-768.

Kazmann, R. W. 1946. Notes on determining the effective distance to a line of recharge. Trans. Amer. Geo. Union. v. 27, no. 6, pp. 854-859.

Kruseman, G. P. and N. A. de Ridder. 1970. Analysis and evaluation of pumping test data. International Institute for Land Reclamation and Improvement, Wageningen, The Netherlands.

Lohman, S. W. 1972. Groundwater hydraulics. USGS Professional Paper 708.

Miller, R. F., L. Farrel, and P. F. Karrow. 1979. Bedrock topography of the Cambridge area, southern Ontario. Ont. Geol. Surv. Prelim. Map P-1985.

Muskat, M. 1937. The Flow of Homogeneous Fluids through Porous Media. McGraw-Hill Book Co., New York.

Ophori, D. U. 1982. Evaluation of the Forwell induced infiltration site, Kitchener-Waterloo area. M.Sc. Thesis, University of Waterloo, Waterloo, Ontario.

Pinder, G. F. and E. O. Frind. 1972. Application of Galerkin's procedure to aquifer analysis. Water Resour. Res. v. 8, no. 1, pp. 108-120.

Rorabaugh, M. I. 1956. Ground water in northeastern Louisville, Kentucky. U.S. Geol. Surv. Water-Supply Paper 1360-B.

Walton, W. C. 1970. Ground Water Resource Evaluation. McGraw-Hill Book Co., New York.

Walton, W. C. and E. A. Ackroyd. 1966. Effects of induced streambed infiltration on water levels in wells during aquifer tests. Minn. Water Resour. Res. Center, Bull. 2.

Walton, W. C. and E. J. Schaefer. 1956. Report on new ground water supply in the Eagle City area for the City of Springfield, Ohio. Typewritten report prepared for Black and Veatch, Consulting Engineers, Kansas City, Missouri.

Walton, W. C. and W. H. Walker. 1961. Evaluation wells and aquifers by analytical methods. J. Geophys. Res. v. 66, no. 10.

* * * * *

Duke U. Ophori obtained his B.Sc. in Geology in 1976 from the University of Ibadan, Ibadan, Nigeria, and his M.Sc. in Hydrogeology in 1982 from the University of Waterloo, Waterloo, Ontario, Canada. He is presently pursuing studies toward a Ph.D. at the University of Alberta, Edmonton, Alberta, Canada.

Bob Farvolden received his B.Sc. and M.Sc. in Geology from the University of Alberta, Edmonton, and was first Head of Groundwater Division of the Research Council of Alberta. After earning his Ph.D. from the University of Illinois, Urbana, he worked for the Desert Research Institute in Reno, and then held faculty appointments at the University of Illinois, Urbana and University of Western Ontario, London. In 1970, he was appointed Chairman of the Department of Earth Sciences at Waterloo, to set up the ground-water program. After 11 years as Chairman and Dean of Science, he is now back with the Institute for Groundwater Research in the Department of Earth Sciences at the University of Waterloo. His research interests include ground-water resources development and the application of modern techniques in physical hydrology and geochemistry to solve field problems.

APPENDIX 3

NUMERICAL SIMULATIONS TO INVESTIGATE MOISTURE-RETENTION CHARACTERISTICS IN THE DESIGN OF OXYGEN-LIMITING COVERS FOR REACTIVE MINE TAILINGS

Reprinted by kind permission of the
Canadian Geotechnical Journal
(Ref: Canadian Geotechnical Journal, v. 23, pp. 446-451, 1991)

Numerical simulations to investigate moisture-retention characteristics in the design of oxygen-limiting covers for reactive mine tailings

FESTUS F. AKINDUNNI,[1] R. W. GILLHAM, AND R. V. NICHOLSON

Waterloo Centre for Groundwater Research, University of Waterloo, Waterloo, Ont., Canada N2L 3G1

Received June 18, 1990

Accepted January 16, 1991

Acid generation in reactive mine tailings is an oxidation process that is dependent on availability of molecular oxygen. As a consequence of the diffusion coefficient of oxygen being several orders of magnitude higher in air than in water, influx of atmospheric oxygen into a material at depth can theoretically be minimized by maintaining a protective cover layer at high moisture content. Such oxygen-limiting covers are generally of finer texture than the material being protected. A numerical model was used to investigate the importance of moisture-retention characteristics in the transient drainage of such two-layer systems. The results show that the effectiveness of a material as a moisture-retaining cover is dependent on the magnitude of its air-entry value. The thickness of the cover maintained at full saturation after prolonged drainage also depends on the pressure head at which the underlying material approaches residual saturation.

Key words: geologic covers, tailings, numerical simulations, air-entry value, residual saturation, textural layering.

La génération d'acide dans les résidus miniers réactifs résulte d'un processus d'oxydation qui est dépendant de la disponibilité d'oxygène. Comme conséquence du fait que le coefficient de diffusion de l'oxygène est plusieurs ordres de grandeur plus élevé dans l'air que dans l'eau, l'influx d'oxygène atmosphérique dans un matériau en profondeur peut être minimisé théoriquement en maintenant une couche protectrice de recouvrement à forte teneur en eau. De tels recouvrements limitant l'influx d'oxygène sont généralement d'une texture plus fine que le matériau à protéger. Un modèle numérique a été utilisé pour étudier l'importance des caractéristiques de rétention d'eau sur le drainage transitoire de tels systèmes bicouches. Les résultats démontrent que l'efficacité d'un matériau comme recouvrement hydrophile dépend de l'amplitude de la valeur d'entrée d'air. L'épaisseur d'un recouvrement qui reste complètement saturé après un drainage prolongé dépend également de la charge de pression à laquelle le matériau sous-jacent s'approche de la saturation résiduelle.

Mots clés : recouvrements géologiques, résidus miniers, simulations numériques, valeur d'entrée d'air, saturation résiduelle, couches de différentes textures.

[Traduit par la rédaction]

Can. Geotech. J. 28, 446-451 (1991)

Introduction

Nicholson *et al.* (1989) discussed the hydraulic principles involved in the use of fine-textured materials as protective covers for reactive mine tailings. Using schematics and assuming static flow conditions, they demonstrated how fine-textured materials could remain at high moisture content above relatively coarser granular materials, even when the water table is at some arbitrary depth, far from the ground surface. The authors concluded that such a layered system would effectively reduce the influx of oxygen, thereby inhibiting oxidation of the underlying sulphide-bearing tailings. They showed that a necessary requirement to maintaining a cover material in a fully saturated state after prolonged drainage is that the magnitude of the air-entry value (AEV) be greater than or equal to the sum of the cover thickness and the magnitude of the pressure head at which the underlying coarse layer approaches the residual moisture content. Although the authors suggested that the base of the fine cover layer represents a "drip surface," it is shown here to be a limiting condition.

Nicholson *et al.* (1989) recognized that under conditions of static equilibrium, the cover layer would indeed drain. It was the contention of the authors, however, that as the underlying coarse material drained such that the residual moisture content was approached, the hydraulic conductivity would become so small that further drainage would be exceedingly slow. As a result, the pressure head in the coarse material would be essentially constant and at a value corresponding to the residual moisture content. Though far from hydraulic equilibrium, for practical purposes and over time scales corresponding to the interval between rainfall events, the flow system could be considered static. Though critical to the model presented by Nicholson *et al.*, it should be noted that the occurrence of "static" nonequilibrium pressure-head profiles in coarse materials under conditions of prolonged drainage has not been confirmed.

Discussing the paper by Nicholson *et al.* (1989), Barbour (1990) used steady-state flow relationships to analyse a two-layer system. Unlike the work of Nicholson *et al.*, dynamic equilibrium conditions were assumed. Barbour concluded that the analysis of Nicholson *et al.* (1989) placed unnecessary restrictions on the moisture-retention characteristics of the cover material. The analysis also indicated that for the materials selected, the moisture-content profile that develops within the cover layer may be quite variable and dependent on the magnitude of water flux (in the form of infiltration) across the ground surface. Although Nicholson *et al.* (1990) clarified the concerns raised by Barbour, they also indicated the limitations of the static (Nicholson *et al.* 1989) and

[1]Present address: Beak Consultants Ltd., 14 Abacus Road, Brampton, Ont., Canada L6T 5B7.

Printed in Canada / Imprimé au Canada

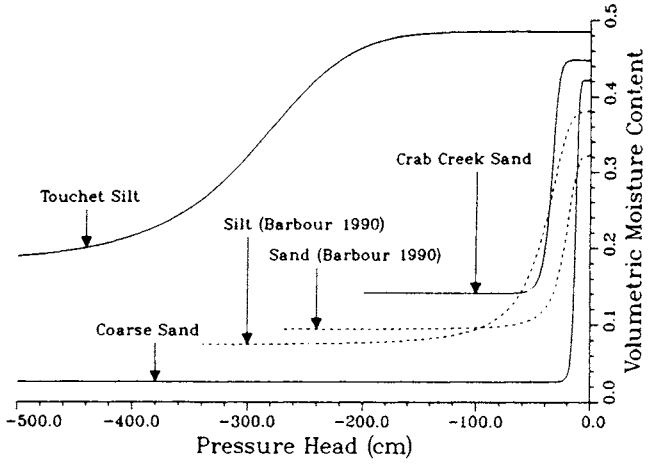

FIG. 1. Moisture-retention characteristics of the selected materials.

steady-state (Barbour 1990) approaches to the analysis of the problem. It was further indicated that a transient analysis of drainage was necessary to demonstrate the anticipated behaviour. Consideration of drainage separately (with no infiltration) would provide a conservative analysis. The objective of this paper is to demonstrate the feasibility of the concept introduced by Nicholson *et al.* (1989) using a transient numerical model and to show that transient disequilibrium is the basis for moisture retention in fine cover layers. More specifically, the purpose is to show numerically that "static" nonequilibrium conditions would prevail in the coarse layer for prolonged periods of time, such that the finer cover material would not drain.

Methodology

A one-dimensional, finite-element, saturated-unsaturated flow model (Abdul 1985) was applied to the problem of drainage through a two-layer vertical profile. The program was originally developed for two-dimensional, homogeneous, anisotropic, variably saturated, and hysteretic flow in slightly compressible porous media. The governing equation applicable to this study is somewhat simpler and is of the form

$$[1] \quad K_s k_r(\psi) \frac{\partial}{\partial z}\left(\frac{\partial \psi}{\partial z} + 1\right) = [C(\psi) + S(\psi) S_s] \frac{\partial \psi}{\partial t}$$

where K_s is the saturated hydraulic conductivity (LT^{-1}), k_r is the relative hydraulic conductivity ($0 \leq k_r \leq 1$), C is the specific moisture capacity (L^{-1}), S is the degree of saturation (normalized moisture content), S_s is the specific storage (L^{-1}), ψ is the pressure head (L), z is the coordinate in the vertical direction (L), and t is time (T).

To accommodate layering, the original version of the program was modified to allow for variation of soil properties with location. Specific storage was evaluated using

$$[2] \quad S_s = \rho g(a + bn)$$

where ρ is the density of water, g is the acceleration owing to gravity, a is the compressibility of the soil material, b is the compressibility of water, and n is the porosity.

Freeze and Cherry (1979) gave the value for b and estimates of a for different materials. Values of compressibility used were 4.4×10^{-10}, 3.3×10^{-8}, and 1×10^{-7} m^2/N for water, sand, and silt, respectively. For the simulations of this study, changes in storage caused by compressibility effects were extremely small, and thus the term could have been neglected with no perceptible change in the results.

Three sets of simulations were conducted, involving five different porous media. These included (*i*) the "silt" and "sand" used by Barbour (1990), (*ii*) Touchet silt loam overlying a medium sand (Crab Creek sand described by Brooks and Corey 1964), and (*iii*) Touchet silt loam overlying a coarse sand.

Moisture-retention characteristics of the different materials are shown in Fig. 1. The relative hydraulic conductivity for each porous medium was calculated from the corresponding moisture-retention curve using the method of Mualem (1976), as suggested by van Genuchten (1980), such that the moisture content (θ) at any arbitrary pressure head was given by

$$[3] \quad \theta(\psi) = \left[(\theta_s - \theta_r)\left(\frac{1}{1 + (\alpha|\psi|)^q}\right)^p\right] + \theta_r \qquad \psi \leq 0$$

and the relative hydraulic conductivity was calculated as

$$[4] \quad k_r(\psi) = \frac{\{1 - (\alpha|\psi|)^{q-1}[1 + (\alpha|\psi|)^q]^{-p}\}^2}{[1 + (\alpha|\psi|)^q]^{\frac{p}{2}}}$$

where θ_r is the residual moisture content, θ_s is the saturated moisture content, and α and q are the curve-fitting parameters (α has a dimension L^{-1} and

$$[5] \quad p = 1 - \frac{1}{q} \qquad (0 < p < 1, q > 1)$$

The parameter α is a measure of the reciprocal of the AEV for the material and q relates to the maximum slope of the moisture-retention curve. Table 1 contains a summary of the hydraulic and the curve-fitting parameters for each material. In [1] and [4], the hydraulic conductivity at a specified pressure head (or moisture content) is assumed to be the product of the hydraulic conductivity at saturation and the relative hydraulic conductivity, such that the relative hydraulic conductivity attains unity as the moisture content approaches its saturated value and becomes zero at residual moisture content.

Each layered system consists of 250 cm of the coarse-grained material overlaid by 100 cm of a finer cover material. The choice of this geometry was a deliberate attempt to be consistent with the system discussed by Barbour (1990) and Nicholson *et al.* (1990). Furthermore, Nicholson *et al.* (1989) had shown that the effectiveness of a cover material as a barrier to influx of oxygen increases appreciably within the first metre of cover thickness, beyond which it does not change much. Other simulations (not shown here), with more than 250 cm of underlying coarse material, gave results that are consistent with the discussion that follows.

The initial condition considered the entire profile to be saturated, with the water table at the surface. The boundary conditions include zero flux across the top boundary and a time-dependent pressure head at the bottom which, in effect, lowered the water table linearly from the top of the profile to the bottom over the 1st h of the simulation period. This boundary was used to relax the constraint on the numerical model caused by large and sudden changes in the boundary condition. Within the time frame of the simula-

TABLE 1. Summary of the hydraulic and curve-fitting parameters for the selected materials

Material	AEV (cm)	θ_r	θ_s	K_s (cm/min)	α (cm^{-1})	q
Silt*	10.0	0.074	0.381	0.045	0.028	3.60
Sand*	8.0	0.095	0.322	0.331	0.050	4.05
Touchet silt	165.0	0.18	0.485	0.035	0.004	7.05
Crab Creek sand	24.0	0.141	0.448	0.431	0.029	10.21
Coarse sand	8.0	0.026	0.422	7.80	0.077	9.74

NOTE: α and q are curve-fitting parameters in the van Genuchten (1980) model; all other parameters are measurable properties of the porous media.
* As presented by Barbour (1990).

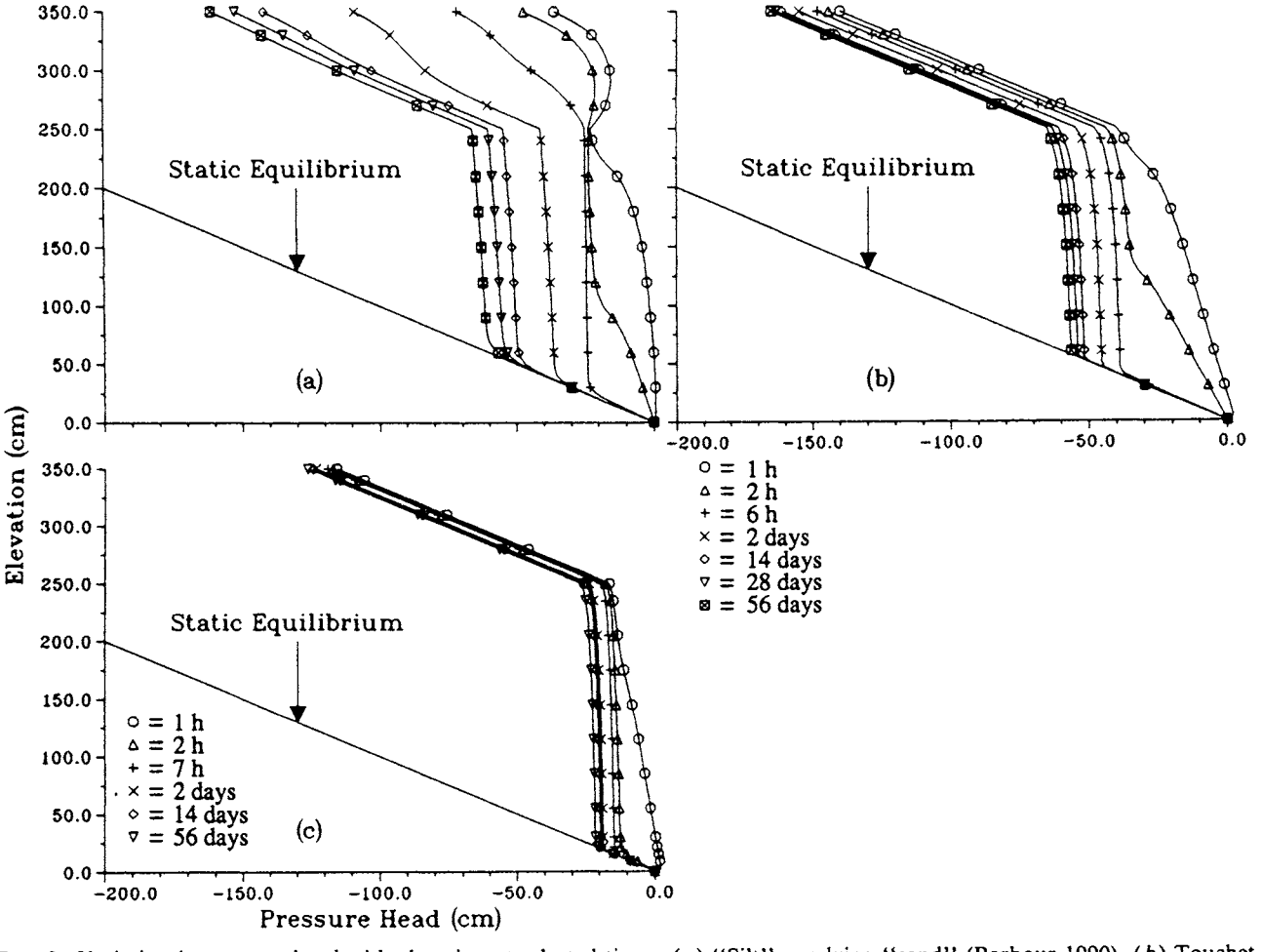

FIG. 2. Variation in pressure head with elevation at selected times. (*a*) "Silt" overlying "sand" (Barbour 1990). (*b*) Touchet silt overlying a medium sand. (*c*) Touchet silt overlying a coarse sand.

tions (56 days), this boundary condition is physically equivalent to an "instantaneous" lowering of the water table to the base of the profile. Variations in pressure head, total hydraulic head, and degree of saturation were tabulated for specified elevations over a period of 56 days.

Results and discussion

The results are summarized in Figs. 2–4. Because the water table was initially at the top of the column, an increasingly positive (hydrostatic) pressure head profile would extend below the surface. To reduce the x-axes and because late-time data are of greatest relevance, only times corresponding to negative pressure head profiles are shown. The graphs are plotted for selected times to show the general trends of the hydraulic response.

The pressure-head profiles for the three pairs of soil materials (Figs. 2*a*–2*c*) changed rapidly during early time and, in all cases, appear to be approaching a static condition by 14 days. Relatively small changes occurred between 14 days and the conclusion of the simulations at 56 days. The final profiles are very similar for all pairs of soil materials. In

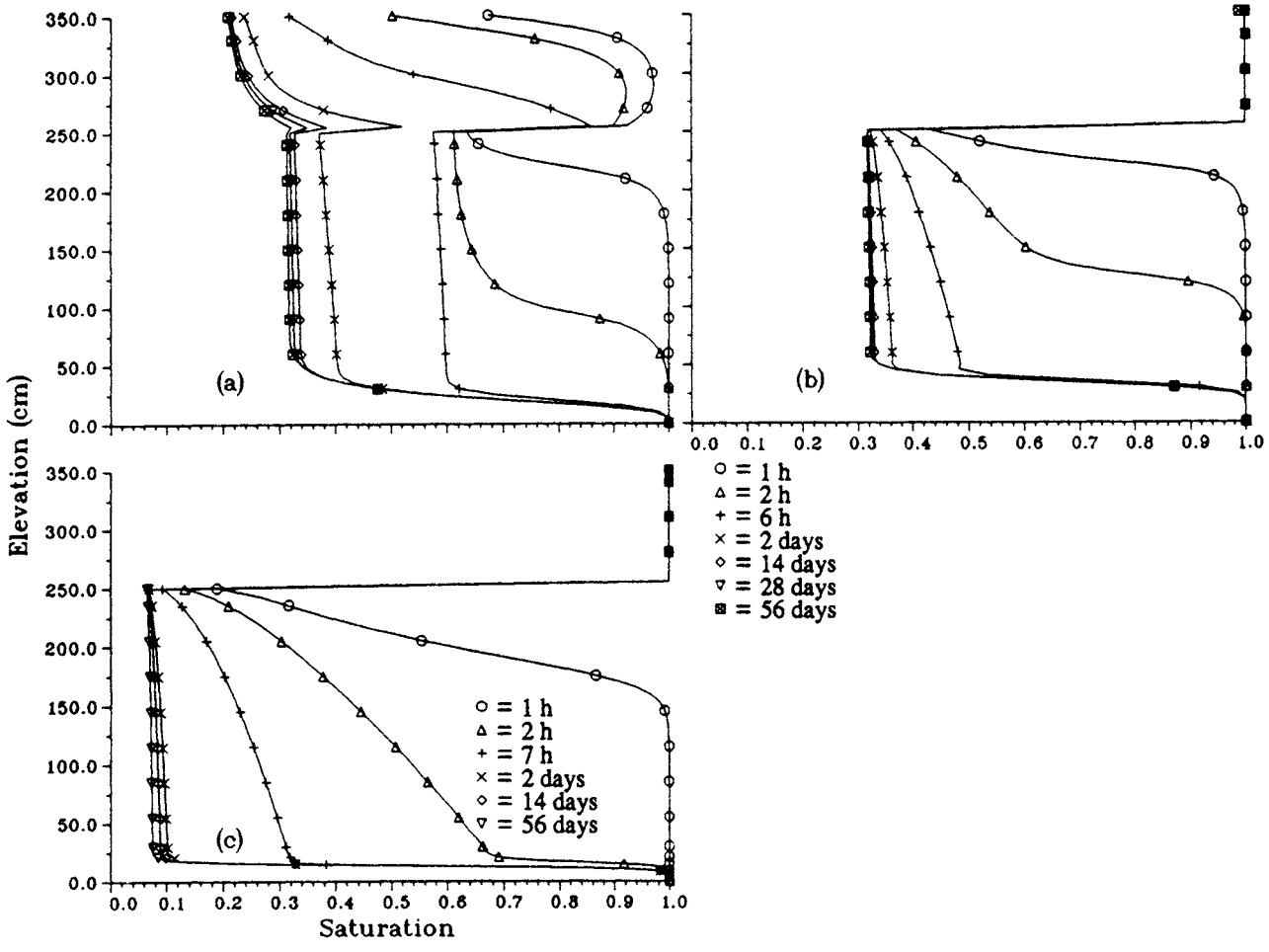

FIG. 3. Variation in saturation with elevation at selected times. (*a*) "Silt" overlying "sand" (Barbour 1990). (*b*) Touchet silt overlying a medium sand. (*c*) Touchet silt overlying a coarse sand.

particular, within the cover layer, which remains saturated or at a relatively high moisture content, the pressure head approaches the 1:1 hydraulic equilibrium condition. For a distance below the cover, the pressure head is almost constant and is close to the pressure head at which the moisture content approaches the residual value for the respective coarse-layer materials (Fig. 1). At greater depth, as the water table is approached, the pressure-head profile again approaches the 1:1 hydrostatic condition. Although the final profiles appear to be approaching a static condition, they are far from the static equilibrium condition indicated on each graph. This is a consequence of the low value of relative hydraulic conductivity when moisture content approaches the residual value.

The results of these simulations can be extended to address the situation that might lead to a zero pressure head (i.e., atmospheric) at the interface. The pressure head at the interface between the medium-size material and the cover changed from about −40 cm at 1 h to about −65 cm at 56 days (Fig. 2*b*). For the case of a coarse underlying material, the pressure head at which the residual saturation is first approached is about −10 cm (Fig. 1). Furthermore, the pressure head at the interface dropped only marginally throughout the duration of the simulation (Fig. 2*c*), keeping the interface pressure head at values more positive than −30 cm at 56 days. One can envision coarser materials with less negative pressure head values at residual saturation, resulting in an interface pressure head that could practically be zero. It is therefore suggested that a condition of "drip" surface at the interface would be an end member of the continuous spectrum, satisfied only by a very coarse underlying material.

The changes in saturation for the three cases simulated are given in Fig. 3. For the materials considered by Barbour (1990), the degree of saturation in the sand declines more rapidly than in the silt (Fig. 3*a*). Nevertheless, even at a time of 2 h, the entire cover layer was at a water content less than saturation, which would substantially reduce the cover's effectiveness as an oxygen barrier. Thus, although Barbour showed that the moisture content could be increased by application of a constant flux, under natural conditions, the cover material considered by Barbour would be an ineffective barrier after only a few hours of redistribution and drainage following precipitation events.

The saturation profiles for the Touchet silt over Crab Creek sand are substantially different (Fig. 3*b*). In particular, although the sand drained rapidly, the silt remained fully saturated over its entire thickness for almost the entire duration of simulation. This observation is readily explained by reference to the pressure-head profiles. The maximum negative pressure head at the bottom of the silt layer is about −65 cm, corresponding to the pressure head at which the

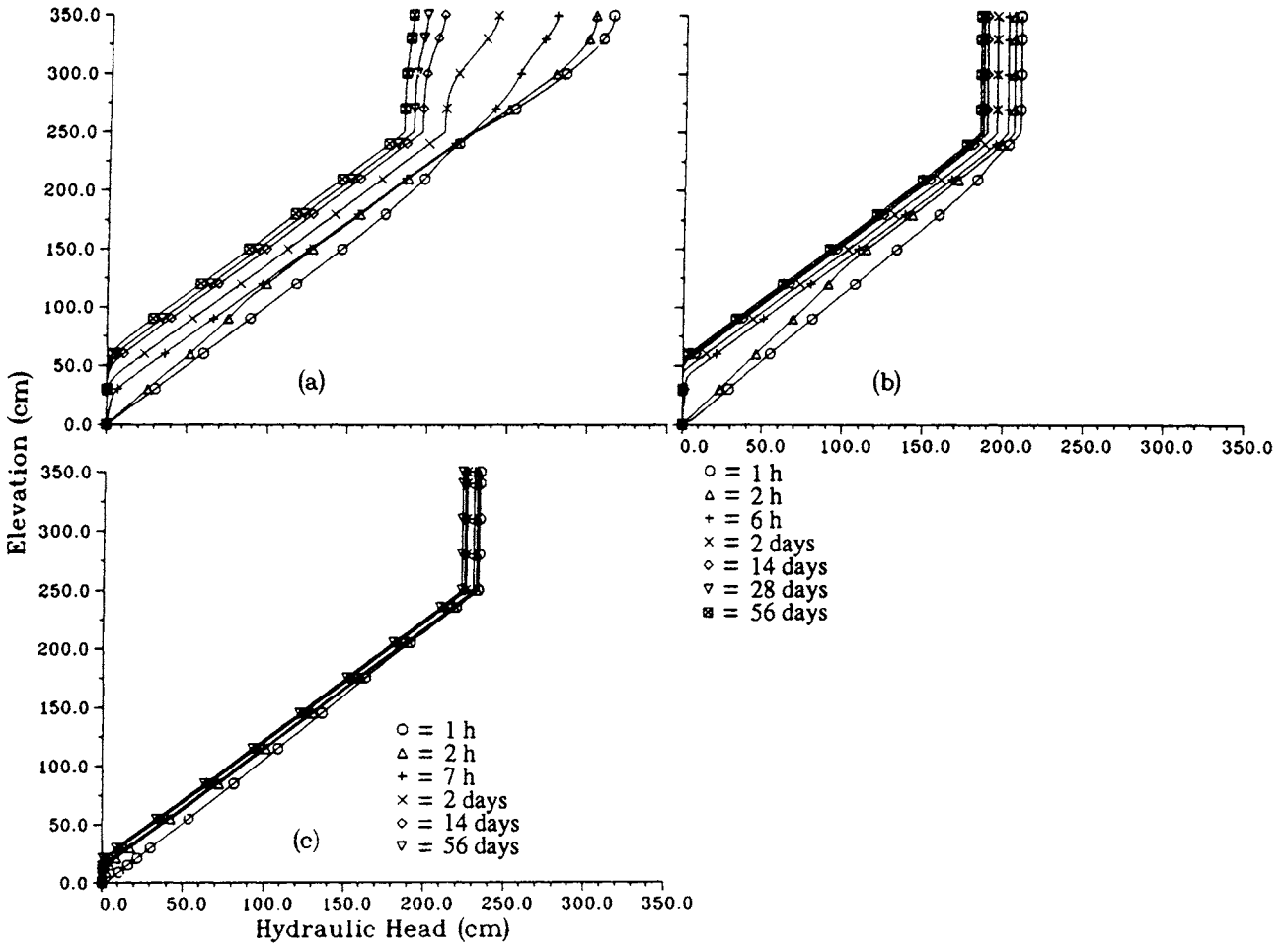

FIG. 4. Variation in hydraulic head with elevation at selected times. (*a*) "Silt" overlying sand (Barbour 1990). (*b*) Touchet silt overlying a medium sand. (*c*) Touchet silt overlying a coarse sand.

underlying sand approaches its residual moisture content value (Fig. 1). The maximum negative pressure head of about −165 cm occurs at the surface of the cover, reflecting an equilibrium pressure head distribution in the cover. Thus at no point in the cover layer does the pressure head significantly exceed the AEV of the Touchet silt material (−165 cm, Fig. 1). The silt therefore remains saturated. For the case of Touchet silt overlying coarse sand, the silt remained fully saturated over its entire thickness throughout the duration of the simulation (Fig. 3*c*). In this case, the maximum negative pressure at the base of the silt layer is only about −25 cm, which again corresponds to the pressure head at which the coarse sand approaches the residual moisture content (Fig. 1).

The hydraulic-head profiles for each soil pair are shown in Fig. 4. For both cases where the Touchet silt is the cover material (Figs. 4*b* and 4*c*), there is a negligible hydraulic gradient across the cover layer throughout the duration of simulation. This is consistent with the static equilibrium pressure head profiles discussed previously. Clearly, if there is no hydraulic gradient across the cover layer, there can be no flow of water across the layer. In the absence of a surface flux, as assumed in the present simulations, this implies that there is no drainage of the surface layer. This is consistent with the fact that the magnitude of the pressure head did not exceed the AEV of the silt. In contrast with the cover layer, the value of hydraulic gradient in the underlying material is close to unity at all times in the zones at residual saturation. Hence drainage would proceed at the rate of the prevailing hydraulic conductivity within the drained zone, diminishing with time as the degree of saturation decreases. At late time, the profiles become almost static, though far from equilibrium, as a result of slow drainage caused by the very low values of hydraulic conductivity. The materials analysed by Barbour (1990) exhibit profiles across the cover layer that are significantly different from other pairs of material simulated, particularly at early time when the hydraulic gradient is appreciable (Fig. 4*a*) while saturation is high (Fig. 2*a*). Under these circumstances, the relative hydraulic conductivity (k_r) would have a significant magnitude and drainage of the cover would be inevitable.

Conclusions

The numerical results showed that over periods of prolonged drainage the pressure head in the underlying coarse layer approached a constant "static" value corresponding to the pressure head at which the coarse material approached residual saturation. As a consequence, the results demonstrated that it is hydraulically possible to maintain a fully saturated layer of fine-texture material above a coarse material, even though the water table may be far from the ground

surface. Neglecting water losses by evapotranspiration and for an appropriate choice of cover material with an appropriate thickness, no infiltration would be necessary to maintain a fully saturated cover layer. Two fundamental characteristics are important in assessing what thickness of a particular material can be maintained fully saturated. The first is the AEV of the cover layer. The second characteristic is the pressure head at which the underlying material approaches residual saturation, in as much as this determines the pressure head at the interface. The thickness of the cover layer that would remain saturated after prolonged drainage and redistribution would be the difference in the magnitude of AEV of the cover material and the magnitude of the pressure head at the interface.

Though the results of the numerical study support the model of Nicholson *et al.* (1990), experimental verification is required. It is also recognised that the simulations do not address all of the practical design considerations for fine-grained covers. In particular, hysteretic effects caused by alternate cycles of wetting and drying conditions, reduced moisture content caused by evapotranspiration, and the effects of freezing and thawing on the integrity of the cover are important questions that need to be addressed. Further laboratory and modelling studies are in progress to better define the limitations of the concept. Preliminary results of the laboratory experiments show trends that are consistent with the discussion above.

Acknowledgements

Funding for this study was provided through Natural Sciences and Engineering Research Council of Canada operating grant 6414 and the Noranda Technology Centre as a subcontract to a research project funded by Environment Canada.

ABDUL, A.S. 1985. Experimental and numerical studies of the effect of the capillary fringe on streamflow generation. Ph.D. thesis, Earth Sciences Department, University of Waterloo, Waterloo, Ont.

BARBOUR, S.L. 1990. Reduction of acid generation in mine tailings through the use of moisture retaining cover layers as oxygen barriers: Discussion. Canadian Geotechnical Journal, **27**: 398–401.

BROOKS, R.H., and COREY, A.T. 1964. Hydraulic properties of porous medium. Colorado State University, Fort Collins, Hydrology Paper No. 3, pp. 1–27.

FREEZE, R.A., and CHERRY, J.A. 1979. Groundwater. Prentice-Hall, Englewood Cliffs, NJ.

MUALEM, Y. 1976. A new model for predicting the hydraulic conductivity of unsaturated porous media. Water Resources Research, **12**: 513–522.

NICHOLSON, R.V., GILLHAM, R.W., CHERRY, J.A., and REARDON, E.J. 1989. Reduction of acid generation in mine tailings through the use of moisture-retaining cover layers as oxygen barriers. Canadian Geotechnical Journal, **26**: 1–8.

_____ 1990. Reduction of acid generation in mine tailings through the use of moisture-retaining cover layers as oxygen barriers: Reply. Canadian Geotechnical Journal, **27**: 402–403.

VAN GENUCHTEN, M.TH. 1980. A closed-form equation for predicting the hydraulic conductivity of unsaturated soils. Soil Science Society of America Journal, **44**: 892–898.

APPENDIX 4

WCGR/IGR SOFTWARE LIST

(Can be obtained directly from

WCGR/IGR or through:

Dr. Festus Akindunni

Beak Consultants Limited

14 Abacus Road

Brampton, Ontario, Canada L6T 5B7)

IGR Software List – December 11, 1991

BLOB3D

Description: 3-D, transient solute tranport with a parallelopiped source. Finite thickness medium. Constant, uniform groundwater velocity. Computes concentration of solute at any time and distance from source. Can handle source or solute decay. Can handle solute retardation.

Solution technique: Analytical.

Cost: $ 150

Programming language: Fortran 77

Documentation: Descriptive comments interspersed with the source code.

Distribution notes: The program source code, example data sets and output are distributed as machine readable files on an IBM compatible floppy disk (5.25 or 3.5 inch disks are available). The user can inspect and modify the source code as desired.

System Requirements: Any computer with a Fortran 77 compiler. NOTE: Ability to read an IBM formatted diskette is required.

CFEMTRAN

Description: 2-D, transient solute transport in cross-section. Computes concentration of solute by solving the advection-dispersion equation. Mesh generation option for rectangular grids. Can also read a manually generated grid. Groundwater velocities are element-wise variable and can be read directly from a FLONETS output file. Can handle solute decay and retardation.

Solution technique: Numerical, Galerkin finite-element approach, matrix solution by Cholesky decomposition method.

Cost: $ 1000

Programming language: Fortran 77

Documentation: Descriptive comments interspersed with the source code.

Distribution notes: The program source code, example data sets and output are distributed as machine readable files on an IBM compatible floppy disk (5.25 or 3.5 inch disks are available). The user can inspect and modify the source code as desired.

System Requirements: A computer with sufficient memory for handling finite-element programs (640 Kb is recommended) and a Fortran 77 compiler. NOTE: Ability to read an IBM formatted diskette is required.

CGAQUFEM

Description: 2-D, transient groundwater flow in plan-view. Computes distribution of heads and groundwater velocities. Confined, unconfined or mixed aquifer. Can handle areal recharge when unconfined (or leakage through an aquitard from a water table aquifer if confined). Aquifer and aquitard thickness and hydraulic conductivity, initial head, water table head, recharge and pumping (or injection) rates are node-wise variable.

Solution technique: Numerical, Galerkin finite-element approach, matrix solution by incomplete Cholesky decomposition and conjugate-gradient acceleration for efficiency. Solver reduces core storage requirements significantly for large problems.

Cost: $ 1000

Programming language: Fortran 77

Documentation: Descriptive comments interspersed with the source code.

Distribution notes: The program source code, example data sets and output are distributed as machine readable files on an IBM compatible floppy disk (5.25 or 3.5 inch disks are available). The user can inspect and modify the source code as desired.

System Requirements: A computer with sufficient memory for handling finite-element programs (640 Kb is recommended) and a Fortran 77 compiler. NOTE: Ability to read an IBM formatted diskette is required.

CRAFLUSH

Description: 2-D, transient solute tranport in a series of parallel fractures. Can handle diffusion of solute into matrix. Computes concentration of solute at any time and distance from source.

Solution technique: Analytical.

Cost: $ 350

Programming language: Fortran 77

Documentation: Descriptive comments interspersed with the source code.

Distribution notes: The program source code, example data sets and output are distributed as machine readable files on an IBM compatible floppy disk (5.25 or 3.5 inch disks are available). The user can inspect and modify the source code as desired.

System Requirements: Any computer with a Fortran 77 compiler. NOTE: Ability to read an IBM formatted diskette is required.

FLONETS

Description: 2-D, steady-state groundwater flow in cross-section. Computes distribution of heads, stream functions and groundwater velocities. Mesh generation option for rectangular grids (can seek the water table in this case). Can also read a manually generated grid. Vertical and horizontal hydraulic conductivity, porosity and principal direction angle are element-wise variable.

Solution technique: Numerical, Galerkin finite-element approach, matrix solution by Cholesky decomposition method.

Cost: $ 500

Programming language: Fortran 77

Documentation: Descriptive comments interspersed with the source code and a short read.me file on the distribution disk. Two published papers which discuss (1) the mathematical theory and (2) a practical application of an earlier version of the program to the Borden plume.

Distribution notes: The program source code, two example data sets and output and brief documentation are distributed as machine readable files on an IBM compatible floppy disk (5.25 or 3.5 inch disks are available). The user can inspect and modify the source code as desired.

System Requirements: A computer with sufficient memory for handling finite-element programs (640 Kb is recommended) and a Fortran 77 compiler. NOTE: Ability to read an IBM formatted diskette is required.

FRACTRAN

Description: A 2-D cross-sectional model of groundwater flow and contaminant transport in a discretely fractured, porous medium. Fractures are represented by line elements while matrix blocks are represented by rectangular elements. The program computes both the steady-state flow solution and the transient evolution of a contaminant plume. Groundwater flow, and advective and diffusive contaminant transport

within the porous media matrix blocks is rigorously treated. Retardation and first-order decay of the contaminant can be simulated. The algorithm makes use of the LTG scheme which does not require timestepping when evaluating the solution at any future time and permits coarser grids than conventional finite-element models. A separate preprocessor program is provided for ease in assigning fracture and porous media properties within zones having diffferent physical properties. The model also has the option to solve for flow and transport in a non-fractured porous medium.

Solution technique: Numerical, Laplace Transform Galerkin(LTG) finite-element approach, second-order ILU preconditioned iterative solver with ORTHOMIN acceleration.

Cost: $ 2500

Programming language: Fortran 77

Documentation: A comprehensive user's manual and descriptive comments interspersed with the source code. Several example problem data files are supplied.

Distribution notes: The PREFRAC, FRACTRAN, POSTFRAC and FPLOT executable and source codes, example data sets and output are distributed as machine readable files on an IBM compatible floppy disk (5.25 or 3.5 inch disks are available).

System Requirements: Executable code is provided for IBM-compatible 386 based machines. Source code is provided which can be compiled with any suitable Fortran 77 compiler. Plotting routines are provided for 386 based machines and VMS machines running DISSPLA. NOTE: Ability to read an IBM formatted diskette is required.

HPATCH3D

Description: 3-D, transient solute tranport with a horizontal patch source which can be located at any depth in the aquifer. Finite thickness medium. Constant, uniform groundwater velocity. Computes concentration of solute at any time and distance from source. Can handle source or solute decay. Can handle solute retardation.

Solution technique: Analytical.

Cost: $ 150

Programming language: Fortran 77

Documentation: Descriptive comments interspersed with the source code.

Distribution notes: The program source code, example data sets and output are distributed as machine readable files on an IBM compatible floppy disk (5.25 or 3.5 inch disks are available). The user can inspect and modify the source code as desired.

System Requirements: Any computer with a Fortran 77 compiler. NOTE: Ability to read an IBM formatted diskette is required.

LINE2D

Description: 2-D, transient solute tranport with a vertical line source at x=0. Finite thickness medium. Constant, uniform groundwater velocity. Computes concentration of solute at any time and distance from source. Can handle source or solute decay. Can handle solute retardation.

Solution technique: Analytical.

Cost: $ 150

Programming language: Fortran 77

Documentation: Descriptive comments interspersed with the source code.

Distribution notes: The program source code, example data sets and output are distributed as machine readable files on an IBM compatible floppy disk (5.25 or 3.5 inch disks are available). The user can inspect and modify the source code as desired.

System Requirements: Any computer with a Fortran 77 compiler. NOTE: Ability to read an IBM formatted diskette is required.

LTGPLAN

Description: A quasi 3-D model of contaminant transport in a system consisting of an optional layered aquitard overlying an aquifer. The aquifer may be semi-confined, unconfined or of mixed type. Uniform groundwater fluxes can be assigned or variable fluxes can be imported from a separate flow solution. Contaminant movement in the aquitard is assumed to be vertical and is coupled (through the contaminant flux at the aquifer/aquitard interface) to a 2-D areal transport model for the aquifer. A 1-D finite element model is used to calculate the contaminant flux entering the aquifer and a 2-D triangular finite-element model is used to compute the aquifer concentrations. Numerous sources, with varying strengths and durations, can be located anywhere in the aquitard or on the aquifer surface. Retardation and first-order decay of the contaminant can be simulated. The aquitard layering may be different under each source area, allowing the user to simulate changes in stratigraphy due to the emplacement of the source. The program computes concentration versus time at the aquifer node points. The algorithm makes use of the LTG scheme which does not require timestepping when evaluating the solution at any future time and permits coarser grids than conventional finite-element models.

Solution technique: Numerical, Laplace Transform Galerkin(LTG) finite-element approach, ILU pre-conditioned, iterative solver with ORTHOMIN acceleration.

Cost: $ 1000

Programming language: Fortran 77

Documentation: Descriptive comments interspersed with the source code portion of LTGPLAN. An example problem with data files is supplied.

Distribution notes: The LTGPLAN executable code, a portion of the LTGPLAN source code, INVERT postprocessor executable code, example data sets and output are distributed as machine readable files on an IBM compatible floppy disk (5.25 or 3.5 inch disks are available).

System Requirements: Executable code is available for most commonly used systems including those running VAX Fortran, 80386's and Unix-based machines. NOTE: Ability to read an IBM formatted diskette is required.

OGATA

Description: 1-D, transient solute tranport. Computes concentration and flux of solute at any time and distance from source. Can handle solute retardation. **Identical to SUPER1D except it can't handle time-variant source.**

Solution technique: Analytical. Ogata-Banks solution.

Cost: $ 50

Programming language: Fortran 77

Documentation: Descriptive comments interspersed with the source code.

Distribution notes: The program source code, example data sets and output are distributed as machine readable files on an IBM compatible floppy disk (5.25 or 3.5 inch disks are available). The user can inspect and modify the source code as desired.

System Requirements: Any computer with a Fortran 77 compiler. NOTE: Ability to read an IBM formatted diskette is required.

ORTHOFEM

Description: Subroutines implementing the iterative, preconditioned conjugate gradient and ORTHOMIN methods for solving banded or sparse matrix equations. The conjugate gradient acceleration technique is appropriate for symmetric matrices, while ORTHOMIN acceleration is applicable for asymmetric matrices. Preconditioning of the coefficient matrix is by first-order, incomplete lower-upper (ILU) factorization. The subroutines are designed for efficient incorporation into finite-element programs with any arbitrary element type. Modifications may need to be made to accommodate either mixed element types of the same dimensionality or finite-difference programs.

Solution technique: Numerical.

Cost: $ 400

Programming language: Fortran 77

Documentation: A short manual outlining the theory, summarizing the algorithms and describing the steps necessary for incorporating the subroutines into a finite-element code. An example implementation is outlined. Descriptive comments are interspersed with the source code.

Distribution notes: The subroutine source code is distributed as machine readable files on an IBM compatible floppy disk (5.25 or 3.5 inch disks are available). The source code may be modified and customized as necessary to be compatible with the user's main program.

System Requirements: Any computer with a Fortran 77 compiler. NOTE: Ability to read an IBM formatted diskette is required.

PATCH3D

Description: 3-D, transient solute tranport with a vertical patch source at x=0. Finite thickness medium. Constant, uniform groundwater velocity. Computes concentration of solute at any time and distance from source. Can handle source or solute decay. Can handle solute retardation.

Solution technique: Analytical.

Cost: $ 150

Programming language: Fortran 77

Documentation: Descriptive comments interspersed with the source code.

Distribution notes: The program source code, example data sets and output are distributed as machine readable files on an IBM compatible floppy disk (5.25 or 3.5 inch disks are available). The user can inspect and modify the source code as desired.

System Requirements: Any computer with a Fortran 77 compiler. NOTE: Ability to read an IBM formatted diskette is required.

RCRACK

Description: 2-D, radially symetric, transient solute tranport along a single fracture. Can handle diffusion of solute into matrix. Computes concentration of solute at any time and distance from source.

Solution technique: Analytical.

Cost: $ 150

Programming language: Fortran 77

Documentation: Descriptive comments interspersed with the source code.

Distribution notes: The program source code, example data sets and output are distributed as machine readable files on an IBM compatible floppy disk (5.25 or 3.5 inch disks are available). The user can inspect and modify the source code as desired.

System Requirements: Any computer with a Fortran 77 compiler. NOTE: Ability to read an IBM formatted diskette is required.

SUPER1D

Description: 1-D, transient solute tranport. Computes concentration and flux of solute at any time and distance from source. Source strength can vary with time. Can handle solute retardation.

Solution technique: Analytical. Ogata-Banks solution with superposition to handle time-variant source.

Cost: $ 50

Programming language: Fortran 77

Documentation: Descriptive comments interspersed with the source code.

Distribution notes: The program source code, example data sets and output are distributed as machine readable files on an IBM compatible floppy disk (5.25 or 3.5 inch disks are available). The user can inspect and modify the source code as desired.

System Requirements: Any computer with a Fortran 77 compiler. NOTE: Ability to read an IBM formatted diskette is required.

WCGR Software List – December 11, 1991

CROSSFLO

Description: 2-D, steady-state groundwater flow in cross-section. Menu-driven, graphical interface for all steps of problem solution including mesh generation (for simple layered grids), data input and plotting of results. (can seek the water table in the upper layer). Computes distribution of heads, stream functions and groundwater velocities.

Vertical and horizontal hydraulic conductivity, porosity and principal direction angle are element-wise variable.

Solution technique: Numerical, Galerkin finite-element approach, matrix solution by Cholesky decomposition method.

Cost: $ 2000

Programming language: GFA-BASIC

Documentation: Comprehensive 60-page User's Manual with a chapter on model verification and illustrative examples. Two published papers which discuss (1) the mathematical theory and (2) a practical application of an earlier version of the program to the Borden plume.

Distribution notes: The program *executable* code and example data sets are distributed as machine readable files on an Atari formatted 3.5 inch floppy disk. Copies of the source are *not* distributed.

System Requirements: An Atari ST computer with sufficient memory for handling finite-element programs (1040 Kb is recommended).

GRID BUILDER

Description: 2-D, triangular element mesh generator. Interactive, menu-driven, graphical interface. Can generate a completely irregular mesh with internal subdivisions. Can refine any subset of elements. Zoom feature facilitates extremely detailed refinement. Up to 32000 elements, 16000 nodes capacity (with 4 Mb of RAM). Built-in node-numbering scheme for bandwidth optimization. Flexible I/O routines allow export of grid data to any 2-D triangular finite element model (which uses triangular elements) or import of the user's existing grids.

Cost: $ 2000

Programming language: FTN77/386 (University of Salford Fortran 77 compiler). Interacter graphics subroutine library (Interactive Software Limited)

Documentation: Comprehensive User's Manual with a step-by-step hands-on demonstration exercise. Extensive, context-sensitive, on-line help screens.

Distribution notes: The program *executable* code and example data sets are distributed as machine readable files on an IBM formatted floppy disk (5.25 or 3.5 inch disks are available). Copies of the source are *not* distributed. The FTN77/386 run-time disk is distributed free-of-charge as part of the package.

System Requirements: An IBM compatible 80386 microcomputer with Microsoft compatible mouse, VGA card and monitor (colour recommended), hard disk, 2 Mb RAM (4 Mb recommended). An HP-GL compatible plotter is supported and recommended.

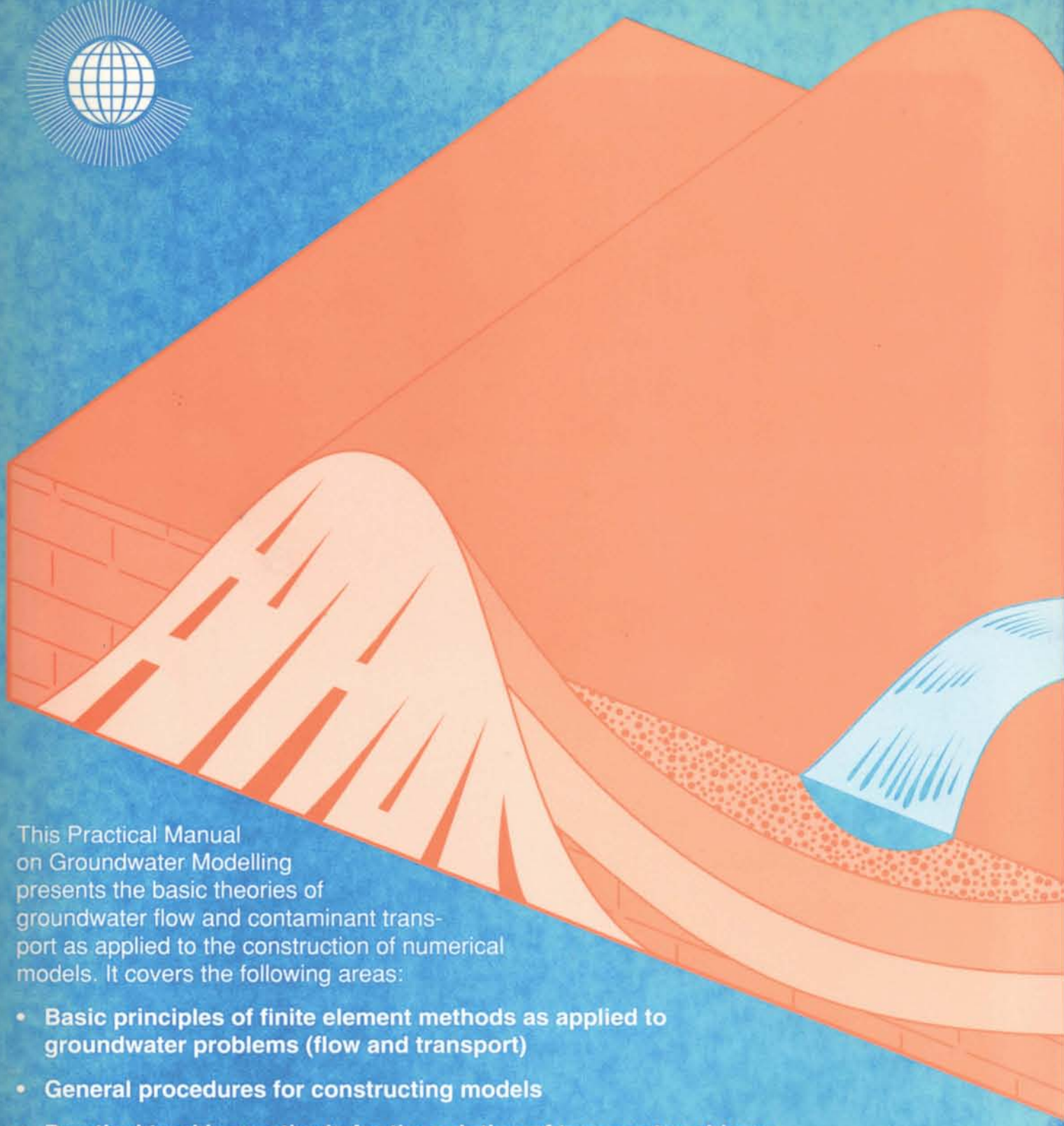

This Practical Manual on Groundwater Modelling presents the basic theories of groundwater flow and contaminant transport as applied to the construction of numerical models. It covers the following areas:

- **Basic principles of finite element methods as applied to groundwater problems (flow and transport)**
- **General procedures for constructing models**
- **Practical tracking methods for the solution of transport problems**
- **Illustrative examples and case studies**

The manual is designed for practising hydrologists, environmental engineers and scientists who require a primer in groundwater modelling. It is also suitable for graduate students of groundwater hydrology.

February 1993
Technical Paper 292
CSC(93)WMR-16
ISBN 0-85092-393-X

ISBN 978-1-84859-500-2
9 781848 595002